

# **Oil & Natural Gas Technology**

**DOE Award No.: DE-NT0005665**

## **Final Technical Report (October 2008 – September 2012)**

### **Source characterization and temporal variation of methane seepage from thermokarst lakes on the Alaska North Slope in response to Arctic climate change**

Submitted by:  
University of Alaska  
Fairbanks, AK 99775

Prepared for:  
United States Department of Energy  
National Energy Technology Laboratory

**May 29<sup>th</sup> 2013**



**Office of Fossil Energy**

## **DISCLAIMER**

This report was prepared as an account of work sponsored by an agency of the United States Government. Neither the United States Government nor any agency thereof, nor any of their employees, makes any warranty, express or implied, or assumes any legal liability or responsibility for the accuracy, completeness, or usefulness of any information, apparatus, product, or process disclosed, or represents that its use would not infringe privately owned rights. Reference herein to any specific commercial product, process, or service by trade name, trademark, manufacturer, or otherwise does not necessarily constitute or imply its endorsement, recommendation, or favoring by the United States Government or any agency thereof. The views and opinions of authors expressed herein do not necessarily state or reflect those of the United States Government or any agency thereof.

## ABSTRACT

The goals of this research were to characterize the source, magnitude and temporal variability of methane seepage from thermokarst lakes (TKL) within the Alaska North Slope gas hydrate province, assess the vulnerability of these areas to ongoing and future arctic climate change and determine if gas hydrate dissociation resulting from permafrost melting is contributing to the current lake emissions. Analyses were focused on four main lake locations referred to in this report: Lake Qalluuraq (referred to as Lake Q) and Lake Teshekpuk (both on Alaska's North Slope) and Lake Killarney and Goldstream Bill Lake (both in Alaska's interior). From analyses of gases coming from lakes in Alaska, we showed that ecological seeps are common in Alaska and they account for a larger source of atmospheric methane today than geologic subcap seeps. Emissions from the geologic source could increase with potential implications for climate warming feedbacks. Our analyses of TKL sites showing gas ebullition were complemented with geophysical surveys, providing important insight about the distribution of shallow gas in the sediments and the lake bottom manifestation of seepage (e.g., pockmarks). In Lake Q, Chirp data were limited in their capacity to image deeper sediments and did not capture the thaw bulb. The failure to capture the thaw bulb at Lake Q may in part be related to the fact that the present day lake is a remnant of an older, larger, and now-partially drained lake. These suggestions are consistent with our analyses of a dated core of sediment from the lake that shows that a wetland has been present at the site of Lake Q since approximately 12,000 thousand years ago. Chemical analyses of the core indicate that the availability of methane at the site has changed during the past and is correlated with past environmental changes (i.e. temperature and hydrology) in the Arctic. Discovery of methane seeps in Lake Teshekpuk in the northernmost part of the lake during 2009 reconnaissance surveys provided a strong impetus to visit this area in 2010. The seismic methods applied in Lake Teshekpuk were able to image pockmarks, widespread shallow gas in the sediments, and the relationship among different sediment packages on the lake's bottom, but even boomer seismics did not detect permafrost beneath the northern part of the lake. By characterizing the biogeochemistry of shallow TKL with methane seeps we showed that the radical seasonal shifts in ice cover and temperature. These seasonal environmental differences result in distinct consumption and production processes of biologically-relevant compounds. The combined effects of temperature, ice-volume and other lithological factors linked to seepage from the lake are manifest in the distribution of sedimentary methane in Lake Q during ice-covered and ice-free conditions. The biogeochemistry results illustrated very active methanotrophy in TKLs. Substantial effort was subsequently made to characterize the nature of methanotrophic communities in TKLs. We applied stable isotope probing approaches to genetically characterize the methanotrophs most active in utilizing methane in TKLs. Our study is the first to identify methane oxidizing organisms active in arctic TKLs, and revealing that type I methanotrophs and type II methanotrophs are abundant and active in assimilating methane in TKLs. These organisms play an important role in limiting the flux of methane from these sites. Our investigations indicate that as temperatures increase in the Arctic, oxidation rates and active methanotrophic populations will also shift. Whether these changes can offset predicted increases in methanogenesis is an important question underlying models of future methane flux and resultant climate change. Overall our findings indicate that TKLs and their ability to act as both source and sink of methane are exceedingly sensitive to environmental change.

## TABLE OF CONTENTS

Contents	Page
Final Scientific Report	1
DOE Award #: NT0005665	1
DISCLAIMER	2
ABSTRACT	3
TABLE OF CONTENTS	4
EXECUTIVE SUMMARY	5
Summary Conclusions	6
Setting and Background	6
Completion of Proposed Tasks	11
Project Results Dissemination	12
Published Abstracts	12
Newsletters	14
Peer-reviewed Publications	14
Manuscripts In-preparation	15
1 Quantifying the short-term variability in methane emissions, gas sources, and biogeochemistry	15
1.1 Materials and Methods	18
1.2 Results and Discussion	22
1.2.1 Geologic subcap seeps geospatially related to cryosphere disintegration	24
1.2.2 Upscaling superficial (ecological) and subcap (geologic) ebullition	25
1.2.3 Gas and aqueous chemistry	26
1.2.4 Sediment Methane Distribution	27
1.2.5 Noble Gas Fingerprinting of Seep Gases	31
1.3 Conclusions	31
2 Geophysical Surveys of Thermokarst Lakes	32
2.1 Materials and Methods	33
2.1.1 Equipment	33
2.1.2 Operations	35
2.2 Results and Discussion	36
2.2.1 Lake Q	36
2.2.2 Lake Teshekpuk	41
2.3 Conclusions	42
3 Methane Oxidation in Thermokarst Lakes	44
3.1 Materials and Methods	45
3.1.1 Methane oxidation potential measurements	45
3.2 Results and Discussion	47
3.2.1 Culture-based studies	51
3.2.2 Comparison of methanotrophs among lakes	54
3.2.3 Effect of temperature on the identity of methane oxidizing bacteria	55
3.3 Conclusions	58
4 Establishing a long-term record of the variability in methane emissions in relation to arctic climate change	59
4.1 Materials and Methods	60
4.2 Results and Discussion	62
4.3 Conclusions	63
LIST OF FIGURES	66
LIST OF TABLES	70
REFERENCES	71
LIST OF ACRONYMS AND ABBREVIATIONS	73



## EXECUTIVE SUMMARY

In recent years, there has been increased attention to the proposition that an “Arctic methane catastrophe” may be imminent as climate warming continues. Some scientific studies have demonstrated increased methane emissions as permafrost thaws (Schuur et al., 2009; Walter Anthony, 2012), but NOAA measurements taken at Barrow appear to record no significant increase in methane in recent years. In shallow waters offshore Siberia, researchers have recorded high concentrations of water column methane and calculated enhanced emissions across the ocean-atmosphere interface (Shakhova et al., 2010). Thawing subsea permafrost and dissociating gas hydrates may respectively be contributing to methane production and methane release in this setting. Prior to 2008, it had been postulated that thermokarst lakes (TKLs)—lakes set in thawing permafrost—might be contributing substantial and as-yet-unaccounted-for methane to the atmosphere. This project’s goals were related to directly testing this hypothesis, as well as determining whether any component of thermokarst methane emissions could be attributable to the degradation of methane hydrates. The project described here was jointly conducted by researchers from the University of Alaska Fairbanks, the USGS Gas Hydrates Project, and University of California-Santa Barbara (Table 1).

**Table 1. Researchers involved in this project. Table does not include support personnel from UAF and the USGS.**

Personnel	Institution	Role	Funding mechanism
Matthew Wooller	UAF	Project Director	DOE NETL
Mary Beth Leigh	UAF	Co-PI	DOE NETL
Katey Walter Anthony	UAF	Co-PI	DOE NETL
Ruo He	UAF	Post doc	DOE NETL
Benjamin Gaglioti	UAF	PhD student (Wooller)	DOE NETL
John Pohlman	USGS	Co-PI for USGS	Interagency
Carolyn Ruppel	USGS	Lead PI for USGS	Interagency
Kai-Uwe Hinrichs	Bremen	Professor/Lab Director	Self-funded (matching)
Marcus Elvert	Bremen	Research scientist	Self-funded (matching)
Monica Heintz	UC Santa Barbara	Ph.D. student (Valentine)	DOE NETL-NRC fellow
Dragos Vas	UAF	Masters student	DOE NETL

The project goals were to: (a) determine methane flux over a range of timescales at thermokarst lakes; (b) discriminate among methane sources to determine the relative contributions of the thermokarst lake thaw bulbs, coalbeds, the conventional hydrocarbon system, and gas hydrates to net methane emissions; (c) constrain methane sinks through analysis of methane oxidation pathways in lake water and lake bottom sediments; and (d) build a millennial-scale history of methane emissions and past temperatures using lake bottom sediment cores and infer the impact of past and future climate change on thermokarst lakes/thaw bulbs, permafrost/gas hydrate, and methane sources/sinks. Through fieldwork and subsequent analyses, the research has addressed each of these goals and reached important conclusions about methane dynamics on the Alaskan North Slope (ANS).

## Summary Conclusions:

In summary and in relation to the goals (a – d) stated above we concluded that: (a) A first-order estimate of subcap macroseep emissions in Alaska ( $0.08 \pm 0.1$  Tg methane  $\text{yr}^{-1}$ ) following the scaling guidelines for point-source emissions. We assumed that the point-source macroseeps observed along the flight surveys in each of the Northern Alaska continuous permafrost region ( $3,562,800$  kg methane  $\text{yr}^{-1}$  for  $793$   $\text{km}^2$  of lakes surveyed), the Interior Alaska region ( $6,951$  kg methane  $\text{yr}^{-1}$  for  $38$   $\text{km}^2$  of lakes surveyed), and the previously glaciated South Central Alaska region ( $168,931$  kg methane  $\text{yr}^{-1}$  for  $169$   $\text{km}^2$  of lakes surveyed) were a representative sample of subcap seeps for all lakes in these zones across the rest of Alaska. Geophysical techniques provide important insight about the distribution of shallow gas in the sediments of TKL systems and the lake bottom manifestation of seepage. (b) Geospatial and geochemical field data support the hypothesis that cryosphere degradation leads to the release of  $^{14}\text{C}$ -depleted methane previously trapped by the cryosphere, an extension can be made to this hypothesis that in a warmer world, thawing permafrost and wastage of glaciers and ice sheets could lead to a significant transitional degassing of subcap methane. Noble gas analyses of samples from our main study site (Lake Q) do not show any enrichment in  $^{132}\text{Xe}$  and  $^{84}\text{Kr}$  gases, suggesting the gas is not derived from gas hydrate or a petroleum system. The  $\delta^{13}\text{C}$  of seep methane ( $-58\%$ ) is consistent with a slightly degraded microbial source, which could be derived from degradation of thawed permafrost or coal beds. However, an absence of elevated  $^{84}\text{Kr}$  or  $^{132}\text{Xe}$  that have been shown to be released during coal biodegradation suggests a microbial source derived from thawed permafrost or modern organic matter. (c) Methane oxidation processes could temper future methane emissions. Our study is the first to identify methane oxidizing organisms active in arctic lakes. Additionally, we describe for the first time how methanotrophic communities in arctic lake sediments respond to temperature variation. Our findings provide new fundamental information regarding the activity and diversity of methanotrophs in cold regions that may aid predicting and modeling future methane flux from warming arctic and sub-arctic environments. (d) We applied an innovative approach to reconstruct methane availability in lakes covering thousands of years. Our data imply that past methane production has changed over the last  $\sim 12,300$  cal yr BP in response to climate change in the Arctic. A most notable period of methane availability in one of our study lakes at  $\sim 4,000$  cal yr BP correlated with a peak change in lake hydrology as well as temperature.

## Setting and Background

Field research for this project was carried out in two parts of the Alaskan North Slope (ANS) and at reference locations within the discontinuous permafrost near Fairbanks, Alaska (Figure 1). The ANS study sites included Lake Qalluuraq (Lake Q) and some small surrounding lakes in 2009 and Lake Teshekpuk and nearby lakes in 2010. Lake Q and the proximal lakes are generally shallow (less than  $2.5$  m deep) and small ( $<1.2$   $\text{km}^2$ ) features about  $10$  km from the native village of Atqasuk within fine-grained sediments of the Meade River floodplain. The lake is set within a treeless, tundra landscape, and much of the annual sedimentation is due to fine-grained, windblown material being deposited in the lake during the ice-free periods. A well-known methane seep has made Lake Q the focus of numerous studies.

**Figure 1. Location map showing primary study sites (Lake Q and Lake Teshekpuk) and the reference sites (Fairbanks lakes).**

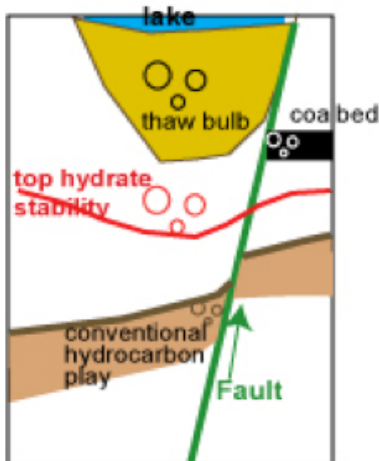


In contrast to Lake Q, Lake Teshekpuk, the second ANS study site, is the largest lake on the ANS at roughly 32 x 40 km. The lake has a maximum depth of ~10 m and is located in an area of coarser-grained sediments within the tundra of the central part of the North Slope, only 17 km from the Beaufort Sea. Small methane seeps were first discovered in the northern part of Lake Teshekpuk in 2009. There is controversy over the degree of thermokarsting that characterizes Lake Teshekpuk. The reference sites near Fairbanks included Goldstream Bill, Killarney, and Smith Lakes. All are small lakes within discontinuous permafrost and are experiencing various degrees of thermokarsting. The lakes are set within forested/meadow vegetation and serve as

the internal drainage basins for some of the surrounding areas. All three lakes have episodes of periodic methane ebullition, but none has the continuous and dramatic ebullition that characterizes Lake Q.

The ANS is a wide coastal plain stretching from the Brooks Range on the south to the shoreline of the Beaufort Sea on the north. The coastal plain consists of layered sedimentary deposits laid down in the foreland of the Brooks Range. Within the study, bedrock geology is of Cretaceous Age with a veneer of younger, unconsolidated sediments. These sediments are derived by northward riverine transport of mountain-derived erosional material and from marine

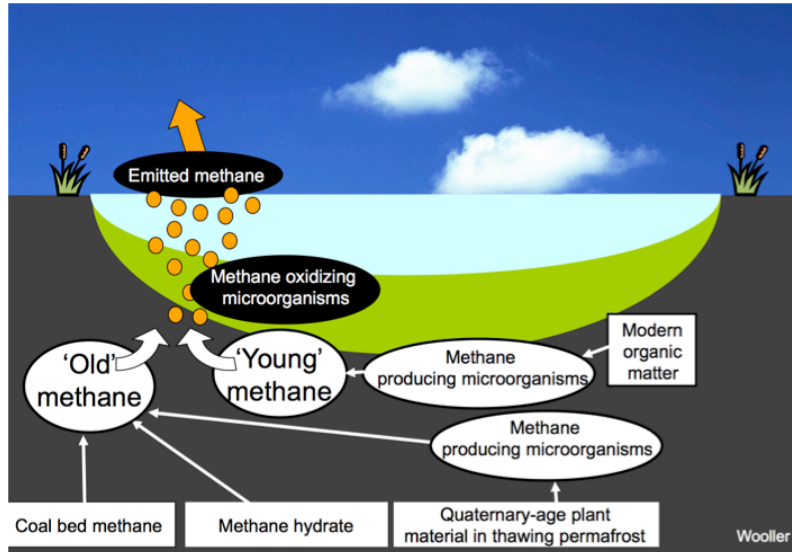
**Figure 2. Sources and sinks for methane beneath a thermokarst lake (TKL) with a well-developed thaw bulb.**



transgressions and regressions, which have affected a zone within tens of kilometers of the present day shoreline. Aeolian transport has also played a role in sedimentary processes, particularly on the central part of the ANS where wind-driven sand deposits are present at the surface. However, the thick, organic-rich loess deposits that characterize the Siberian Arctic are not present on the ANS.

Much of the ANS was exposed sub aerially (not-glaciated) through the Late Pleistocene and early Holocene. As a consequence, the ANS developed continuous permafrost that ranges from ~300 m thick near Barrow to 600-700 m in the vicinity of Prudhoe Bay. Permafrost thickness near Lake Q is estimated at ~200 m based on temperature data obtained from a USGS borehole near Meade River (e.g., Lachenbruch et

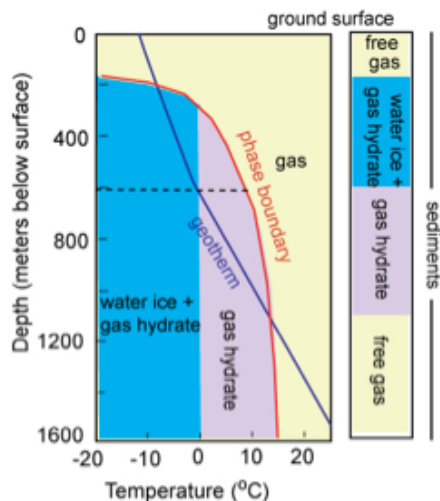
**Figure 3. Schematic of potential sources of methane that could be emitted at or near a thermokarst lake.**



al., 1982). The condition and existence of permafrost beneath Lake Teshekpuk is the subject of some controversy. Some researchers interpret seismic data as indicating that the permafrost is missing beneath Lake Teshekpuk. Yet USGS boreholes on the lake's margins clearly indicate that permafrost remains intact up to at least the lake's edge.

arid in terms of annual precipitation, the annual thawing of near-surface permafrost leads to widespread marsh like conditions and, in some places, to the development of thermokarst lakes (TKL) that dominate the landscape. On the ANS, these TKL vary in size and are preferentially oriented NNW. Beneath some TKL, the permafrost remains permanently thawed in features called thaw bulbs, which may deepen or remain static, depending on a number of factors (e.g. Figure 2). Thaw bulbs are important to carbon cycling and methane dynamics on the ANS.

**Figure 4. Nominal relationship among permafrost, gas hydrate, and gas-charged sediments in a permafrost area, from Ruppel (2007).**



three key components: coalbeds, conventional oil/gas deposits, and gas hydrates. USGS maps show that coal of various grades is distributed beneath nearly the entire ANS as far east as Harrison Bay and certainly occurs beneath the ANS locations used for this study. Not all

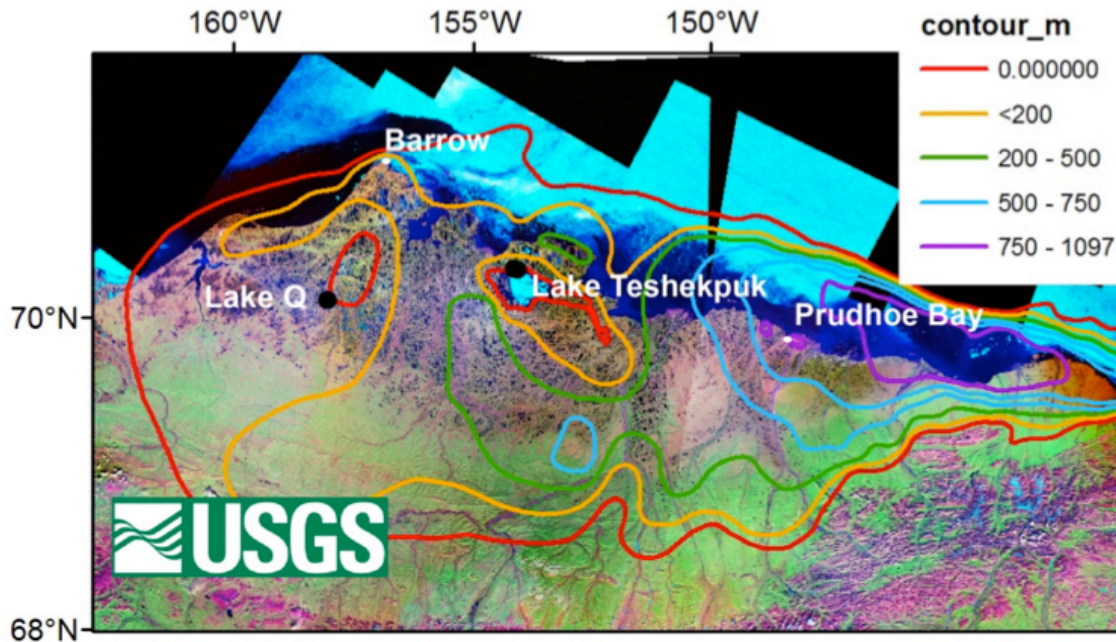
coalbeds emit methane, but those that do can generate large volumes of gas with the light stable carbon isotopic signatures characteristic of a microbial generation. Anthracitic coals and those that are deeply buried are typically more prone to emit methane than are other types. The USGS identifies subbituminous coal of mineable thickness in the Lake Q area, and outcrops of this coal are visible between Lake Q and the native village of Atqasuk (~10 km away). The coal that lies beneath the Lake Teshekpuk area is also classified as subbituminous, but of unknown thickness. Lignitic coals were encountered in the South Meade borehole 32 km NNE of the Lake Q site, but these were generally at several hundred meters depth.

On the ANS, oil and/or conventional gas are commercially produced from the west of the Colville River to Mikkelson Bay on the east. Conventional gas is widely produced and used in the vicinity of Barrow as well. Gas leases have been proposed in the vicinity of Lake Teshekpuk by BLM testifying to the likelihood of gas deposits in this area. There has been little consideration of conventional hydrocarbons in the immediate vicinity of Lake Q. USGS analyses of the South Meade borehole 32 km NNE of Lake Q revealed no liquid hydrocarbons and only sporadic, non-commercially viable gas shows relatively deep in the section. Gas hydrates are an ice-like form of low molecular weight gas (usually mostly methane) and water that is stable within permafrost at depths greater than ~225 m (Figure 4). Gas hydrates remain stable throughout the lower part of the permafrost-bearing section and up to hundreds of meters below the base of permafrost. Gas hydrates in permafrost areas normally form through ‘freezing’ of thermogenic gas that is in place or migrating through the section. Depending on the mixture of thermogenic gases, the top of the gas hydrate stability zone can be shifted to shallow depths, possibly less than 200 m.

The calculated thickness of the theoretical gas hydrate stability zone (Figure 5) based on temperature fields calibrated with borehole data ranges from < 200 m in the vicinity of Barrow to over 750 m near Prudhoe Bay. Both Lake Q and Lake Teshekpuk apparently lie near zones of minimal gas hydrate thickness (Collett, 1997), but these interpretations are based on a single, repeatedly sampled borehole near the South Meade River and on the presumption of no permafrost beneath Lake Teshekpuk, respectively. However, if there is only a minimal gas hydrate stability zone in the vicinity of Lake Q and Lake Teshekpuk, these areas are particularly apt locations for this study since those gas hydrate stability zones would be thin and thus more susceptible to dissociation during thermal perturbations.



**Figure 5.** Calculated thickness of gas hydrate stability zone on the Alaskan North Slope based on analyses by T. Collett of USGS borehole temperature data and supplementary data. The positions of the Lake Q and Lake Teshekpuk study sites are also shown.



There is considerable uncertainty about the degree to which TKL thaw bulbs may perturb the underlying thermal regime and potentially lead to dissociation of gas hydrate. Since the shallowest gas hydrate in permafrost would normally occur at 225 m or greater, thaw bulbs would have to be deep and at least several kilometers wide to perturb underlying geotherms to great enough depths to affect the gas hydrate stability zone. Furthermore, given that gas hydrate in permafrost areas generally forms by freezing of migrating thermogenic gas, it is not clear how common gas hydrate occurrences are at minimal depths of gas hydrate stability. Nonetheless, some of the low-velocity zones associated with thaw bulbs imaged by Bellefleur et al. (2009) in the Mackenzie Delta area based on 3D seismic data are hundreds of meters thick and could perturb gas hydrate stability. Based on modeling and field-based studies (West et al., 2008; Kessler et al., 2012), ANS thaw bulbs could range from a few meters to tens of meters thick depending on lake depth, area, and other characteristics, although that dependence has been challenged by recent work (Minsley et al., 2012; Jepsen et al., 2013). Thaw bulbs even tens of meters thick are unlikely to affect thermal regimes at the depths where gas hydrates would be stable.

## Completion of Proposed Tasks

The tasks enumerated below were proposed for the DE-NT0005665 to address the project goals described above. The following summary outlines the progress toward completion for each of these objectives by addressing the series of tasks proposed in the original management plan. The original numbering of these tasks from the project management plan is indicated in each results section.

**Project goal a and b: Quantifying the short-term variability in methane emissions and gas sources.** The goal of this task (Management Plan Task 5 and 10) was to characterize the short-term variability in methane emissions from TKL sites. An additional goal was to use chemical analyses of the gases being emitted from TKLs to characterize their most likely source. This goal was completed for Lake Q as well as a number of other lakes across Alaska and was published in international peer reviewed journal articles (Walter-Anthony et al., 2012, Walter-Anthony et al., 2010) (reference details listed below).

**Project goal b: Geophysical surveying of thermokarst lakes.** The goal of this task (Management Plan Task 9) was to use myriad geophysical methods to image shallow sediments, determine the distribution of shallow sub-lake gas, detect gas migration pathways, and possibly image thaw bulbs. This goal was completed for Lake Q, Lake Teshekpuk and a number of lakes in the Fairbanks area.

**Project goal c: Methane oxidation in Alaskan thermokarst lakes.** The goal of this task (Management Plan Task 11) was divided into two sub-tasks (Subtask 11.1 and 11.2). The goal of the first sub-task was to characterize and quantify aerobic methane oxidation. This was conducted by analyzing both methane oxidation and the biogeochemistry in TKL sediments and water. The goal of the second sub-task was to characterize methanotrophs in TKLs using stable isotope probing and lipid biomarker analysis. This goal was completed and the results have been published in a series of papers led by the UAF post doc supported by this award (Dr. Ruo He) (reference details listed below).

**Project goal d: Establishing a long-term record of the variability in methane emissions in relation to arctic climate change.** The overall goal of the section (Management Plan Task 12) was to examine whether dated sediments from TKLs with seeps preserved evidence of the long-term (thousands of years) history of methane availability. The goal of this task was broken down into 4 sub-tasks (12.1-12.4). The goal of the first sub-task was to establish the depositional chronology of lake sediments taken as cores from TKLs. The goal of the second subtask was to establish a long-term record of past methane emissions using chemical markers of methane preserved in lake sediments. The goal of the third sub-task was to establish a long-term record of past climate using chemical markers of climate preserved in lake sediments. The goal of the final sub-task was to synthesize and compare long-term records to evaluate the influence of past climate on methane emissions. The overall goal was completed and the results have been published in an international peer-reviewed journal (Wooller et al., 2012) (reference details listed below)

## Project Results Dissemination

Project results (Management Plan Task 20) have been detailed in a final report to the government, which describes the final disposition of each task outlined above. In addition, project investigators have made presentations to national and international scientific associations to describe and discuss their findings. Many of the final results have already been published in peer-reviewed scientific journal articles that acknowledge the support of DOE-NETL. Remaining data are actively being included in articles being prepared for peer-reviewed scientific journals and will also acknowledge the support of DOE-NETL. The contributions from this project are list below.

## Published Abstracts

- Corinne Disenhof, Matthew Wooller, John W. Pohlman, Kelly Rose. 2012. Lithology of Alaskan Thermokarst Lake Facilitates Methane Flux, AGU
- Brosius, L., Walter Anthony, K.M., Chanton, J. 2009: Determining Organic Matter Sources to CH<sub>4</sub> Production and Bubbling from Alaskan Lakes using Stable Isotopes and Radiocarbon Ages. Eos Trans. AGU, 90(52), Fall Meet. Suppl., Abstract B41C-0327.
- Chanton, J., Walter Anthony, K.M., Prater, J., Whiting, G. (2009): Contrasting natural abundance radiocarbon signatures of methane released upon permafrost decomposition. Eos Trans. AGU, 90(52), Fall Meet. Suppl., Abstract B44B-04.
- Elvert, M, Hinrichs, K-U, Wooller, M., Gaglioti, B., Becker, K., Pohlman, J.W. 2011. Carbon and hydrogen isotope biomarker records of methane release and hydroclimatic variability from a thermokarst lake in the Alaskan Arctic. International Meeting on Organic Geochemistry. Interlaken, Switzerland.
- Geai M-L, Walter Anthony KM, Grosse G (2010): Climate Change and Methane Emissions: Pan Arctic Lake Ice Methane Monitoring Network (PALIMMN). International Polar Year Conference, Oslo, Norway, 8-12 June, 2010.
- Grosse G, Jones B, Walter Anthony K, Romanovsky V, Marchenko S (2010): Classification of Lakes in Pan-Arctic Permafrost Regions. Third European Conference on Permafrost, Longyearbyen, Svalbard, Norway, June 13-17, 2010.
- Grosse G, K. Walter Anthony, B. Jones, L. Plug, V. Romanovsky (2010): Thermokarst lake drainage in the continuous permafrost zone of NW Alaska and climate feedbacks. EGU General Assembly, 2-7 May 2010, Vienna, Austria.
- Grosse G, Walter Anthony K, Romanovsky V, Marchenko S, Jones B, Plug L, Edwards M (2010): Pan-Arctic thermokarst lakes, methane emissions, and future permafrost thaw. International Polar Year Conference, Oslo, Norway, 8-12 June, 2010.
- Leigh, MB. (2011). Into the black box: Carbon and contaminant cycling in Alaskan ecosystems. Institute of Arctic Biology Life Sciences Seminar. University of Alaska Fairbanks.
- Nolan J, Parsekian A, Slater L, Plug L, Walter Anthony K, Grosse G (2010): Thaw Bulb Dimension Imaging Using Continuous Resistivity Soundings, Seward Peninsula, Alaska. State of the Arctic Conference, Miami, Florida.
- Pohlman, J.W., Elvert, M, Hinrichs, K-U., Gaglioti, B., Wooller, M. 2011. Holocene methane emissions from an Alaskan thermokarst lake: A multiproxy reconstruction. USGS-DOE Climate-Hydrates workshop. Boston MA.



- Ruo He, M. Wooller and MB Leigh. (2011). Methane oxidizing microbes in Alaskan lakes. Platform presentation. American Society for Microbiology Alaska Branch Meeting, Anchorage, AK.
- Ruo He, Matthew Wooller and Mary Beth Leigh. (2011). Methane oxidizing microbes in Alaskan lakes. Oral presentation. ASM Alaska branch meeting, April 22-23,
- Ruo He, Matthew J. Wooller, Mary Beth Leigh. (2010). Community structure and activity of methanotrophs in arctic lakes. Poster 13th International symposium on Microbial Ecology.
- Ruo He, Wooller MJ, Leigh MB (2010). Stable isotope probing analysis of methane oxidation activity and community structure in arctic lakes. Poster 7th Isotopes In Ecology Conference.
- Ruo He, Matthew J. Wooller, Mary Beth Leigh. Characterization of Methane Oxidation and Methanotrophic Community Structure in a lake on the North Slope of Alaska. Poster. ASM Alaska branch meeting, February 26-27, 2010
- Ruppel, C., Climate change and methane hydrates onshore and offshore Northern Alaska, Alaska Environmental Forum (outreach), Anchorage, AK, February 2010.
- Ruppel, C., Climate change and methane in the Arctic, WHOI Summer Student Fellow seminar series (outreach), Woods Hole Oceanographic Institution, June 2010. [talk also given to public as part of USGS Earth Day celebration, April 2010]
- Ruppel, C., Global warming on the North Slope: a tale of permafrost and methane ice (hydrate), Schoolyard lecture series (outreach) hosted by Barrow Arctic Science Center, July 2010. [same talk also given to MIT's Dept of Earth, Atmospheric, and Planetary Sciences undergraduate seminar series, November 2010].
- Ruppel, C., Methane hydrate degassing and global climate change—past, present, and future, Lawrence Livermore National Laboratory, April 2010.
- Ruppel, C., USGS Gas Hydrates Project: Arctic methane-climate research, EU COST PERGAMON Arctic Methane meeting, Brussels, Belgium, February 2011.
- Ruppel, C., Overview of USGS climate-methane hydrates research, USGS-DOE Climate-Hydrates workshop, Boston, MA, March 2011.
- Walter Anthony, K.W. (2010): Methane emissions from thermokarst lakes, ABISKO Scientific Research Station Invited Speaker, December 17, 2010.
- Walter Anthony, K. W. 2011, Methane ebullition from thermokarst lakes in the Arctic, Invited Talk, Physics of Sustainable Energy II: Using Energy Efficiently and Producing It Renewably; The American Physical Society's Forum on Physics and Society Topical Group on Energy Research and Application & The American Association of Physics Teachers, University of California, Berkeley, March 5, 2011.
- Walter Anthony, K.M., Grosse, G., Jones, B.M. (2009): Positive and negative feedbacks to climate change associated with methane emissions from arctic permafrost systems. Eos Trans. AGU, 90(52), Fall Meet. Suppl., Abstract B43F-06.
- Walter Anthony, K.M., Zimov, S.A. (2009): Greenhouse gas release from arctic permafrost: positive feedback to climate warming. Eos Trans. AGU, 90(52), Fall Meet. Suppl., Abstract U44A-02.
- Walter KM, Grosse G, Finlay J, Chandra S, Michelle MC (2009): Disappearing permafrost and the response of Arctic lakes. Advancing the Science of Limnology and Oceanography Meeting, 25-30 January, 2009, Nice, France.

Wooller, M.J. 2011. Stable Isotopes role in addressing oil spills in ice covered water. ASF workshop, University of Alaska Fairbanks.

### Newsletters

- Ruppel, C., J. Pohlman, and C. Worley, 2009, Studying the link between Arctic methane seep and degassing methane hydrates, Soundwaves USGS national newsletter, October edition, cover article (<http://soundwaves.usgs.gov/2009/10/>)
- Wooller, M.J., Ruppel, C., Pohlman, J.W., Leigh, M.B., Heintz, M., and Walter Anthony, K., Permafrost gas hydrates and climate change; lake-based seep studies on the Alaskan North Slope: Fire in the Ice (U.S. Department of Energy, National Energy Technology Laboratory Methane Hydrate Newsletter), summer 2009, p. 6-9 [<http://www.netl.doe.gov/technologies/oilgas/FutureSupply/MethaneHydrates/newsletter/newsletter.htm>].

### Peer-reviewed Publications

- Brosius LS, Walter Anthony KM, Grosse G, Chanton JP, Farquarson LM, Overduin PP, Meyer H (2012): Using the deuterium isotope composition of permafrost melt water to constrain thermokarst lake contributions to atmospheric CH<sub>4</sub> during the last deglaciation. *Journal of Geophysical Research – Biogeosciences*, 117, G01022, doi:10.1029/2011JG001810.
- Grosse, G., V. Romanovsky, T. Jorgenson, K. Walter Anthony, J. Brown, P. P. Overduin. 2011. Vulnerability and feedbacks of arctic permafrost to climate change. *EOS Transactions, American Geophysical Union*. In press.
- He, R. M. J. Wooller, J. W. Pohlman, J. Quensen, J. M. Tiedje, M. B. Leigh. 2012a. Diversity of active aerobic methanotrophs along depth profiles of arctic and subarctic lake water column and sediments. *The ISME Journal*. doi:10.1038/ismej.2012.34
- He, R. M. J. Wooller, J. W. Pohlman, J. Quensen, J. M. Tiedje, M. B. Leigh. 2012b. Shifts in identity and activity of methanotrophs in arctic lake sediments in response to temperature changes. *Applied and Environmental Microbiology* 78(13):4715-4723.
- He, R. M. J. Wooller, J. W. Pohlman, C. Catranis, J. Quensen, J. M. Tiedje, M. B. Leigh. 2012c. Identification of functionally active aerobic methanotrophs in sediments from an arctic lake using stable isotope probing. *Environmental Microbiology* 14(6):1403-1419.
- Hunt, A.G., Stern, L., Pohlman, J.W., Ruppel, C., Moscati, R.J., Landis, G.P. 2013. Mass fractionation of noble gases in synthetic methane hydrate: Implications for naturally occurring gas hydrate dissociation. *Chemical Geology*. In Press.
- Isaksen, I. S. A., M. Gauss, G. Myhre, K. M. Walter Anthony, and C. Ruppel. 2011. Strong atmospheric chemistry feedback to climate warming from Arctic methane emissions, *Global Biogeochem. Cycles*, 25, GB2002, doi:10.1029/2010GB003845.
- Ruppel, C., 2011, Methane Hydrates and Contemporary Climate Change, *Nature Education Knowledge*, 2(12):12.
- Scandella, B.P., C. Varadharajan, H. F. Hemond, C. Ruppel and R. Juanes, 2011, *Geophysical Research Letters*, 38, L06408, doi:10.1029/2011GL046768
- Sepulveda-Jauregui, A., K. Martinez-Cruz, A. Strohm, K. M. Walter Anthony, F. Thalasso, 2012. New method for on-site measurement of dissolved gas in water using Infrared

- tunable diode laser absorption spectroscopy. *Limnology and Oceanography Methods*, 10:560-567, DOI: 10.4319/lom.2012.10.560.
- Walter Anthony, K. M., P. Anthony, G. Grosse, J. Chanton. 2012. Geologic methane seeps along boundaries of arctic permafrost thaw and melting glaciers, *Nature Geoscience*, DOI doi.org/10.1038/Ngeo1480.
- Walter Anthony, K. Vas, D., Brosius, L., Chapin, F. S. III, Zimov, S.A., and Zhuang, Q. 2010. Estimating methane emissions from northern lakes using ice bubble surveys. *Limnol. Oceanogr.: Methods* 8, 2010, 592–609.
- Wooller, M. J., Pohlman, J. W., Gaglioti, B. V., Langdon, P., Jones, M., Walter Anthony, K. M., Becker, K. W., Hinrichs, K. U., Elvert, M. 2012. Reconstruction of past methane availability in an Arctic Alaska wetland indicates climate influenced methane release during the past ~12,000 years. *Journal of Paleolimnology* DOI 10.1007/s10933-012-9591-8.
- Wooller, Matthew J. et al. 2012. An ~11,200 year paleolimnological perspective for emerging archeological findings at Quartz Lake, Alaska. *Journal of Paleolimnology*. DOI 10.1007/s10933-012-9594-9

### **Manuscripts In-preparation**

- Ruo He, Matthew J. Wooller, John W. Pohlman, Catharine Catranis, John Quensen, James M. Tiedje, Mary Beth Leigh. (in review) Identification of functionally active aerobic methanotrophs in sediments from an arctic lake using stable isotope probing. *Environmental Microbiology*
- Vas, D.A., K. M. Walter Anthony, R. Barry, P. Anthony. Understanding the plumbing methane ebullition seeps in interior Alaska thermokarst-lake sediments from high temporal resolution seep monitoring, *Limnol. Oceanogr.*
- Wooller, Matthew J. et al. (in preparation) A record of Late Quaternary climate change in the northwestern Brooks Range, Alaska derived from stable isotopic analyses of chironomids. *Quaternary Research*.
- Wooller, Matthew J. et al. 11,000 years of climate and limnological change from Quartz Lake, Alaska. *Journal of Paleolimnology*.

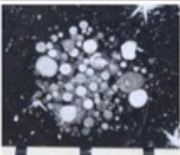
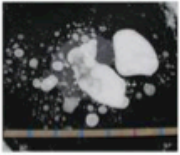
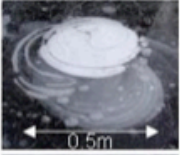

### **1 Quantifying the short-term variability in methane emissions, gas sources, and biogeochemistry**

Ebullition (bubbling) is often the dominant pathway of methane release (Figure 6) from aquatic ecosystems, but methane in bubbles can originate from a variety of sources with different implications for resource availability and climate change feedbacks. In this project Walter Anthony's UAF group worked to distinguish two types of methane ebullition seeps in Alaskan lakes using field and laboratory measurements: Superficial and subcap seeps. This work was published primarily in two articles, summarized here in this report:

- Walter Anthony, K. M., D. Vas, L. Brosius, F. S. Chapin III, S. A. Zimov, Q. Zhuang. 2010. Estimating methane emissions from northern lakes using ice bubble surveys. *Limnology and Oceanography Methods* 8, 592–609.

Walter Anthony, K. M., P. Anthony, G. Grosse, J. Chanton. 2012. Geologic methane seeps along boundaries of arctic permafrost thaw and melting glaciers, Nature Geoscience, DOI doi.org/10.1038/Ngeo1480.

**Figure 6. Classification of superficial (ecological) ebullition seeps by methane bubble-clusters patterns in lake ice; methane concentrations in bubble gas; and summer, winter, and annual ebullition determined by long-term flux measurements. Error estimates (standard error of n seeps) represent differences in methane concentrations and ebullition between individual seeps in each category. The lines on the meter sticks in the photos of type A and B mark 10cm wide intervals. [From Walter Anthony et al. 2010].**

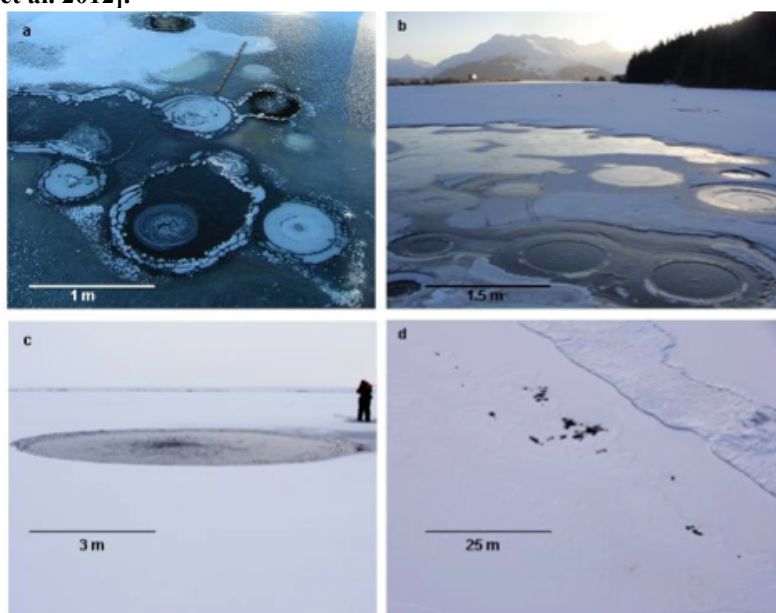
Seep	Description	CH <sub>4</sub> (%)	Ebullition (mg CH <sub>4</sub> d <sup>-1</sup> )		
			Summer	Winter	Annual
	<b>A</b> Isolated bubbles in multiple ice layers	73 ± 11, n=6	28 ± 19, n=3	8 ± 5, n=8	16 ± 10
	<b>B</b> Merged bubbles in multiple ice layers	75 ± 3, n=35	210 ± 8, n=2	81 ± 29, n=4	131 ± 20
	<b>C</b> Single gas pockets stacked in ice	76 ± 3, n=41	1042 ± 210, n=6	925 ± 98, n=9	971 ± 142
	<b>Hotspot</b> Relatively open hole in winter lake ice	78 ± 2, n=52	3130 ± 244, n=4	3240 ± 412, n=10	3197 ± 346

Superficial seepage (also referred to here as ecological seeps) refers to the continuous formation and release of ‘ecosystem’ methane, which is formed over relatively recent time scales without storage for geologic time. Examples of superficial methane systems include shallow lake and wetland sediments where methane is produced by microbes through anaerobic decomposition of relatively modern organic matter. A second example would be thawed zones under thermokarst lakes, such as our Fairbanks area study lakes (e.g., Killarney L. and Goldstream L.) formed by degradation of icy, organic-rich yedoma permafrost, where the radiocarbon age of microbial methane reflects the age of recently thawed Pleistocene organic matter (Zimov et al. 1997, Walter et al. 2006). In contrast, subcap seeps release <sup>14</sup>C-depleted methane that has been trapped or impeded by the cryosphere. Subcap methane may originate from microbial, thermogenic or mixed microbial-thermogenic processes within sedimentary basins, including buried organics associated with glacial sequences, coal beds, conventional natural gas reservoirs, and potentially methane hydrates. Emissions from superficial seeps can be scaled based on ecological methods that were further developed through coupling ice-bubble surveys to long-term flux measurements

by this project (Walter Anthony et al. 2010). Quantification of subcap seepage is more challenging because methane accumulations are distributed beneath complex, site-specific geologic and cryospheric settings.

Seasonal ice cover on water bodies in the Arctic provides a unique opportunity to more accurately assess methane ebullition from both seep types. Relatively slow bubbling from superficial seeps produces distinct in-ice bubble patterns and occasionally small holes (0.01-0.3 m<sup>2</sup>) that remain ice-free for several days to weeks following freeze-up (Figure 7a). In contrast,

**Figure 7. The effect on lake ice formation of the largest superficial seeps (a) and the smallest (b) and largest (c) subcap macroseeps. Even the strongest superficial seeps are ice-covered in late winter. Further, ebullition does not occur simultaneously among superficial seeps (a). In contrast, bubbles breaking the surface of all open holes indicate high, simultaneous ebullition among subcap seeps (b). Clustering of subcap seeps is apparent in the aerial photograph (d). Photographs were taken near Fairbanks, Interior Alaska (a), Cook Inlet, Southcentral Alaska (b), and (Lake Q) Atkasuk, Northern Alaska (c, d) one, eight, and three weeks respectively following freeze-up. Locations are shown in Figure 8. [From Walter Anthony et al. 2012].**



convection associated with anomalously high bubbling rates in subcap seeps maintains large (up to 300 m<sup>2</sup>) open holes in ice 0.2-2 m thick that we detected during aerial surveys in winter (Figure 7b-d). We used aerial and ground surveys combined with ebullition flux measurements, gas collection, and isotope analyses to map the occurrence of superficial and subcap methane seeps along a north-south transect in Alaska (Figure 8).

Despite concerns that accelerated methane emissions from northern lakes will exacerbate climate warming, knowledge of the sediment biogeochemistry controlling the production and fate of methane in northern lake sediments remains poorly understood, particularly given the diversity in permafrost characteristics and the wide variety of lake types in the Arctic.

## 1.1 Materials and Methods

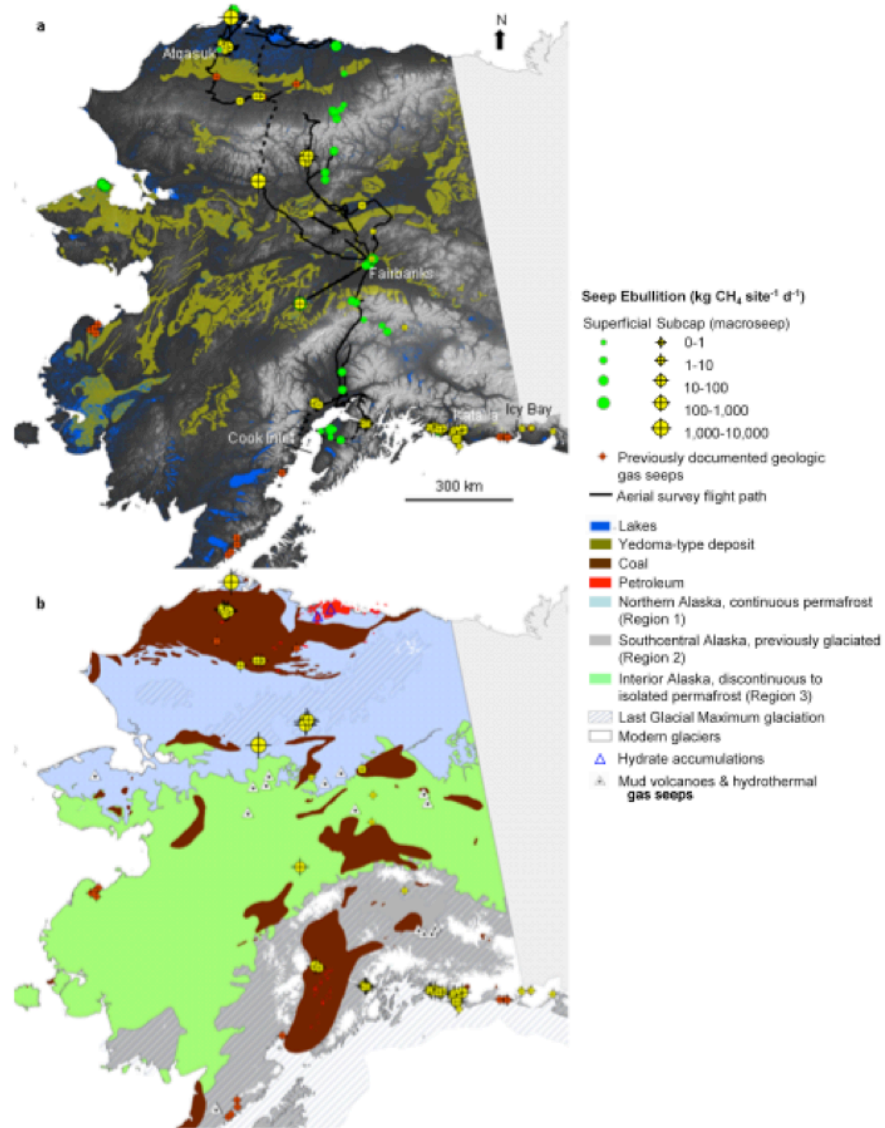
We conducted aerial surveys (Table 2) on approximately 6,700 lakes in an 11,260 km<sup>2</sup> area along a north-south transect in Alaska during ice-cover seasons from 2008-2010 (Figure 8). From the airplane directly and from photographs obtained during flights, we counted the number of open holes observed in the ice cover of frozen water bodies (usually lakes). We classified the likelihood of open ice holes indicating subcap seeps as ‘very likely’ or ‘maybe’ at each site according to the number and size of holes observed, their morphology, clustering and distribution, and the overall ice conditions on lakes. Ground-truth expeditions were conducted in concert with aerial-survey flights (Table 2: North Slope surveys supported in large part by this project; southern Alaska surveys supported by other projects). Of the 290 sites for which we initially observed seep-size open water holes, 77 sites were classified as ‘very likely’ containing subcap seeps and were the basis of our emission estimates. We ground-truthed 50 of the 77 ‘very likely’ sites, including Lake Q, and confirmed that subcap seeps were present at all of these sites based on observations of high ebullition ( $>10 \text{ L seep}^{-1} \text{ d}^{-1}$  on 72 measured seeps) and isotopic and geochemical gas composition (Figure 9). At individual subcap seep sites we counted the number of bubble streams (seeps) per open hole and measured fluxes in replicated holes to statistically estimate the number of ‘macroseeps’ and their cumulative flux per site. For sites where we counted open holes but did not measure flux, we applied the mean fluxes measured at nearby sites.

**Table 2. Dates of aerial surveys and ground truth field campaigns for subcap seeps, supported by this project (North Slope) and other projects. From Walter Anthony et al. (2012).**

Region	Aerial Survey	Field work
North Slope Alaska		July 2007
		January 2008
		April 2008
	October 2008	October 2008
		May 2009
	October 2009	October 2009
		March 2010
		July 2010
Brooks Range Alaska	October 2009	-
	February 2010	February 2010
		September 2010
		April 2011
Interior Alaska	October 2009	-
	February 2010	February 2010
		April 2010
	October 2010	October 2010
	November 2010	November 2010
		April 2011
Southcentral Alaska	February 2009	February 2009
		August 2009
	January 2010	January 2010
	February 2010	February 2010
		April 2010
		May 2010
		June 2010

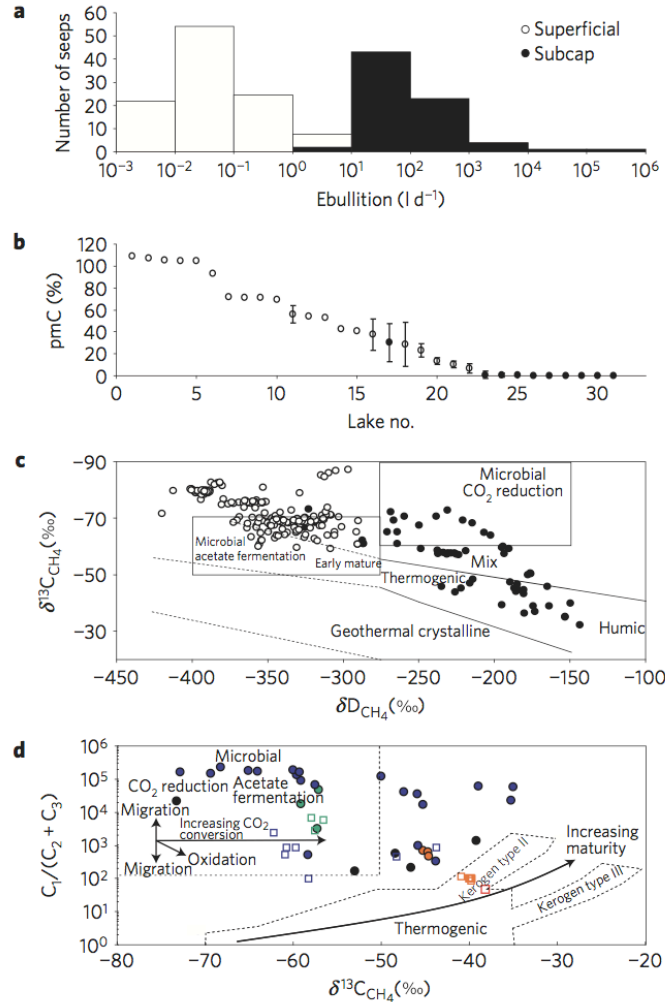


**Figure 8. Map of Alaska seeps, aerial flight path, study regions, lakes, yedoma deposits and hydrocarbon basins. Yellow dots, representing 77 subcap seep sites identified across Alaska in this study, and green dots (superficial study lakes, panel a) are scaled by the magnitude of methane flux ( $\text{kg CH}_4 \text{ site}^{-1} \text{ d}^{-1}$ ) at each site. Black dashed lines show sections of the flight path omitted from analysis due to fog. Additional information is provided in *Walter Anthony et al.* [2012].**



To analyze subcap macroseep emissions by latitude, we divided our Alaska north-south flight survey transect into 25 latitudinal bins (50 km in N-S direction and 1 km left and right of the flight transect) and used the intersect tool in ArcGIS 9.3 to determine the total land surface area, lake area, and number of lakes surveyed within each bin. Following the EMEP-EEA Guidelines (2009), we converted our point-source emissions into an areal extent by aggregating the observed point-source emissions within each latitudinal bin and dividing by the area surveyed within each bin.

**Figure 9. Distinctions between seep types based on bubbling rates and isotope compositions.** Alaska subcap ebullition seeps (solid symbols) were distinct from superficial seeps (open circles and bars) based on (a) vigorous rates of bubbling; (b) predominately fossil radiocarbon ages [percent modern carbon (pmC), mean  $\pm$  SE of 1-12 seeps per lake]; and (c) enriched stable isotope values originating from thermogenic and microbial hydrocarbon reservoirs or buried glacial organics. In (d)  $\delta^{13}\text{C}$ -methane and  $\text{C}_1/(\text{C}_2+\text{C}_3)$  ratios in subcap seeps (solid circles) were similar to those in nearby gas wells (open squares) in South Central Alaska (Cook Inlet, blue) and Northern Alaska near the Meade River (green, Burruss et al. 2003) and Walakpa (orange). [From Walter Anthony et al. 2012].





We derived a first-order estimate of subcap macroseep emissions in Alaska ( $0.08 \pm 0.1$  Tg methane  $\text{yr}^{-1}$ ) following the scaling guidelines for point-source emissions. We assumed that the point-source macroseeps observed along the flight surveys in each of the Northern Alaska continuous permafrost region ( $3,562,800$  kg methane  $\text{yr}^{-1}$  for  $793$   $\text{km}^2$  of lakes surveyed), the Interior Alaska region ( $6,951$  kg methane  $\text{yr}^{-1}$  for  $38$   $\text{km}^2$  of lakes surveyed), and the previously glaciated South Central Alaska region ( $168,931$  kg methane  $\text{yr}^{-1}$  for  $169$   $\text{km}^2$  of lakes surveyed) were a representative sample of subcap seeps for all lakes in these zones across the rest of Alaska. We quantified the uncertainty of the emission value by propagating errors of the estimates of number of seeps per site and seep flux (kg methane seep $^{-1}$  d $^{-1}$ ) for all measured and estimated sites in the three Alaska study regions at the 95% confidence limits. Additionally, we observed 103-104 ebullition ‘miniseeps’ at each of eight subcap sites visited in summer. Miniseeps were isotopically similar to macroseeps, but were invisible in winter due to lower bubbling rates. We quantified miniseepage based on measured miniseep densities and ebullition rates at three sites. To scale up subcap emissions to the state of Alaska, we assumed that the observed ratio of miniseep-to-macroseep fluxes ( $2.0 \pm 0.4$ , standard deviation) applies to all Alaska macroseep sites.

We estimated the potential magnitude of present day subcap methane emissions from pan-arctic lakes overlying assumed natural gas fields in the continuous permafrost zone north of  $\sim 60^\circ\text{N}$  based on the U.S. Geological Survey’s Circum-Arctic Resource Appraisal. Our first-order estimate of  $0.7 \pm 0.1$  Tg methane  $\text{yr}^{-1}$  for macroseep subcap emissions is the product of the emission factor observed along our survey flight path in the northern Alaska continuous permafrost zone and the area of large pan-arctic lakes overlying assumed natural gas fields ( $150,000$   $\text{km}^2$ ). Additional subcap emissions in the pan-Arctic associated with permafrost degradation south of  $60^\circ\text{N}$  and with wastage of glaciers and ice sheets were not assessed, but would further increase the pan-arctic emission estimate.

To investigate the detailed sediment biogeochemistry of TKL emitting methane we conducted biogeochemical analyses of sediment cores taken from TKL (Tables 3).

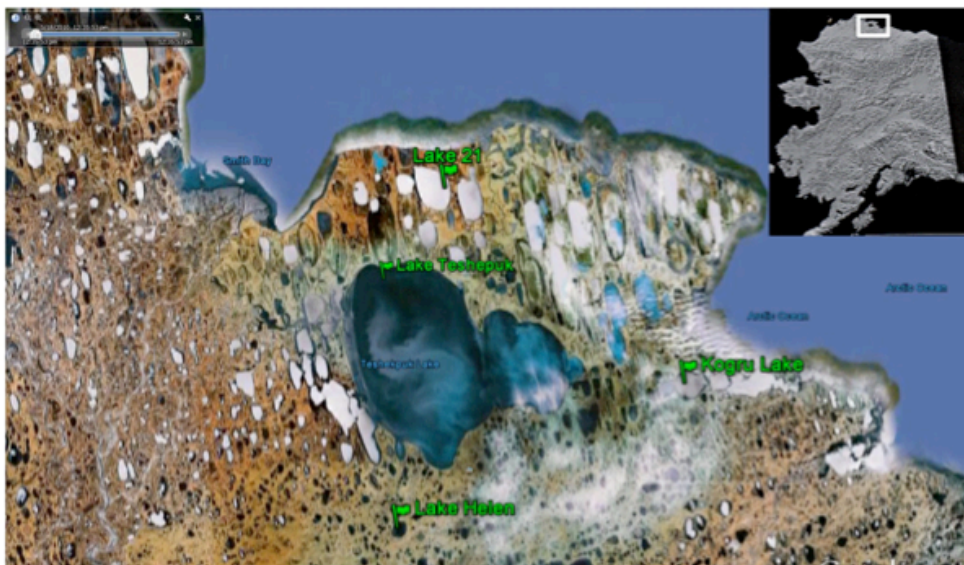
**Table 3. Core locations for sediment biogeochemistry studies.**

Core Site Name	Coordinates	Location	Date Cored
Seep Core	N70 22.669 W157 20.925	Lake Q	May and July 2009
Inside Ground Ice Core	N70 22.672 W157 20.926	Lake Q	May 2009
Outside Ground Ice Core	N70 22.691 W157 20.921	Lake Q	May 2009
BGC Core	N70 22.674 W157 20.936	Lake Q	July 2009
Camp Monica Core	N70 22.739 W157 20.861	Lake Q	May and July 2009
Worley Seep	N70 42.308 W153 44.100	Teshekpuk Lake	April 2010
Lake Helen Seep	N70 21.534 W153 39.983	Lake Helen	April 2010
Lake 21	N70 49.826 W153 28.841	Naluakruk Lake	April 2010
Kogru East	N70 33.630 W152 29.877	Lake Kogru	April 2010

Analysis of fluids and gases from pore fluids and lake water for several Alaskan North Slope (ANS) lakes was utilized to characterize the distribution of methane and infer methane sources and sinks. The most extensive coring was conducted at Lake Q during May 2009, when the lake was ice-covered, and July 2009, when the lake was ice-free. In May, a series of four gravity cores was collected at Lake Q along a 140 m transect extending from the active seep to a location identified as Camp Monica. The ‘Seep Core’ and ‘Inside Ground Ice Core’ were located within

an estimated 10 m diameter ring of open water beneath a 1.8 to 2 m ice cap. Based on multiple ice auger holes drilled around the seep, we believe the ground ice largely isolates the seep from the rest of the lake. The ‘Outside Ground Ice Core’ and ‘Camp Monica Core’ were both located outside the ground ice ring and are presumably isolated from the area of seep. In July, when the lake was free of ice, the seep site and Camp Monica were cored again. Additionally, a site of intermediate distance from the seep (‘BGC Core’) was collected in lieu of the inside and outside ice cores. To our knowledge, these include the most deeply-penetrating continuous ANS lake sediment records for both depth (5.12 m sediment depth) and time (>12,500 years before present). The lake types cored include a classic thermokarst lake with ice-rich silty substrate (Lake 21), a deep-clear lake with ice-poor aeolian sand (Lake Helen), a lake infiltrated with seawater and fine-grained marine sand (Kogru Lake), and the largest Arctic lake in Alaska and one of complex origin (Lake Teshekpuk) (Figure 10).

**Figure 10. Lake sediment core locations on the Alaskan North Slope, near Lake Teshekpuk. The white rectangle in the Alaska map inset demarcates the area of the larger map.**

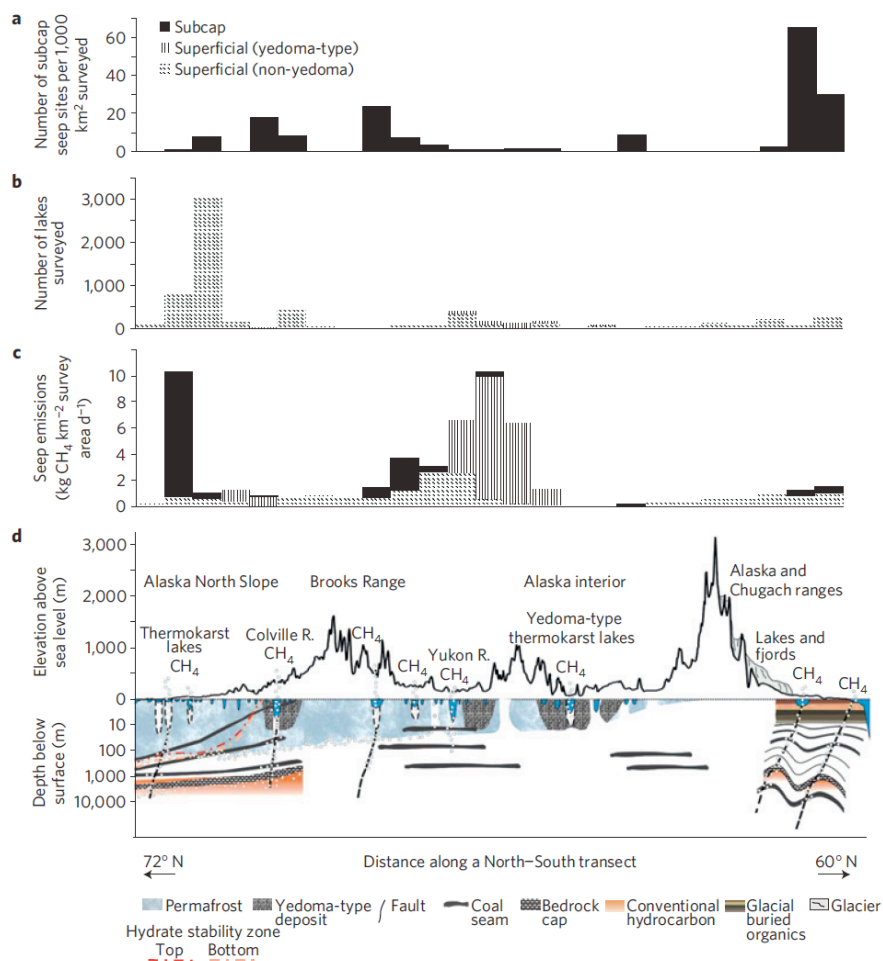


## 1.2 Results and Discussion

Subcap seeps exhibited exceedingly high ebullition rates (up to 141,600 L seep-1 d<sup>-1</sup>, Figure 9a), isotopic and geochemical signatures that frequently matched those of locally identified coalbed methane and natural gas (Figure 9b-d), and spatial clustering. Pockmarks up to 3 m diameter in bottom sediments frequently characterized subcap seep sites. Geologic seeps of similar size are known to occur on the sea floor. However, much of marine seep methane dissolves out of bubbles during their ascent through deep water and is lost to microbial oxidation in the ocean’s water column (Reeburgh 2007). In contrast, subcap seepage through relatively shallow lakes, rivers and fjord margins in Alaska escaped directly to the atmosphere with bubble methane concentrations as high as 99.5% by volume.

We conservatively treated each lake or region of a river containing one or more seep fields as a single subcap seep site, and based our analysis on ebullition macroseeps that were visually detectable during winter surveys. Survey results increased the number of previously documented geologic seep-site occurrences by state and federal agencies in Alaska 4-fold. Ninety percent of Alaska subcap seep sites occurred in sedimentary basins, but only 33% overlapped regions of known coal and conventional natural gas basins. Aerial seep surveys appear to be an excellent tool for hydrocarbon exploration.

**Figure 11. Subcap (macroseep) and superficial methane seep emissions in Alaska. In 50-km wide bins along the north-south Alaska transect, (a) the number of subcap-seep sites normalized by survey area; (b) total number of lakes surveyed; (c) methane emissions from subcap macroseeps and superficial seeps (yedoma-type and non-yedoma lakes); and a schematic cross-section (d, not to scale) of major topographic and subsurface features along the Alaska transect: permafrost distribution and thickness; examples of open and closed thaw bulbs in conjunction with faults and permeable strata providing gas migration conduits; examples of primary structural and stratigraphic gas traps beneath the secondary cryosphere cap; and potential methane sources contributing to ebullition emissions in Alaska including superficial ecosystem methane from surface lake and taberal (thawed permafrost) sediments and five subcap sources: microbial methane in buried glacial sediments, coalbed methane (biogenic or thermogenic), thermogenic methane from deep conventional hydrocarbons; and possibly methane derived from hydrate dissociation. [From Walter Anthony et al. 2012].**



### 1.2.1 Geologic subcap seeps geospatially related to cryosphere disintegration

Hydrocarbon seepage worldwide is a function of the occurrence of pressurized fluid reservoirs and permeability of the overlying rocks. Outside of the ice-rich cryosphere, natural gas and coalbed methane escaping from primary structural and stratigraphic traps migrates to the surface through permeable strata, open joints, and activated faults and fissures. In Alaska and across the pan-Arctic, researchers have demonstrated that massive glacial ice and permafrost with ice-filled pore space serve as an additional impermeable confining layer that restricts gas flow and impedes, slows, or focuses gas migration to the surface. Models predict that the disintegration of the cryosphere cap would lead to transient release of gas trapped beneath and within permafrost or through faults, joints and fractures previously sealed by ice, hydrates or the normal stress of glacial ice overburden (Formolo et al., 2008, Grassmann et al., 2010). We used geospatial analysis to test hypotheses about geologic methane release specific to Northern and Interior Alaska, two regions distinct according to the character of the cryosphere cap.

Northern Alaska (Figure 11b) represents a type of cryosphere cap where geologic methane reservoirs are sealed long-term by thick continuous permafrost. Warming of permafrost and melting of ground ice during the formation of deep or open thaw bulbs beneath old lakes, large rivers, and high-discharge springs substantially increases permafrost permeability locally. For this region we hypothesized that sites with subcap seeps should be disproportionately associated with low-ground ice content and fluvial deposits, substrate characteristics most likely to enhance thaw-bulb formation and permeability.

Interior Alaska (Figure 11b) is characterized by a cryosphere cap that degraded from thinner, but continuous permafrost during the Late Pleistocene glacial period to a strongly disintegrated discontinuous to isolated permafrost today. Geologic seeps are more likely to occur in association with neotectonic activity unrelated to cryosphere dynamics, with site-specific geological controls similar to those of regions outside the Arctic.

Geospatial analysis confirmed our first hypothesis. In the ice-rich continuous permafrost zone of Northern Alaska, subcap seeps sites were disproportionately located in isolated areas of low-ice content and fluvial deposits beneath deep lakes or near rivers (Table 4), features that together suggest steep thaw gradients.

Examples include numerous seep fields identified in lakes in the vicinities of known coal and natural gas deposits in Northern Alaska adjacent to the Meade River, in the drainages of the Brooks Range, and along the upper Colville River where recent geophysical investigation determined a deep or through-going thaw bulb. The relationship of subcap seeps to fluvial deposits was stronger in the northern continuous permafrost region than in the rest of Alaska, possibly because there are additional potential escape routes for gas, such as surface faults and unfrozen, unconsolidated sediments in the Interior and Southcentral regions. Relative to the North, we found a paucity of geologic subcap seeps in Interior Alaska except along the boundary of continuous-discontinuous permafrost (Figure 11).

### 1.2.2 Upscaling superficial (ecological) and subcap (geologic) ebullition

Both subcap seeps and some superficial seeps (e.g., those in yedoma-type lakes) release  $^{14}\text{C}$ -depleted methane to the atmosphere (Figure 9). While the isotope geochemistry of all superficial seeps showed clear microbial origin (Figure 9), that of the subcap seeps varied. The majority of subcap seeps emitted  $^{14}\text{C}$ -dead methane. Their stable isotope and geochemical signatures were consistent with microbially-produced coalbed or thermogenic methane observed in nearby deep gas wells (Figure 9) and in hydrocarbon reservoirs common throughout Alaska.

First-order extrapolation of geospatial seep relationships across Alaska for superficial seeps ( $0.75 \pm 0.12 \text{ Tg methane yr}^{-1}$ ), subcap macroseeps ( $0.08 \pm 0.01 \text{ Tg methane yr}^{-1}$ ) and miniseeps ( $0.17 \pm 0.03 \text{ Tg methane yr}^{-1}$ ), and other potential non-subcap geologic microseepage from unfrozen soils overlying hydrocarbon-prone sedimentary basins ( $0.5\text{-}1.1 \text{ Tg methane yr}^{-1}$ ), results in an estimate of  $1.5\text{-}2 \text{ Tg methane yr}^{-1}$ . Our extrapolation increases the current estimate of Alaska's natural methane emissions ( $3 \text{ Tg methane yr}^{-1}$ ) to the atmosphere by 50-70%.

A conservative first order extrapolation based on geospatial relationships observed in the Northern Alaska continuous permafrost region, would place the magnitude of subcap macroseep ( $0.7 \pm 0.1 \text{ Tg methane yr}^{-1}$ ) and miniseep ( $1.4 \pm 0.3 \text{ Tg methane yr}^{-1}$ ) emissions from lakes in the natural gas-rich region of the terrestrial Arctic north of  $60^\circ \text{ N}$  at  $\sim 2 \text{ Tg methane yr}^{-1}$ . Emissions associated with glacier and ice sheet wastage are not included in this estimate, but are an additional source of atmospheric methane in the pan-Arctic. In permafrost regions, disintegration of permafrost removes the ice seal from pre-existing faults and from unconsolidated sediments, also creating conduits through the lithosphere that allow gas previously trapped by permafrost to escape to the atmosphere. Accordingly, pan-arctic regions are a special place for gas seepage due to past and ongoing cryosphere disintegration. This may explain why our subcap seep emission estimate ( $\sim 2 \text{ Tg methane yr}^{-1}$ ) is relatively large in comparison with the global geologic seep emission estimates ( $\sim 3\text{-}4 \text{ Tg methane yr}^{-1}$ ).

**Table 4. The occurrence of subcap seep sites in relation to permafrost ice content and soil texture in the Northern Alaska continuous permafrost region.**

		<b>A</b>		<b>B</b>			<b>C</b>		
		Number of Seeps	Percent	Number of lakes	Percent	Seep ratio	Lake area ( $\text{km}^2$ )	Percent	Seep ratio
Permafrost ice content	Low	16	55%	33,014	31%	1.8	4,547	35%	1.6
	Moderate	5	17%	45,113	42%	0.4	5,617	43%	0.4
	Variable	5	17%	9,314	9%	2.0	702	5%	3.2
	High	3	10%	19,523	18%	0.6	2,259	17%	0.6
Texture	Rocky	10	34%	17,328	16%	2.1	1,188	9%	3.8
	Sandy	16	55%	63,004	59%	0.9	8,892	68%	0.8
	Silty	3	10%	26,632	25%	0.4	3,044	23%	0.4

Notes: The Seep Ratio is the ratio of the fraction of seeps located within a specific permafrost-ice or soil texture class to the fraction of randomly selected lakes occurring in these permafrost soil classes. High seep ratios between seep sites (a) and both the number of randomly selected lakes (b) and their area (c) revealed that seeps occurred disproportionately in the low and variable ice classes, and in the coarsest sediment texture class (rocky). These findings support our hypothesis for the North Slope, in that seeps did not occur evenly across all permafrost types, but were disproportionately located in permafrost types indicative of higher permeability for gas flow (e.g. low ground ice content and coarse, fluvial sediments). It is possible that gas migration through fractured bedrock, faults or fractures intersected by extant or relict thaw bulbs, unfrozen saline horizons, or fine-grained sediments with a high unfrozen water content could account for the occurrences of rarer seeps located in lakes situated in other permafrost soil types. [From Walter Anthony et al. 2012].



**Table 5. Comparison of seep association with fluvial deposits among the three Alaska study regions.**

Region	1000 lakes	Seep sites
Northern Alaska continuous permafrost	22%	70%
Interior Alaska	41%	50%
Southcentral Alaska previously glaciated	23%	51%

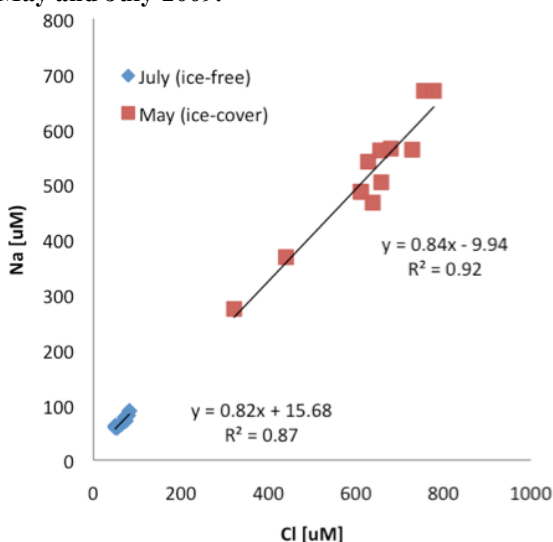
Notes: Northern Alaska continuous permafrost, Interior Alaska, and the previously glaciated Southcentral Alaska region. Percentages reflect the fraction of subcap seep sites or the fraction of 1000 randomly selected lakes that occurred within 3 km of mapped fluvial deposits, a distance that takes into account the mapping inaccuracy for fluvial deposits. Within each of the regions, percentages of seep sites within 3 km of fluvial deposits were greater than the percentages of a random selection of lakes in the regions. The relationship between subcap seeps and fluvial deposits was strongest in the Northern Alaska continuous permafrost region. [From Walter Anthony et al. 2012].

Since our geospatial and geochemical field data support the hypothesis that cryosphere degradation leads to the release of  $^{14}\text{C}$ -depleted methane previously trapped by the cryosphere, an extension can be made to this hypothesis that in a warmer world, thawing permafrost and wastage of glaciers and ice sheets could lead to a significant transitional degassing of subcap methane. Deep permafrost thaw is projected to occur over centuries to millennia. However, already ongoing permafrost warming

leading to higher unfrozen water content, intensification of surface water and subpermafrost groundwater exchange, expansion of existing taliks, and formation of new taliks may increase permeability to gas flow locally on shorter time scales. It is possible that methane oxidation processes could temper future subcap emissions, but at the very least, an injection of methane carbon due to cryosphere degradation will increase surface carbon cycling.

### 1.2.3 Gas and aqueous chemistry

**Figure 12. Crossplot of sodium (Na) and chloride (Cl) concentrations from Lake Q and surrounding lakes in May and July 2009.**



A defining feature of the Lake Q aqueous chemistry is the seasonal shift in dissolved oxygen (DO) saturation and temperature. During ice-free summer conditions, the water temperature is  $17 \pm 0.3\text{ }^{\circ}\text{C}$  and the water is fully saturated with oxygen ( $100 \pm 1.9\%$ ). By contrast, during ice-covered winter-like conditions, the average temperature is  $0.0 \pm 0.2\text{ }^{\circ}\text{C}$  and the DO saturation is  $1.3 \pm 1\%$ . pH is fairly constant during ice-cover and ice-free conditions. Low DO during ice cover is a result of biological activity in the lake water and sediments and limited gas exchange between the lake and atmosphere as a result of ice-cover. Limited oxygen availability has implications for the biogeochemical processes that are possible

in the water column and sediments. Oxygen is required to aerobically oxidize methane in the water column and seasonal shifts in the lake water could alter redox conditions in the sediments where methane is either generated (anaerobically) or consumed (aerobically and aerobically). Dissolved ion concentrations for Lake Q were substantially greater in ice-covered May than ice-free July, a trend that indicates ion concentration due to ice (or brine) formation.

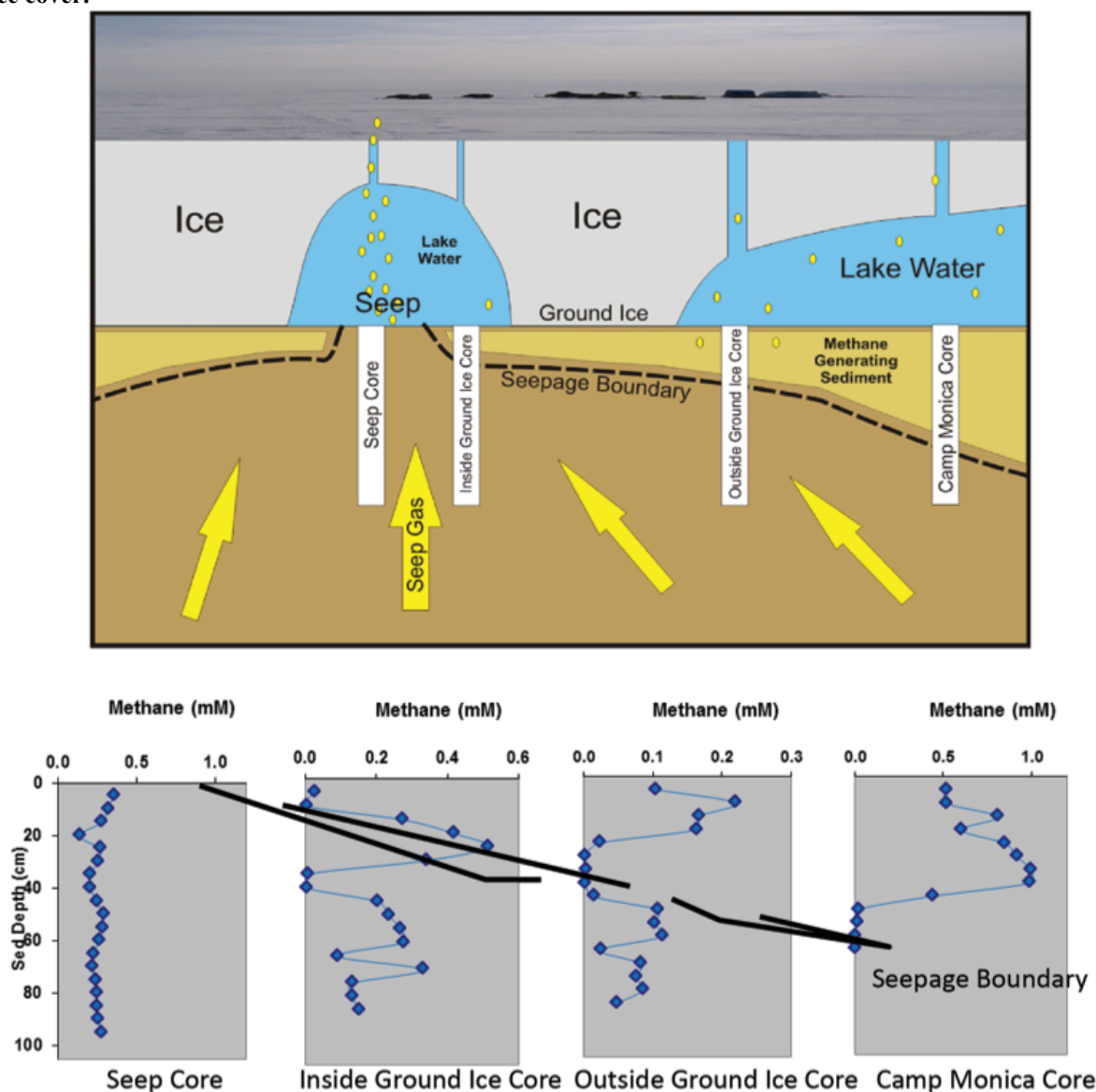
A concentration crossplot of the conservative (non-reactive) ions sodium (Na) and chloride (Cl) illustrates the relationship between the dissolved ion data from both seasons (Figure 12). For the May and July data, the relationship is significantly correlated ( $r^2 = 0.92$ ) and has a slope (0.84) identical to seawater. The May data reflect varying degrees of ice formation and suggest pockets of residual fluid are isolated by extensive ground ice formation. The seawater Na/Cl ratio of 0.85 (slope of the linear regressions) suggests a seawater origin for these ions. Assuming ice formation fully excludes sodium and chloride, the fraction of water lock-up as ice ranges from 91 to 75%, depending in the location and/or the ion used to calculate the fraction of FW residue.

#### 1.2.4 Sediment methane distribution

Sediment methane data from ice-covered Lake Q (May 2009) indicate two methane pools in the lake sediments (Figure 13). The ‘Seep Core’ contained methane throughout the core, indicating a single, deeper gas source at the seep. The remaining cores each contained a subsurface methane minimum (heavy line in bottom panel of Figure 13) ranging from ~30-65 cm below the lake bed that becomes progressively deeper with increasing distance from the seep. The methane minimum is overlain by sediments containing methane with dissolved concentrations ranging from 0.23 to 1.0 mM and underlain by sediments with methane concentrations ranging from 0.08 to 0.26 mM. The methane minimum is described as the ‘seepage boundary’ (Figure 13) because it may represent the boundary between deeper gas source sustaining the seep and shallow gas source supported by degradation of near-surface sediment organic matter (i.e., ‘methane generating sediment’ in Figure 13).

In July 2009, core recovery from Lake Q was less than May. Deeper core penetration was easier from hard ice in May than from the floating coring platform used in July. Thus, the maximum depths from which data are reported from July are shallower than May. With the exception of the nearest lake-bed sediments (<10 cm sediment depth), methane concentrations at the seep were relatively high throughout the core (Figure 14). By contrast methane concentrations were low throughout the near-seep core (‘BGC Core’). At ‘Camp Monica’ core site, where methane concentrations were relatively high to a depth of 40 cm sediment depth in ice-covered May 2009, the near-lake bed methane concentrations were low and increased gradually to 0.8 mM at 19 cm sediment depth.

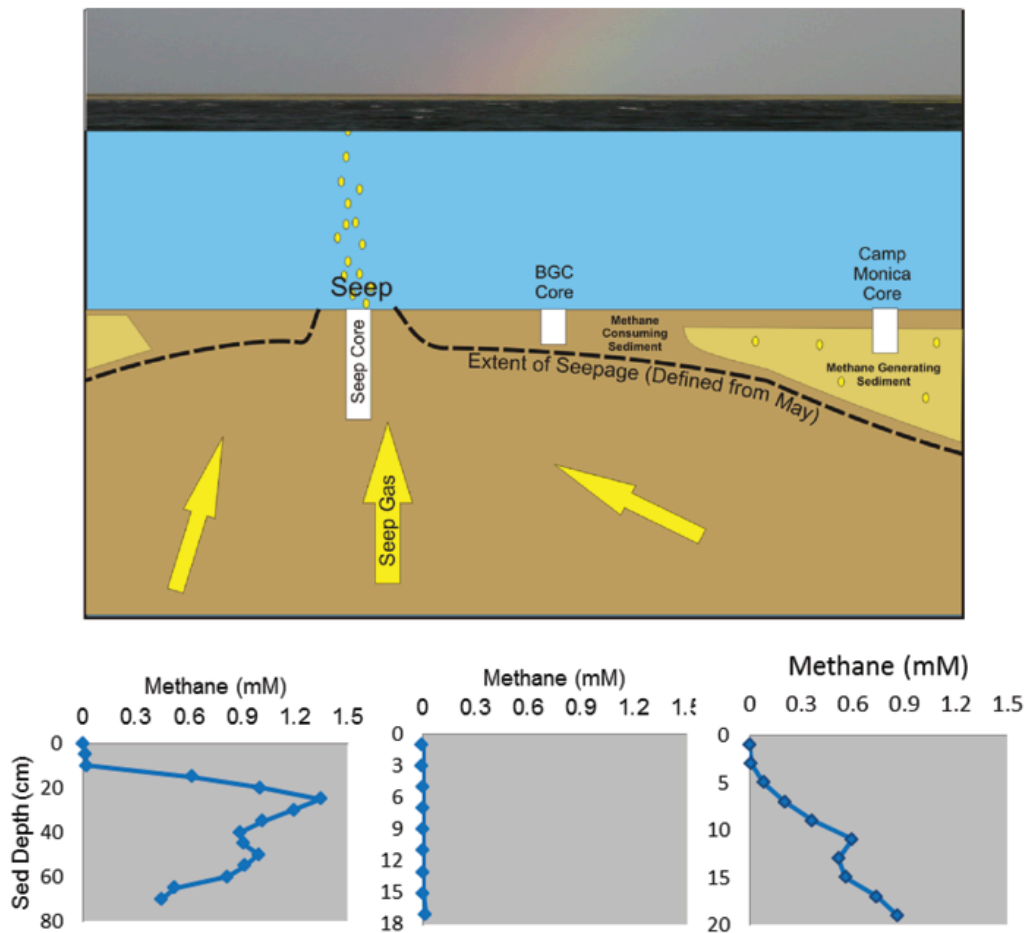
Figure 13. Methane concentration profiles from May 2009 sediment cores from Lake Q (lower panels). The upper panel is a conceptual diagram for factors controlling the sediment methane distribution during ice cover.



Because the water temperature was warmer in July than May, enhanced biological activity that would make conditions more amenable to sedimentary anaerobic methanogenesis might be expected. However, the exceptionally low DO saturation observed in May apparently created more extensive methane generating conditions in the near lake-bed sediments in May (Figure 13) than July (Figure 14). Thus, the occurrence of methane generating sediments was deeper in July such that methane was not observed in the BGC core and accumulated at greater depth in the 'Camp Monica Core.' Core penetration in July was not sufficient to reach the deeper gas reservoir. Its presence in Figure 13 is based on the position defined from the May campaign (see Figure 13).



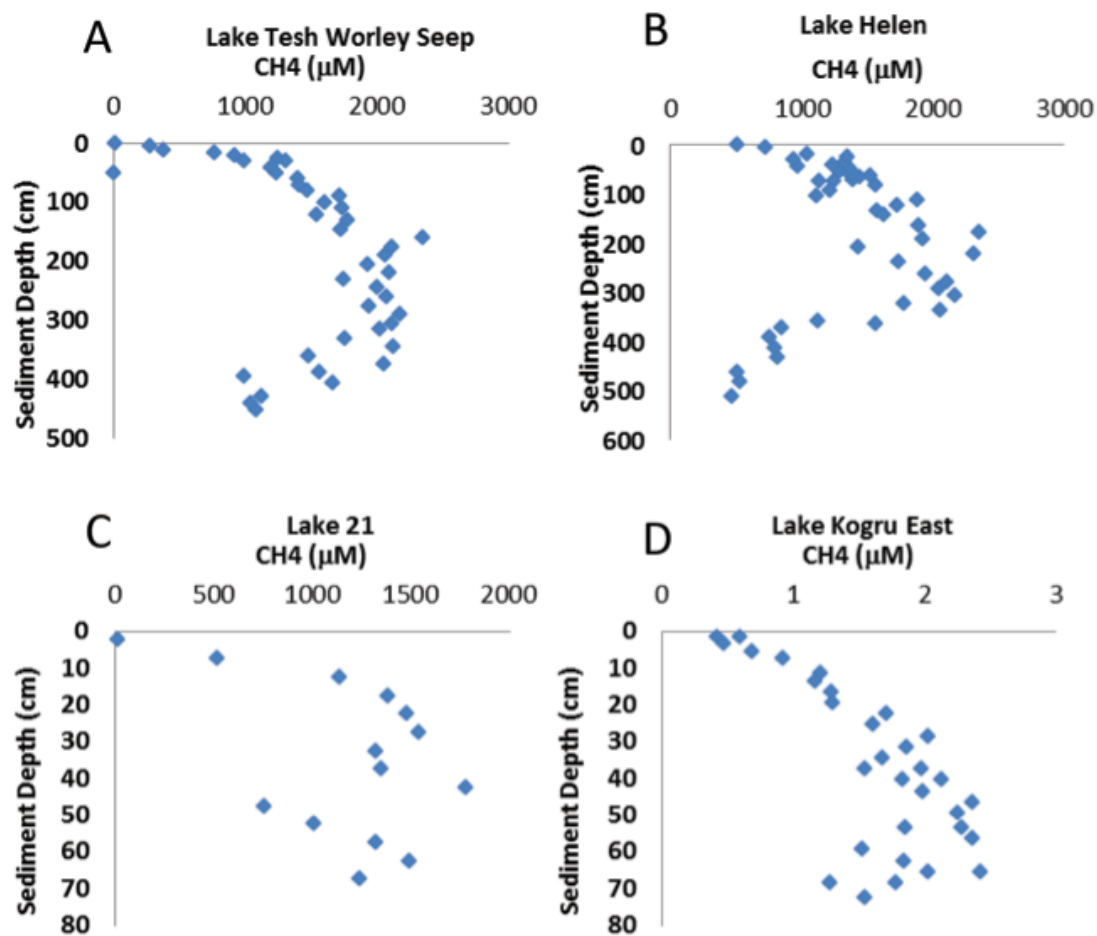
Figure 14. Methane concentration profiles from July 2009 sediment cores from Lake Q (lower panels). The upper panel is a conceptual diagram for factors controlling the sediment methane distribution during ice-free conditions.



Coring at Lake Teshekpuk and smaller surrounding lakes with a Livingston corer allowed us to recover longer intact cores and more easily isolate methane samples in the field. As a result, the sample depths and density are significantly greater than the Lake Q cores. Forty-four samples were collected from a 453 cm core recovered from Lake Teshekpuk.

Methane concentrations increased gradually from the surface to a maximum concentration of 2.4 mM at 161 cm sediment depth. Concentrations decreased gradually to 1.1 mM at the base of the core. The mid-core maximum is consistent with a source of methane at that depth. A similar trend was observed in the 512 cm (46 sample) core from Lake Helen (Figure 15b). The mid-core maximum concentration was 2.4 mM at 177 cm sediment depth. The cores from Lake 21 (Figure 15c) and Lake Kogru (Figure 15d) were shorter, but each also had a mid-core concentration maximum within the extent of the core. The mid-core maximum concentration from the Lake Kogru East core (~2.2 mM) was approximately 3-orders of magnitude less than the mid-core maximum from other three sites. Additional work is being conducted on these cores to determine the origins of the gases and to identify the processes controlling methane production and consumption within these cores.

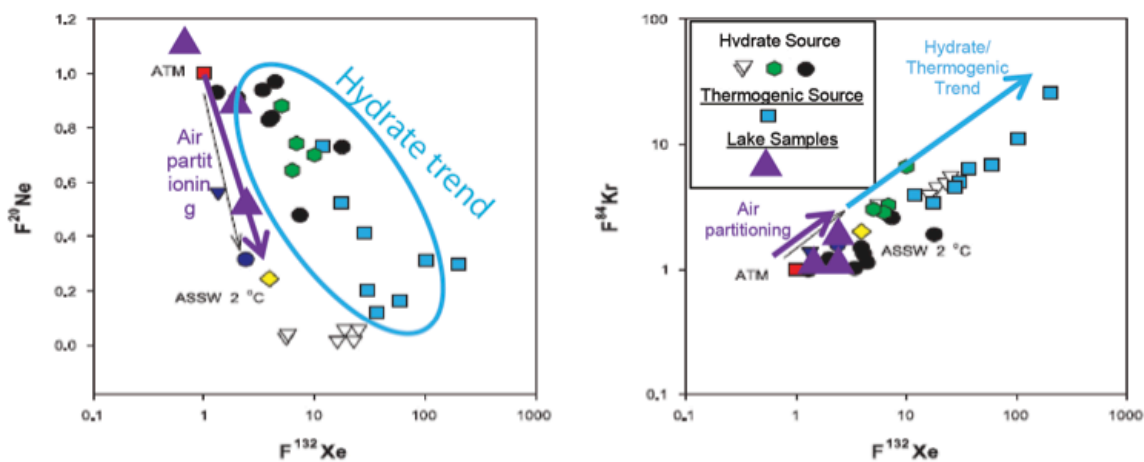
Figure 15. Sediment methane concentration profiles from A) Lake Teshekpuk, B) Lake Helen, C) Lake 21, and D) Lake Kogru.



### 1.2.5 Noble Gas Fingerprinting of Seep Gases

Mass fractionation patterns of noble gases (He, Ne, Ar, Kr and Xe) resulting from gas hydrate formation and dissociation may be useful for differentiating gas hydrate-derived gases from other reservoirs (e.g., petroleum reservoirs and microbial methane). Through funding from this project and other DOE sources, USGS scientists conducted a series of experiments to describe noble gas systematics during gas hydrate formation, storage and dissociation. Three gas samples from the active seep at Lake Q were analyzed to determine if the gas originated from dissociating gas hydrate. Data from those samples are plotted as noble gas ratios of  $^{20}\text{Ne}$ ,  $^{132}\text{Xe}$  and  $^{84}\text{Kr}$  relative to  $^{36}\text{Ar}$  in the sample and normalized to atmospheric values (expressed as ‘F’ values in Figure 16). Higher ‘F’ values indicate a greater relative contribution from the respective noble gas. Included in the plots are ‘F’ ratios of other gas samples collected from gas hydrate and thermogenic sources, the atmosphere, and air saturated seawater. Hydrate and thermogenic sources are frequently enriched with noble gases; in particular,  $^{132}\text{Xe}$  and  $^{84}\text{Kr}$  (Figure 16). The gas samples from Lake Q do not show any enrichment in either of these gases, suggesting the gas are not derived from gas hydrate or a petroleum system. The  $\delta^{13}\text{C}$  of seep methane ( $-58\text{‰}$ ) is consistent with a slightly degraded microbial source, which could be derived from degradation of thawed permafrost or coal beds, both of which are known to occur in this area. However, an absence of elevated  $^{84}\text{Kr}$  or  $^{132}\text{Xe}$  that has been shown to be released during coal biodegradation suggests a microbial source derived from thawed permafrost or modern organic matter.

**Figure 16. Noble gas ratio crossplots of Ne, Kr and Xe, expressed as ‘F’ values. Purple triangles are the samples from Lake Q. The other symbols represent atmospheric (ATM), air saturated seawater (ASSW) and samples from gas hydrate and thermogenic sources. The absence of noble gas enrichment in the Lake Q samples is inconsistent with a gas hydrate derived source.**



### 1.3 Conclusions

We showed that ecological seeps are more common in Alaska and they account for a larger source of atmospheric methane today than geologic subcap seeps. Cryosphere-cap methane seeps were larger on an individual seep basis, and occurred along steep thaw gradients in permafrost. The geospatial association of these seeps with cryosphere boundaries in suggests that if this

relationship holds true for other regions in the Arctic where sedimentary basins are currently capped by permafrost, glaciers and ice sheets, such as northern West Siberia, rich in natural gas and partially underlain by thin permafrost predicted to degrade substantially by 2100, emissions from the geologic source could increase with potential implications for climate warming feedbacks.

The novel aerial survey approach used by this project helped to increase the number of previously documented geologic methane seeps in Alaska by nearly 400%. Since the majority of geologic seeps discovered through this effort were located outside of mapped coal and conventional natural gas basins it is reasonable to conclude that the occurrence of subsurface hydrocarbon reservoirs in Alaska may be more common than previously thought. These findings imply that future research could focus on exploration and assessment for potential development of hydrocarbons underlying the newly mapped geologic methane seeps.

Shallow thaw lakes experience radical seasonal shifts in ice cover and temperature. Ice cover inhibits oxygen exchange, creating anaerobic conditions in the water column and sediments where complex biogeochemical cycles linked to methane production and consumption are active. Biological oxidation under anaerobic conditions requires electron acceptors other than oxygen; some of which are concentrated by the formation of brines when the ice forms. These alternate processes support seasonally-distinct consumption and production biologically-relevant compounds. The combined effects of temperature, ice-volume and other lithological factors linked to seepage from the lake are manifest in the distribution of sedimentary methane in Lake Q during ice-covered and ice-free conditions. Sediment cores from Lake Teshekpuk and surrounding lakes displayed systematic profiles that we hypothesize are controlled by the age and content of the underlying organic matter as well as the seasonal effects from ice-cover and temperature.

## 2 Geophysical Surveys of Thermokarst Lakes

To support a multidisciplinary understanding of methane dynamics in TKL, the USGS conducted some of the first multi-sensory geophysical surveys in these settings during field research in 2009 and 2010. Using a combination of subbottom profiling, ground penetrating radar, towed DC resistivity, and water column imaging, the surveys were designed to reveal shallow sedimentary structure, the distribution of gas-charged sediments, the nature of gas flow pathways in the sediments, water column gas plumes, and, if possible, constraints on thaw bulb morphology. As a practical matter, the geophysical data were the best way to efficiently produce accurate bathymetric maps for some of the lakes and provided important information about the lake-bottom distribution of various sedimentary deposits and the morphology of pockmark features. Water column imaging was helpful for identifying gas plumes in locations where the gas bubbles did not obviously break the water's surface. Initially, it was also hoped that some of the geophysical data might be correlated with lithologic interpretations in shallow cores.

## 2.1 Materials and Methods

### 2.1.1 Equipment

This section reviews the instrumentation deployed in one or more of the TKL that was surveyed by the USGS as part of this project.

**Chirp subbottom profiling:** Motivated by results obtained in a Siberian lake, Chirp seismic data acquisition was considered one of the best tools to potentially image the thaw bulb. Chirp data quality is notoriously dependent on the type of sediments, and the thick loess sediments of Siberia are particularly well-suited to Chirp imaging.

Subbottom profiling was carried out in all of the lakes (Lake Q, Lake Teshekpuk, and Lakes Smith and Killarney near Fairbanks) using an Edgetech 424 towed ‘fish’ (Figure 17) with 4-24 kHz sweep and a small-footprint topside system acquired especially for remote-region research. The fish was modified for this project: Weights were removed, and USGS operations staff rigged flotation to keep the bird at the surface during work in very shallow waters. One drawback of this configuration was degradation of data quality and cavitation during rough water conditions. It is always preferable to run the fish beneath the water’s surface where possible. Power for the Chirp system was supplied by marine batteries or by a generator, depending on the deployment. Data were recorded digitally in SEGY format (already enveloped) on a laptop computer using native Edgetech software. The SEGY headers contained the DGPS navigation. Post-cruise, data were viewed in several types of software. For Lake Q, bottom picks for mapping bathymetry were made in NRC Canada’s freeware and exported directly to ArcGIS shapefiles.

**Figure 17.** Deployment of the Chirp 424 subbottom profiling fish in Lake Teshekpuk in 2010 (left) and use of a waterproofed RTA ground penetrating radar cable in Smith Lake near Fairbanks in 2009 (right).



**Boomer subbottom profiling:** A low-energy portable boomer system deployable on a 20-foot-vessel was used in 2010 in Lake Teshekpuk, but was not used in any other lakes surveyed as part of this project. The key motivation for deployment of the boomer in Lake Teshekpuk was deep penetration that might image the substructure of this lake, which has been the subject of significant controversy over the existence of permafrost. The boomer had center frequency of

~3.5 kHz and provided high-quality imagery of the upper part of the section. However, the time window was limited to 150 ms on this system, yielding penetration of ~100 m maximum for nominal sediment velocity and water depth. Data were recorded on a single channel streamer and digitally logged on a PC in SEGY format. DGPS navigation was independently recorded.

**Ground penetrating radar (GPR):** Freshwater lakes are ideal for the deployment of GPR from either ice or as towed cables behind small vessels because freshwater is largely ‘transparent’ to radar waves, with some exceptions. In contrast to subbottom profiling, whose results depending on contrasts in the seismic response of shallow sediments when subjected to swept frequency acoustic energy, the radar response of sediments depends on their dielectric constant, which is affected by lithology, water content, pore water salinity, and other factors. For 2009 surveys, we used a Mala GPR system borrowed from Rutgers University and coupled this with a 50 kHz unshielded remote terrain antenna (RTA) sheathed in waterproof well liner (Figure 17). This is the first known deployment of an RTA cable for this application as part of a towed (open-water) marine system at the USGS and was documented in an article in the USGS Soundwaves newsletter (Ruppel et al., 2009). Besides sheathing the RTA cable, USGS operations personnel also added flotation to the cable and a drogue to assist in towing the streamer as straight as possible. In contrast to typical GPR configurations that place the transmitter and receiver antennas in parallel and move these along a transect, the RTA cable has the transmitter and receiver arrayed inline. Data were recorded on a PC in Mala’s native RD3 format, and navigational data were recorded separately in Mala-format files. For independent determination of lake bathymetry in Lake Q, a sample of the GPR data was analyzed in Mala software and transformed to SEGY for analysis in other software. Anecdotally, the GPR functioned well in the very clear waters of Lake Q and later in the waters of Lake Smith outside Fairbanks. The waters at Lake Killarney had a brownish color, and the GPR signals were highly attenuated and the data unusable, possibly due to high organic content in the waters. Due to poor weather and time constraints, the GPR system was never deployed in Lake Teshekpuk in 2010.

**Towed DC Resistivity:** The USGS Woods Hole AGI 8-node Supersting towed DC resistivity system was deployed in Lake Q in 2009 (Figure 18). DC resistivity is a well-established and very traditional geophysical method that our project deemed potentially useful for distinguishing low-resistivity lake sediments from very high resistivity underlying permafrost. More routinely, towed DC resistivity surveys are used by the USGS and others to identify areas of submarine

**Figure 18.** Towed AGI Supersting DC resistivity system on Lake Q in 2009 (left) and Humminbird display showing sidescan results and water column image on Lake Teshekpuk in 2010 (right).





groundwater discharge in estuaries. DC resistivity is an electrical method that involves injection of a current at a transmitter and recording of a voltage at a receiver. The resistivity of the intervening Earth materials is then calculated from the current and voltage. On land, modern DC resistivity surveys typically deploy dozens of electrodes, and software is used to switch through many combinations of these electrodes as sources and receivers to provide an image of the subsurface. Although land-based DC resistivity instrumentation was available at Lake Q in 2009, limited time meant that it was never deployed. In the marine setting, towed DC resistivity systems have one transmitting dipole and many receiving dipoles. This means that marine surveys are inherently less reliable since each dipole pair is not used as both a transmitter and receiver, ensuring reciprocity. The outcome of DC resistivity surveys is a pseudo-section, which maps each resistivity reading at a given pseudo-depth. Advanced inversions are required to extract meaning from raw pseudo-sections and to delineate features. DC resistivity is the static limit of electromagnetic methods, which rely on either time- or frequency-domain measurements to provide a far more complete understanding of the subsurface than DC resistivity can. DC resistivity methods should in theory serve an important function in first-order studies like this one, making it possible to quickly determine whether the permafrost is within the depth range imaged by these surveys beneath the lake. In practice, the implementation of DC resistivity methods was not straightforward.

**Water Column Imaging:** We used a Humminbird 512ci fishfinder (Figure 18) to image the water column in Lake Q and other lakes for this project. The fishfinder has a multifrequency (55 kHz, 200 kHz, 455 kHz) transducer and has undergone firmware upgrades that allow it to conduct sidescan imaging. At the time of the initial 2009 deployments, imagery of water column methane plumes was being recorded manually as screen snapshots of the incoming data. By 2010, we were able to continuously record the Humminbird imagery and replay it from sonar-style files.

### 2.1.2 Operations

Geophysical surveys in Lake Q and the lakes near Fairbanks were carried out using a 12' inflatable hard-bottom boat R/V Tundra powered by an electric motor between 8 and 13 July, 2009 under ice-free conditions (Figure 19). The choice of an inflatable vessel, christened the

**Figure 19. Boat operations for geophysical surveys in 2009 at Lake Q (left) and 2010 at Lake Teshekpuk (right).**



R/V Tundra, was dictated in part by the remoteness of Lake Q and the need to transport most equipment on the back of ATVs. Even on the lakes near Fairbanks, it was necessary to carry the boat (and all equipment) overland, making use of the small inflatable necessary. Due to the small size of this boat, geophysical surveys in 2009 were carried out sequentially with the geophysical instrumentation, starting with Chirp, followed by DC resistivity and then GPR in Lake Q. In the lakes near Fairbanks, only Chirp and GPR surveys were conducted.

In 2010, we used a 20' gas-powered open aluminum skiff (R/V Saree) that was owned by Alaska Fish and Game and transported by USGS personnel from the southern to northern end of Lake Teshekpuk (Figure 19). Using a boat already onsite was critical, since the survey location is reachable in summer only by single-engine floatplane from Deadhorse. The 2010 program was carried out between 13 and 19 July, 2010, and the ice had only gone out on the lake in the few days prior to the commencing the geophysical surveys. Most of the lake beyond a few kilometers from its northernmost shore remained ice covered during the entire week of surveys, and even leads in the ice were too treacherous to navigate with geophysical gear being towed behind the vessel. Surveys therefore concentrated on the northernmost part of the lake, where methane seeps had first been imaged in 2009 by USGS researchers and collaborators, including Ben Jones. During the Teshekpuk surveys, we simultaneously acquired Chirp and boomer data, along with Humminbird imagery. Weather conditions during most of the week were poor, and surveys could not be conducted in an open boat for more than a few hours per day. Wind and precipitation conditions were severe enough that no surveys could be conducted on some days.

## 2.2 Results and Discussion

### 2.2.1 Lake Q

The geophysical surveys completed on Lake Q are shown in Figure 20 and comprise roughly 6.3 km of subbottom profiling, 3 km of GPR, and about 5 km of DC resistivity. Some of the geophysical techniques are better at shallow imaging, and these surveys were therefore concentrated near the seep site and in areas where shallow sedimentary structure and gas distribution were to be delineated. Other geophysical techniques should theoretically be better at penetrating deeper layers and possibly detecting the edge of the thaw bulb. Those techniques were preferentially used more near the edges of the lake where the thaw bulb boundary should lie at shallow depths. The distribution of subbasins also affects the patterns of freezing and ice grounding observed in the lake in synthetic aperture radar (SAR) imagery provided by the Alaska Satellite Facility. These data were analyzed to support some of the methane oxidation rate studies carried out by UCSB in an effort to evaluate the possibility that sub-ice waters may be isolated in parts of the lake for several months during the ice-covered season. In Figure 21, the tic marks point into the areas of grounded ice, which correlate well with shallow bathymetry. The seep site lies at the boundary between grounded and floating ice and shallow and deeper bathymetry. This location may be coincidental.



**Figure 20. Tracklines for geophysical surveys at Lake Q: Subbottom profiling with the Chirp 424 system in white; GPR in red; and DC resistivity transects in green. The July 2009 cores are shown in yellow, and the seep site is marked with a blue cross.**

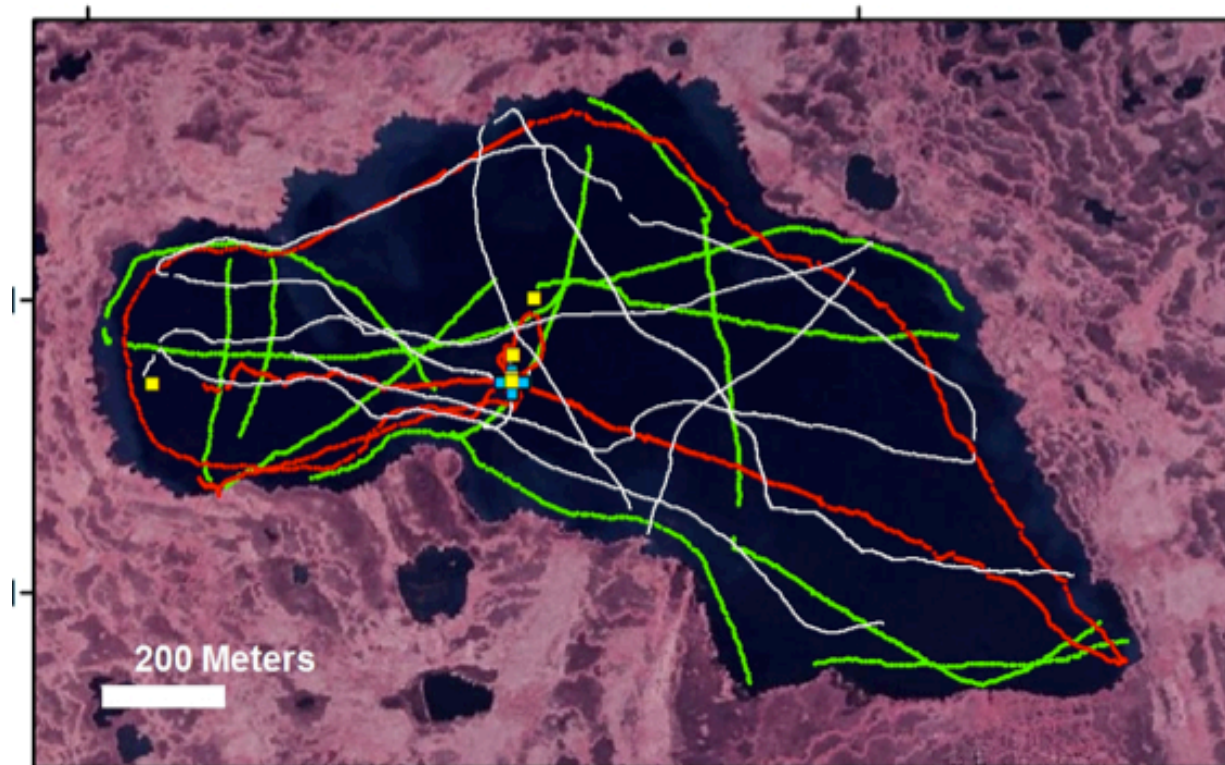
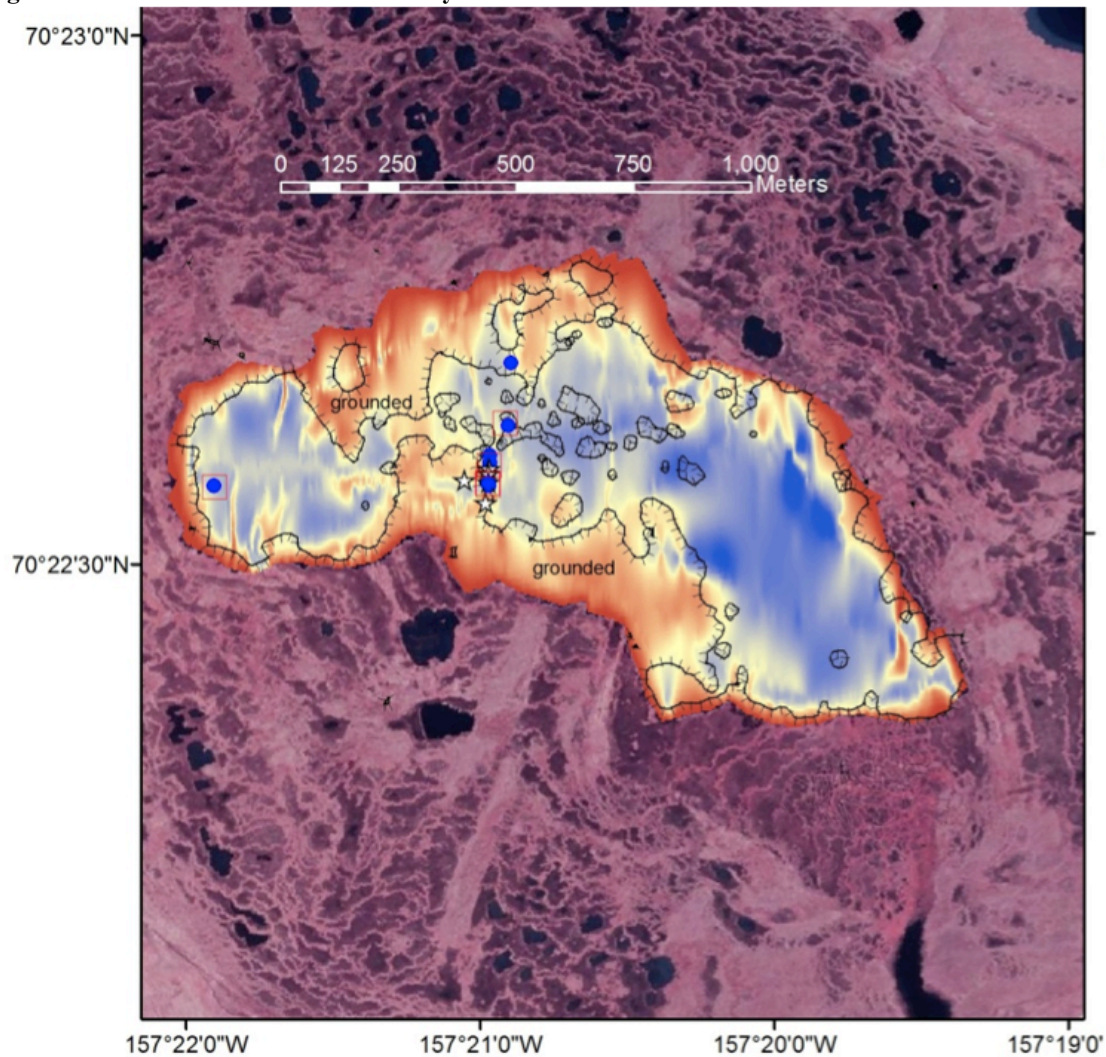


Figure 21. Bathymetry of Lake Q (red to blue shading) mapped by compiling lake bottom first arrival picks from the Chirp 424 data, automatic depth recordings collected during the DC resistivity tows, and lake bottom radar reflections from the GPR data. Standard ArcGIS routines were used to merge and grid the data, and the lake's edge as digitized from the underlying high-resolution photo-mosaic was arbitrarily set to 0 depth. Deepest blue corresponds to ~2.5 m depth. Red areas are less than half a meter deep. The seep is located at the boundary between the two main basins, where the blue circles and red squares overlap close to the star symbols. Blue circles denote locations of July 2009 cores. The area enclosed by the hatched contour bounds the limit of grounded ice (ticks face into the grounded ice) as digitized from SAR data collected in May 2010.



The combined geophysical datasets were used to construct a bathymetric map of Lake Q, one version of which is shown in Figure 21. The bathymetric map that Lake Q is divided into 2 main subbasins, with the eastern basin being further subdivided into a western and southeastern arm. These subbasins may have originated as distinct areas bound by hexagonal faults and ice wedges. Numerous TKL on ANS consist of multiple subbasins that have become flooded and joined. tend to be located at the edges of TKL, and the seep is located at the edge of the eastern subbasin. The advective action at the seep is known to be vigorous enough to transport sediment, and new sediment may be preferentially deposited to the west of the seep in the area of now-shallow bathymetry.

Taken together, the geophysical data provide new information about the Lake Q seep. The seep is associated with a well-developed pockmark about 5 to 6 m across and up to 1.5 m deep. Sediment has accumulated non-uniformly within the pockmark, whose west and south sides have shallower bathymetry than the east and north sides. Unfortunately, the geophysical data do not provide insight into the degree to which the pockmark may control sedimentation patterns. The Chirp data (Figure 22) do not reveal the details of sediment layering (i.e., gas charging masks the layered structure), and the GPR data show no apparent asymmetry in the shallow sediment drape across the pockmark.

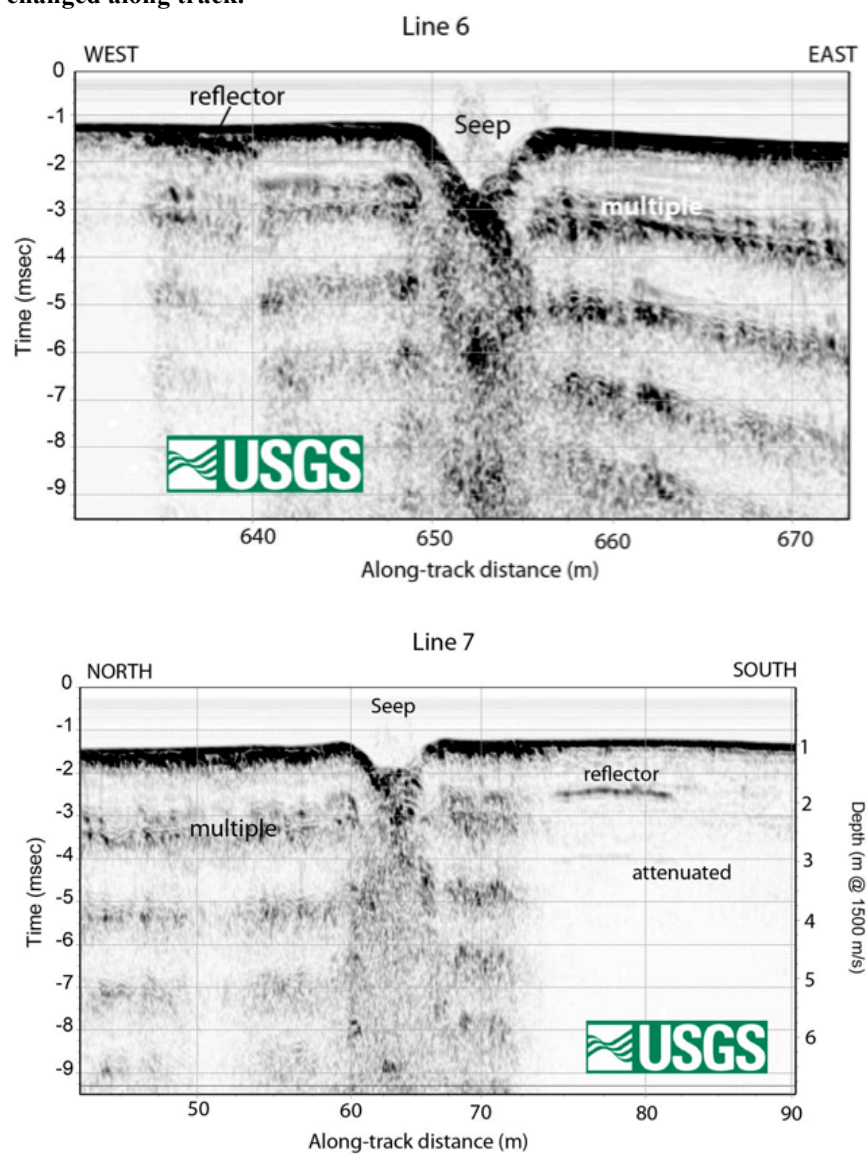
None of the data provides evidence for a deep-seated source for the gas, nor for a migratory pathway that links the seep to a deeper source. The disruption in the GPR data beneath the seep is probably attributable to the near-surface feature, not to a deeper-seated chimney structure. The Chirp data also show no evidence for structures that could be feeding the seep. Given the lateral resolution of the imaging data sets, failure to locate a clear conduit that supplies gas to the seep is not surprising.

In theory, the base of the thaw bulb at Lake Q should be marked by a significant contrast in geophysical properties between overlying thawed sediments and underlying permafrost-bearing sediments. However, the acoustic and GPR data do not constrain the thickness of the thaw bulb at this lake. This does not necessarily mean that the thaw bulb is deeper than the nominal penetration depth for Chirp or GPR data under perfect conditions, since the actual penetration of these signals is limited by the widespread of presence of shallow gas and by coarser-grained sediments in some parts of the lake. The inability of the chosen geophysical methods to determine the thaw bulb thickness did, however, lead to the decision to also deploy lower-frequency, deeper-penetrating seismic methods for the Lake Teshekpuk surveys in 2010.

Besides the challenges posed by the shallow sediments and gas beneath Lake Q, there may be other reasons that the talik was not imaged. First, the high resolution imagery around Lake Q shows that its total basin formerly occupied an area several times larger than the present extent of the lake. Thus, for the undrained Lake Q, thaw bulb edges may actually lie hundreds of meters from the current edge of the lake. The remnant thaw bulb beneath the current lake may therefore be the deepest part. Obviously, the shallower thaw bulb edges are would be easier to detect than the deepest part of the thaw bulb. Second, despite the finding of relatively coarse-grained sediments beneath parts of the lake and the proximity of Lake Q to a meander bend and sand deposits along the Meade River, the regional sediments are known to be relatively fine-grained. Frozen fine-grained sediments sometimes do not have high enough ice content to dramatically

change geophysical properties, particularly seismic properties. Further examination and integration of the geophysical data will be necessary, but it seems unlikely that this particular multisensory geophysical data set will yield substantial constraints on the thaw bulb thickness at Lake Q.

**Figure 22. Raw Chirp 424 subbottom profiling data across the Lake Q seep. Most of the reflectors below the lake bottom are multiples. Line 6 runs from west to east through the seep, and Line 7 runs from north to south, nearly perpendicular to the first line. Note that the seep is vigorous enough that Chirp frequencies (4-24 kHz) can detect the gas in the water column. Depth conversions (right axis on Line 7) are automatically made using 1500 m/s for seismic velocity, which is slightly too fast for this freshwater setting. Note the bright reflector about 8 m south of the seep at ~1 ms below the lake bottom in Line 7 and a bright reflector just beneath the surface to the west of the seep in Line 6. Distance marks along the bottom at 10 m intervals and will not be evenly distributed if the boat's speed changed along track.**

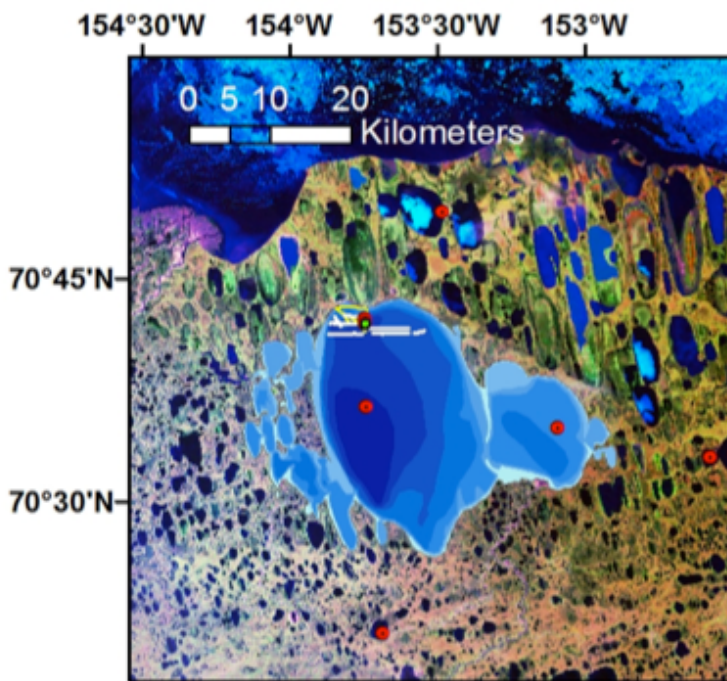




### 2.2.2 Lake Teshekpuk

As noted earlier, ice conditions meant that geophysical data could be acquired only on the very northernmost part of Lake Teshekpuk in July 2010. The map in Figure 23 shows the locations of boomer, Chirp, and Humminbird surveys in July 2010, reconnaissance Chirp surveys in 2009 (Figure 23), and the cores collected from ice by the biogeochemistry collaborators on the project in spring 2010. Boomer surveys were specifically designed to attempt deep penetration with the aim of constraining the existence of permafrost beneath the lake. Only limited high quality boomer data were collected, in part due to a storm event midway through the field effort that

**Figure 23. Lake Teshekpuk and surrounding areas. The Beaufort Sea is at the top of the image. Red circles denote cores collected for this project in April 2010. The white survey lines at the northernmost part of the lake show the geophysical transects acquired in July 2010. Reconnaissance surveys in 2009 had revealed the existence of methane seeps in this part of the lake. Bathymetry provided by Ben Jones, USGS Anchorage. In Lake Teshekpuk, the deepest colors correspond to ~8 m depth.**

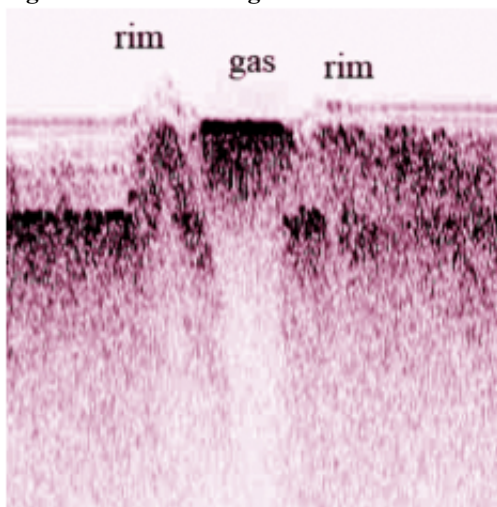


caused (literal) flooding of the electronics. While GPR equipment was available and had been ferried to the lake via floatplane, conditions were too rough to consider its deployment.

The Chirp data collected from Lake Teshekpuk provide unprecedented high resolution imaging of the shallow section in areas where the sediments were conducive to acoustic wave penetration (Figure 24). Two factors contributed to limited Chirp penetration in some locations. First, part of the northwestern most sector of the lake has fairly coarse-grained sediments that are generally not conducive to Chirp imaging. Second, nearly ubiquitous gas-charging of the shallow sediments prevents deep penetration in many locations. Figure 25 shows

one of the best Chirp transects from Lake Teshekpuk. The data show relatively laminated fine-grained sediments on lapping a sandier unit on the right. Gas is on average ~3 m below the lake bottom on the left side of the profile under the presumably low-permeability laminated sediments and rises very close to the seafloor under the shallower, higher-permeability sediments on the right side. Plumes of gas rise through the laminated sediments, and some of these contribute to the formation of lake bottom seep features.

**Figure 24. Chirp image collected with USGS Woods Hole equipment by Ben Jones (USGS Anchorage) and Chuck Worley (USGS Woods Hole) during reconnaissance in July 2009. This image shows a seafloor pockmark with well-developed rims, gas charging directly beneath the lake bottom at the seep, and gas in the water column right above the lake bottom at the pockmark. It was on the basis of imagery like this that the decision was made to pursue work in Lake Teshekpuk for Year 2 of the study. Lake Teshekpuk also had a clear advantage over the Prudhoe Bay area, where entry to the field sites would have been complicated by regulations controlling access.**



inherently frustrates attempts to achieve deep penetration and imaging of the lake bottom sediments with most acoustic-based methods, other techniques (e.g., radar and particularly DC resistivity and electromagnetic methods) deserve more study. In Lake Q, the Chirp data were limited in their capacity to image deeper sediments and did not capture the thaw bulb, in sharp contrast to the image that Schwarmborn et al. (2002) had obtained with Chirp technology in a TKL in Siberia. Despite the fact that Lake Q is set within an area of generally fine-grained sediments, the cores from Lake Q contained quite coarse-grained sediments, particularly near the seep where fine-grained sediments may have been winnowed by the advective flux of fluids. The sediment type, as well as the widespread gas charging in the shallow sediments, contributed to the poor imaging of Lake Q. The resistivity data and GPR data from Lake Q may yet yield more information about the shallow sedimentary section, but do not seem to define the thaw bulb either. As noted above, the failure to capture the thaw bulb at Lake Q may in part be related to the fact that the present day lake is a remnant of an older, larger, and now-drained lake. The edges of the thaw bulb, which are the parts closest to the surface and thus most easily detectable with geophysical methods, are likely located at the edges of the ancient lake, not the present day lake.

As noted above, it was not only the presence of methane plumes, but also the controversy over the existence of permafrost beneath the areally-extensive (but shallow) Lake Teshekpuk that made this an attractive site for 2010 research and led to the acquisition of boomer seismic data there. Earlier inferences that permafrost was lacking beneath the lake was based on interpretation of large-scale land-based refraction data collected decades' ago. However, USGS borehole data show permafrost thickness of  $> 250$  m on the eastern edge of the lake and more than 400 m on the edge of nearby Harrison Bay. The new data sets do not assist in either verifying or denying the existence of permafrost beneath the lake.

## 2.3 Conclusions

Geophysical techniques provide important insight about the distribution of shallow gas in the sediments of TKL systems and the lake bottom manifestation of seepage (e.g., pockmarks). As with any setting, the ability to image sediments with seismic techniques is a complicated function of the types of sediments (fine-grained are superior), the amount of gas (gas-free is best), acquisition conditions (e.g., sea state), and the capacity of the chosen frequencies to provide a good combination of resolution and penetration. Because gas



**Figure 25.** Example Chirp profile in Lake Teshekpuk. Shallow gas occurs nearly everywhere in these profiles. The depth conversion on the right was done automatically with 1500 m/s, which is slightly too fast for freshwater and not reliable within the sedimentary section. Uneven spacing of distance marks on the bottom indicates varying speed of the vessel.

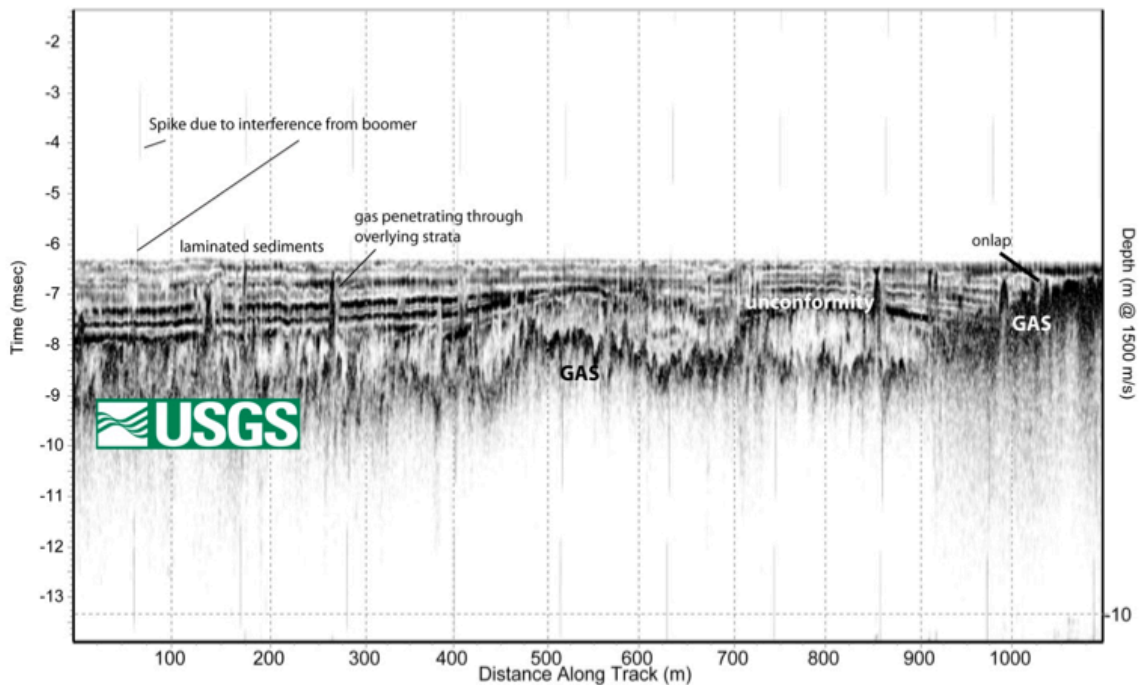
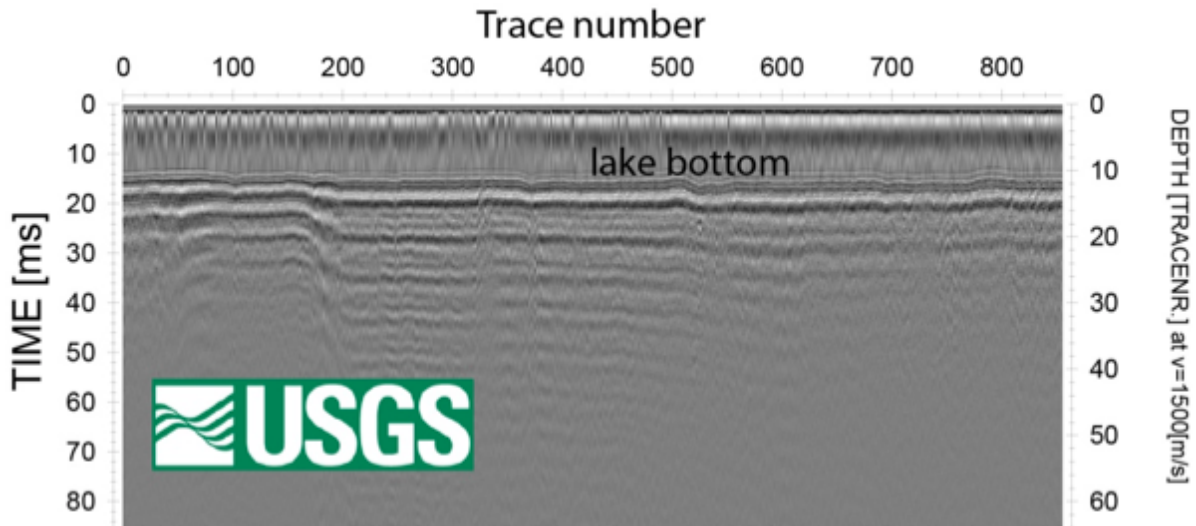


**Figure 26.** Example of mini-boomer data recorded in northern Lake Teshekpuk in 2010.



For Lake Teshekpuk, there has been a long-standing controversy over the existence of permafrost, despite observations of thick permafrost at the lake's eastern edge. Nonetheless, the discovery of methane seeps in the northernmost part of the lake during 2009 reconnaissance surveys provided a strong impetus to visit this area with a slightly different suite of geophysical instruments in 2010. Coupled with the inference that Lake Teshekpuk is likely to end up at the Beaufort coastline in a few centuries if current rates of coastal erosion are sustained, the observations were enough to lead us to Lake Teshekpuk as a prime study site for Year 2 of the

project. The seismic methods applied in Lake Teshekpuk were able to image some pockmarks, widespread shallow gas in the sediments, and the relationship among different sediment packages on the lake's bottom, but even boomer seismics did not detect permafrost beneath the northern part of the lake. It is important to note that this does not constitute confirmation that permafrost is missing, but does provide provocative impetus for further study, perhaps with airborne EM methods.

### 3 Methane Oxidation in Thermokarst Lakes

In this section we describe the UAF led activities related to the assessment of aerobic methane oxidation potential rates in thermokarst lakes and the identification of aerobic methane oxidizing microorganisms in lake sediments and water. We compare these data spatially within and between lakes and assess the effects of temperature on the activity and identity of methane oxidizing microorganisms. Comparisons are also made between organisms and rates associated with different methane sources, specifically a seep of intense methane ebullition and slower, more recent biogenic methane sources. Prior to our study, the sinks for arctic methane and the biological systems involved in methane consumption were poorly understood. Most critically, the role of aerobic methane oxidation in mitigating the flux of methane from lake systems had never been quantified. Despite the large net flux of methane from thermokarst lakes, there was no information on the extent to which oxidation in the sediments and water column of thermokarst lakes regulates the net flux. Nor had organisms responsible for methane oxidation in arctic Alaska been identified. Identification of methane oxidizers is critical, since different methane oxidizing organisms have previously been reported to respond differently to and have different tolerance to environmental change.

In addition to identification of methane oxidizers, this project also used lipid biomarkers to study methane oxidation in TKL. Lipid biomarkers are organic compounds derived from cellular membranes of prokaryotes and eukaryotes that provide a molecular fingerprint of the source organism. Lipids associated with contemporary material (e.g., surface sediments and particulate matter) are used to identify what organisms are active, while lipids preserved in association with older material (i.e., the sediment record) are used to identify organisms that were active. In this study, we utilized lipid biomarkers from a) suspended particulate matter to identify active carbon cycles and b) a radiocarbon-dated sediment core to reconstruct methane dynamics in the lake during the Holocene. The suspended particulate matter lipid biomarker data was paired with rate and microbiological studies describing the active methane carbon cycling in Lake Q. The sediment biomarker record complements the paleo-invertebrate record also used to reconstruct the methane activity in Lake Q during the Holocene (Section 4).

Many of the results reported here have already been published in peer-reviewed scientific journals. Additional details are available in the following articles in print and in review.

## Manuscripts in print

He, R. M. J. Wooller, J. W. Pohlman, J. Quensen, J. M. Tiedje, M. B. Leigh. 2012a. Diversity of active aerobic methanotrophs along depth profiles of arctic and subarctic lake water column and sediments. *The ISME Journal*. doi:10.1038/ismej.2012.34

He, R. M. J. Wooller, J. W. Pohlman, J. Quensen, J. M. Tiedje, M. B. Leigh. 2012b. Shifts in identity and activity of methanotrophs in arctic lake sediments in response to temperature changes. *Applied and Environmental Microbiology* 78(13):4715-4723.

He, R. M. J. Wooller, J. W. Pohlman, C. Catranis, J. Quensen, J. M. Tiedje, M. B. Leigh. 2012c. Identification of functionally active aerobic methanotrophs in sediments from an arctic lake using stable isotope probing. *Environmental Microbiology* 14(6):1403-1419.

## Manuscript in preparation

He, R. M. J. Wooller, J. W. Pohlman, J. Quensen, J. M. Tiedje, M. B. Leigh. Methane-derived carbon flow through arctic lake sediment microbial communities. 2012d. Manuscript in preparation.

## 3.1 Materials and Methods

We quantified and characterized the processes associated with methane oxidation at our study areas by measuring the concentration and stable carbon isotope composition of organic and inorganic species in the pore fluids and sediments, and methane oxidation rates in the water column and surface sediments. We also characterized the phylogenetic identity of microbes that actively oxidize methane in thermokarst lakes. We found that aerobic methane oxidation in the water column and the sediment appear to make important contributions towards mitigating the flux of methane from thermokarst lakes to the atmosphere. The identity of active methane oxidizers also varied spatially among lakes and within lakes, by sediment depth and depending upon the methane source (active seep vs. biogenic sources). Temperature also affected the activity and the identity of methane oxidizers, suggesting that increasing climate warming may affect methane oxidation substantially. Aerobic methane oxidation potential was quantified in sediment and water samples collected from various locations and depths in several different study lakes. Dissolved methane concentrations in sediment pore water were also quantified to examine methane oxidation activity in situ. The primary study sites were Lake Q and Lake Killarney, a subarctic taiga lake with moderate methane ebullition in Fairbanks, Alaska (Figure 27).

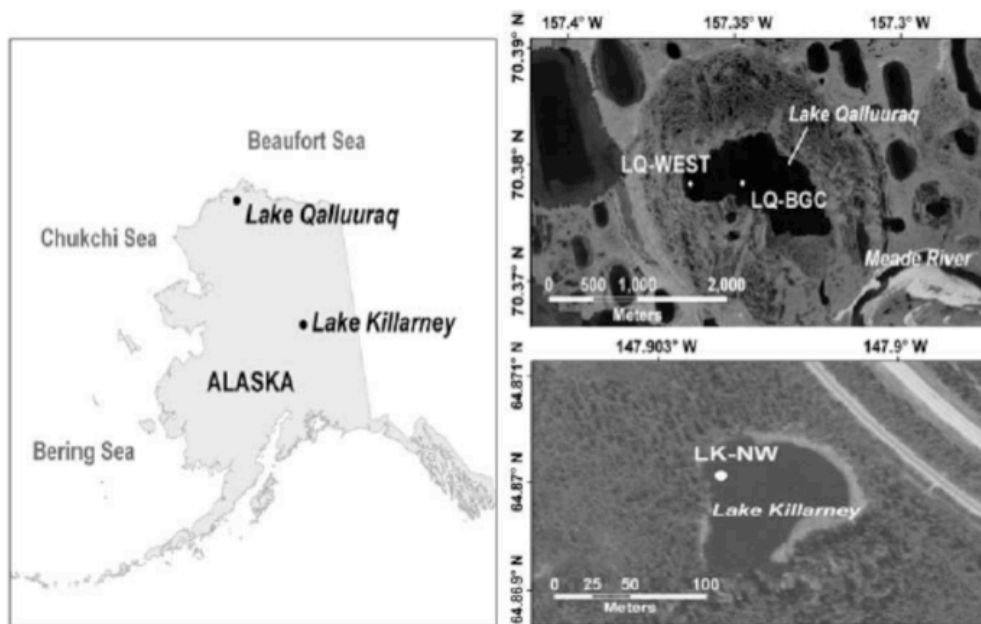
### 3.1.1 Methane oxidation potential measurements

Methane oxidation potential was measured in water and sediment samples (collected in July 2009) using laboratory microcosm experiments (He et al., 2012a, 2012b). Microcosms were constructed in sterile 60 ml glass serum vials, using either 5 g (wet weight) of sediment or 10 ml of water, and then were sealed with butyl rubber stoppers. Microcosms were injected with methane (99.5% pure) to achieve a headspace concentration of 10% methane (v/v) and replicates

were incubated on a rotary platform shaker (100 rpm) at 4°C, 10°C and 21°C. Gas headspace samples were periodically withdrawn from the headspace of microcosms for analyses of residual methane using GC-FID.

The identity of methane oxidizing bacteria active in arctic and subarctic lakes was conducted by UAF using culture-based methods, stable isotope probing (SIP) techniques and other molecular microbial ecological tools like qPCR, total community analyses using 16S rRNA pyrosequencing, and sequence analyses of methane oxidation genes. We determined the identity and diversity of active aerobic methanotrophs in the water columns and sediments (0–25 cm) from an arctic tundra lake (Lake Q) on the north slope of Alaska and a subarctic taiga lake (Lake Killarney) in Alaska's interior (He et al., 2012a, 2012c). We also used SIP to compare the identity of active methanotrophs in sediments from Lake Q when incubated at different temperatures in order to explore the effects of seasonal and climatic temperature change on active populations (He et al., 2012b). Using time-course incubations, we also investigated the flow of carbon from methane into the microbial community with DNA-SIP and PLFA-SIP methods (He et al., 2012d).

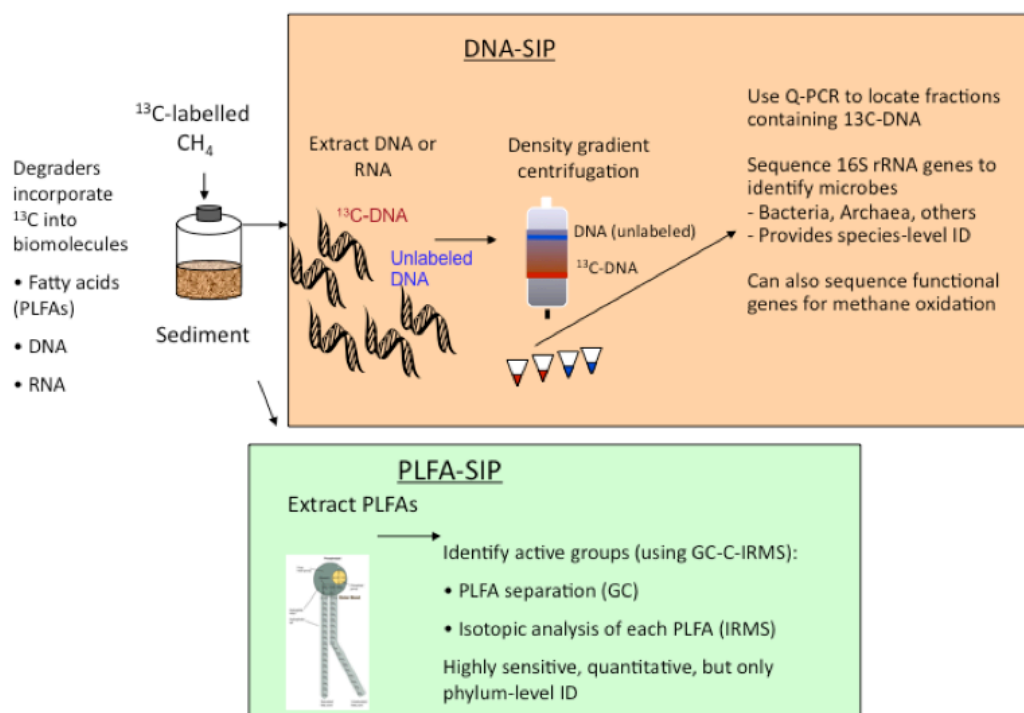
**Figure 27. Primary sampling locations and study sites for methane oxidation and microbial studies: Lake Q, previously discussed in this report, and Lake Killarney, a subarctic taiga lake with moderate methane ebullition in Fairbanks. Reprinted from He et al., 2012a.**



Microbial studies relying on cultivation methods have long been recognized as limited in scope; less than 1% of microbes active in the environment are detectable by cultivation techniques. For this reason, we performed SIP to more accurately determine the identity and relative contributions of different microbial taxa to methane oxidation (Figure 28). The application of SIP has allowed unprecedented and direct phylogenetic identification of microorganisms that derive carbon from a specific compound of interest (i.e., methane) within the context of a

complex microbial community. Briefly, SIP involves incubating a microbial community (e.g. those in the sediment from a lake) with a stable isotopically labeled substrate ( $^{13}\text{C}$ -labeled methane), during which time organisms that utilize the compound incorporate the isotope into their biomass including their genetic material. The  $^{13}\text{C}$ -labeled genetic material is then separated from unlabeled genetic material by isopycnic (density gradient) centrifugation. Commonly the  $^{13}\text{C}$ -labeled nucleic acids are then subjected profiling or sequence analysis of rRNA genes to identify the organisms that derived carbon from the substrate (e.g. methane).

**Figure 28. Stable isotope probing methods overview.**



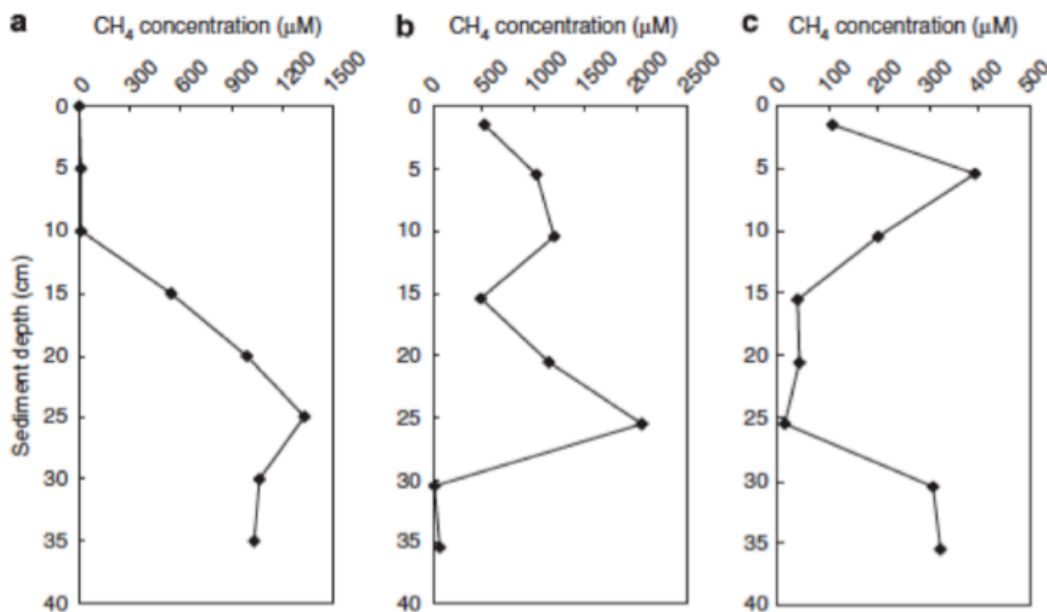
### 3.2 Results and Discussion

Methane concentrations were measured in sediment pore water along depth profiles collected in July 2009 (Figure 29; He et al 2012a, 2012b). At the LQ-BGC (active seep) site, dissolved methane concentrations were 1334 mM at 25 cm sediment depth and decreased to less than 15 mM at the 0-10 cm sediment depth (Figure 29). At the LQ-WEST site, dissolved methane concentrations varied from 483 mM to 2062 mM between the sediment water interface to the 25.5 cm sediment depth and very low dissolved methane concentrations (25-68 mM) were found at 30-36 cm sediment depth, where the substrate was highly sandy. Dissolved methane concentration in the pore water from LK-NW site was lower (about 16-390  $\mu\text{M}$ ) than those observed for Lake Qalluaraq (LQ-BGC and LQ-WEST sites). Declines in methane concentrations near the sediment surface are indicative of active aerobic methane oxidation

providing a sink for methane generated deeper in the sediment. Interestingly, a sharp decrease in dissolved methane concentration was also observed in the pore water from the LK-NW 15-25 cm sediments (Figure 29), which is suggestive of anaerobic methane oxidation activity.

Differences in methane oxidation potential in the water column were observed both between and within our study lakes, Lake Q (a tundra arctic lake) and Lake Killarney (a sub-arctic taiga lake) (Figure 30). A 15 to 60-fold greater methane oxidation potential was observed in the water column above the active methane seep (LQ-BGC) site compared to the non-seep (LQ-WEST) site within the same arctic lake, which may have been due to the seep providing a continuous input of carbon and energy sources that caused increased microbial biomass in the water column. A considerably (4 to 7-fold) higher methane oxidation potential was exhibited by the sub-arctic lake (LK-NW site) water when compared with the arctic lake methane seep. The highest methane oxidation potential was present in the deep water from this sub-arctic lake (LK-NW site), which was a hypoxic zone in situ (He et al 2012a).

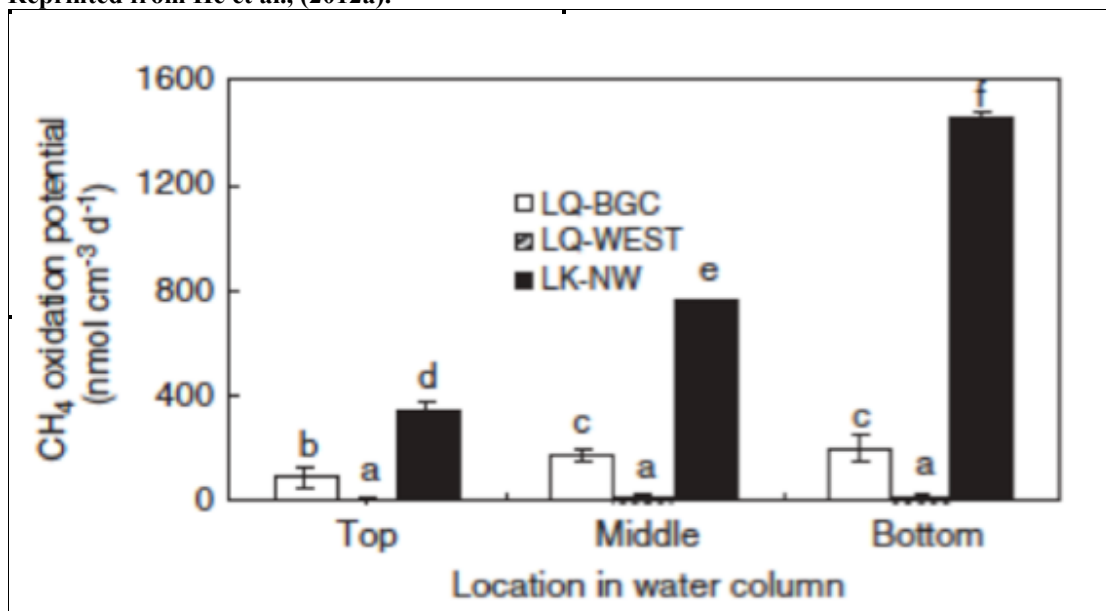
**Figure 29. Sediment depth profile for dissolved methane concentration in the sampling sites. (a) LQ-BGC site; (b) LQ-WEST site; and (c) LK-NW site. Reprinted from He et al., 2012a.**





Methane oxidation potential measurements in sediments were performed at 4°C, 10°C and 21°C. Methane consumptions at 4°C and 10°C were both very slow in the sediments from the LQ-BGC site (Figure 31). For this reason, when investigating the comparative maximum activity and

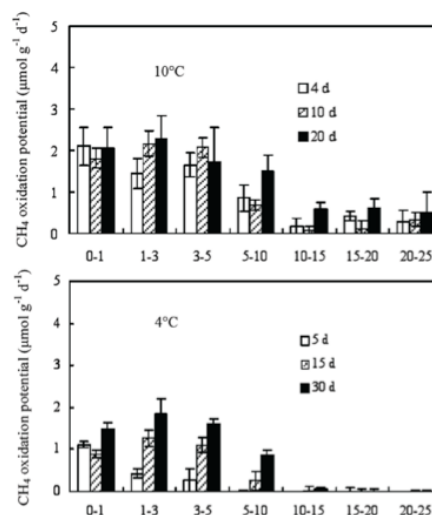
**Figure 30. Methane oxidation at 21°C of water from indicated depths. Different letters within the graph refer to significant differences at 5% level based on the least significant difference (LSD) method. Reprinted from He et al., (2012a).**



community structure of methanotrophs between and within the lakes, we focused on incubations at 21°C. This temperature is similar to the maximum water temperatures of 20°C (July) detected during a 4-year study of arctic lakes and the measured temperature of water at Lake Q in July 2009 when samples were collected.

In sediments, the methane oxidation potential (21°C) of surface sediment (0-1 cm) from the LQ-WEST site (77-80  $\mu\text{mol g}^{-1} \text{d}^{-1}$ ) was found to be over an order of magnitude higher than the LQ-BGC seep site and 1.8-13.0 times higher than surface sediment from the sub-arctic lake site, LK-NW (Figure 31). Measurable methane consumption occurred at the 0-20 cm sediment depths from LQ-BGC and LQ-WEST and at the 0-5 cm depths from the LK-NW site after 2 days of incubation (Figure 31). After 10 days of incubation, methane consumption was detectable in sediments from every depth (0-25 cm), with methane oxidation potentials of 0.7-76.8  $\mu\text{mol g}^{-1} \text{d}^{-1}$ , which likely represented acclimation and growth of methanotrophs in the incubations.

**Figure 31. Methane oxidation potential of sediment from LQ-BGC site at 10°C and 4°C. Reprinted from He et al., 2012a (supplement).**



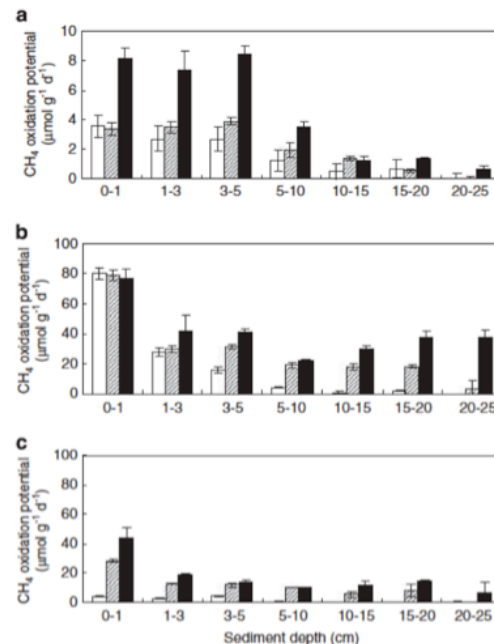
Methane oxidation potentials were compared among different incubation temperatures for sediments from Lake Q (He et al. 2012b). The methane oxidation potentials increased as the incubation temperature increased from 4°C to 21°C. In the 0- to 5-cm sediment depth, the methane oxidation potentials at 21°C (on day 5) were 0.6 to 1.6 times and 37.0 to 160.5 times greater than those at 10°C (on day 4) and 4°C (on day 5), respectively (He et al. 2012b).

The methane oxidation potentials in the sediment samples increased along with increased incubation temperature from 4°C to 21°C (Figure 31). A greater increase in methane oxidation potential occurred from 10°C to 21°C than from 4°C to 10°C, indicating that many of the active methanotrophs in the arctic lake sediments might be psychrotolerant (from <0 to ≤35°C with optimal temperature ≤25°C) rather than psychrophilic (from <0 to ≤20°C with optimal temperature ≤15°C) (He et al. 2012b).

In summary, this portion of our study indicates that arctic and subarctic lake sediments and water possess substantial aerobic methane oxidation potential and represent a potentially important sink for methane. Oxidation potentials varied among lakes and within lakes, which appears to be largely dependent upon sediment composition, organic matter and oxygen availability. Methane concentration profiles in situ provide further evidence that aerobic methane oxidation is an important methane sink, removing a large proportion of methane generated in situ, particularly near the oxic/anoxic interface. Additional evidence of methane losses in deeper sediments and are suggestive that anaerobic methane oxidation may be another important methane sink. As incubation temperatures increased, methane oxidation rates also increased, suggesting that during seasonal shifts and long-term climate warming, the potential sink for methane increases concomitantly. An important area for future study will be to determine if increased methane oxidation rates can mitigate increased methane emissions as the climate warms.

The first order observation regarding the fate of methane in the lake is that rates of methane oxidation were exceptionally high during ice-cover. This observation identifies a previously unknown sink for methane and is intriguing because the quantity of oxygen required to support the measured oxidation rates exceeds its availability during ice-cover. Lipid biomarker data provides details about the active carbon cycle and thus are used to support the rate based evidence for elevated methane oxidation rates during ice-covered conditions. The stable carbon isotope data for lipid biomarkers associated with suspended particles in the lake reveals that

**Figure 32. Methane oxidation potential of sediment from (a) LQ-BGC; (b) LQ-WEST sitte; and (c) LK-NW site at 21oC incubated for 2 (white bar), 5 (shaded bar) and 10 (black bar) days. Note different scales on y-axes. Reprinted from He et al., (2012a).**



methane carbon was transferred into biomarkers associated with methane-consuming (or methanotrophic) bacteria and some photosynthetic products, but not eukaryotic biomass. As expected, the plant wax-derived C24:0 has  $\delta^{13}\text{C}$  values consistent with a photosynthetic source in both seasons. By contrast, diplopterol, a biomarker for aerobic methanotrophic bacteria, has a  $\delta^{13}\text{C}$  value similar to methane, suggesting aerobic methanotrophs were active in May when the lake was ice-covered and the measured methane oxidation rates were high. This signal was absent in July when methane oxidation rates were low. Methane-influenced  $\delta^{13}\text{C}$  values for sitosterol, a plant and algal biomarker, in May suggests carbon dioxide generated during methane oxidation was assimilated by algae during under-ice photosynthesis, which was identified as the mechanism postulated to sustain aerobic methane oxidation during ice-cover. The absence of a methane signal in the eukaryotic biomarker cholesterol suggests the host organisms did not consume an appreciable amount of methanotrophic biomass or algae that grew during ice-cover.

### 3.2.1 Culture-based studies

To identify planktonic methane oxidizers in water, enrichment cultures were established for water samples from the top, middle and bottom of the water column from different lakes and sampling sites (He et al., 2012a). Bacterial community fingerprinting using terminal restriction fragment length polymorphism (T-RFLP) analyses indicated that the enrichment cultures from various depths were generally similar in community structure (He et al. 2012a). For this reason, we combined DNA extracts obtained from the top, middle and bottom depths together at each sampling location for pyrosequencing analysis of 16S rRNA gene amplicons. RDP classification of pyrosequencing reads showed that the type II methanotroph, *Methylocystis*, was dominant in the water sample enrichment cultures (Table 6), while the type I methanotrophs, *Methylomonas*, *Methylobacter* and unclassified Methylococcaceae, represented a small proportion (1.7%) of the enrichment culture from water from the LK-NW site, and were not evident in the sites from Lake Q.

Interestingly, an obligate methylotroph that uses methanol as the sole source of carbon and energy, *Methylophilus*, was present in all enrichment cultures and was particularly abundant in the LK-NW water culture, where it comprised 25.2% of pyrosequencing reads. In addition to the Proteobacteria, members of the Actinobacteria, Bacteroidetes and Verrucomicrobia (note there are three previously known methanotrophs in the phylum Verrucomicrobia) were also found in the enrichment cultures from all the study locations.

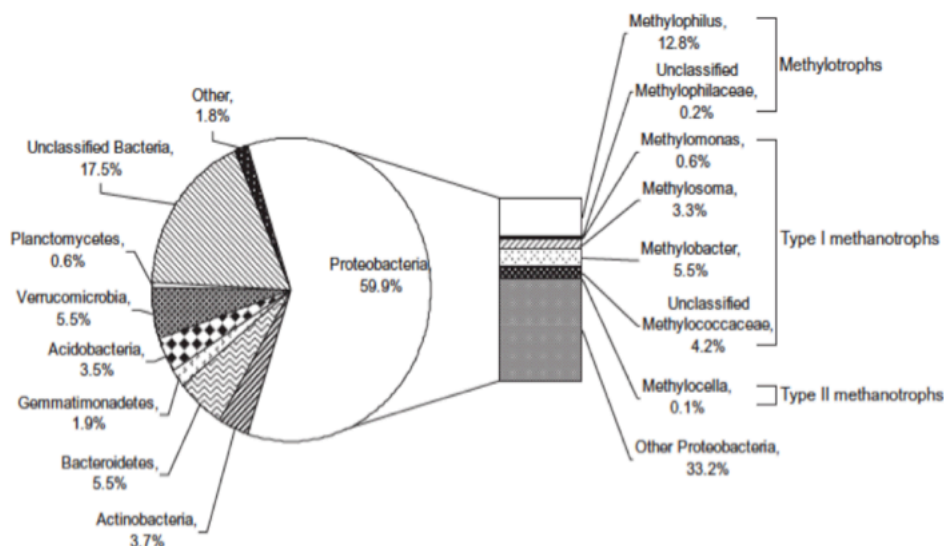
DNA-SIP, direct sequence analyses of methanotrophs, and functional gene analyses were performed on surface sediments (0-1 cm depth) in Lake Q (He et al. 2012c). Using targeted primer sets based on 16S rRNA genes, both type I and type II methanotrophs were directly detected in the upper sediment total communities. SIP was performed to identify which organisms were active in deriving C from  $^{13}\text{C}$ -methane. Using SIP along with sequencing of functional genes (*pmoA* and *mxoF*) and 16S rRNA genes in the  $^{13}\text{C}$ -DNA from the upper sediment, we found that type I methanotrophs, mainly *Methylobacter*, *Methylosoma*, *Methylomonas* and *Methylovulum miyakonense*, dominated the assimilation of methane (e.g. Figure 33). Quantitative PCR (Q-PCR) of 16s rRNA genes of *pmoA*, type I and type II methanotrophs and pyrosequencing of 16S rRNA genes in  $^{13}\text{C}$ -DNA obtained by SIP provided

further confirmation that type I methanotrophs, *Methylobacter*, *Methylomonas* and *Methylosoma*, dominated carbon acquisition from methane in the sediments (He et al. 2012b).

Our findings that type I methanotrophs dominated methane oxidation in arctic lake sediment are consistent with previous reports that low temperatures favor the growth of type I methanotroph populations. Psychrophilic methanotrophs that have been previously isolated (i.e., cells with optimal growth at or below 15°C) have all been found to belong to the type I group of methanotrophs.

The environmental conditions prevalent in our study lake also are consistent with those found to favor type I methanotrophs. The relative numbers and activity of type I and type II

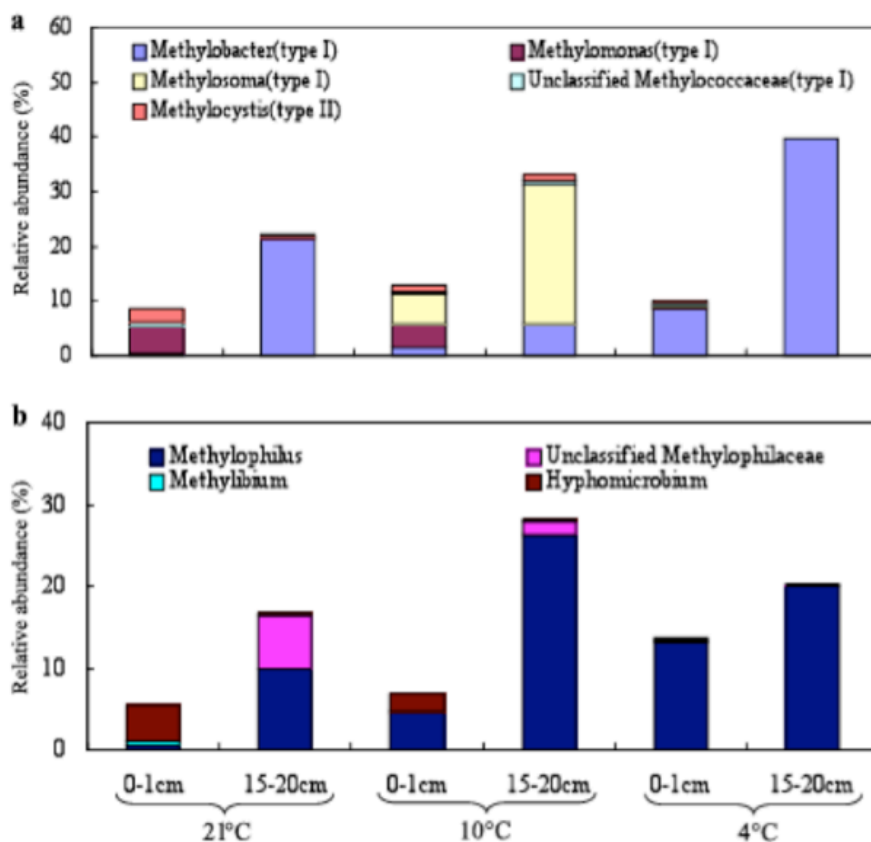
**Figure 33. Phylogenetic distribution of all pyrosequencing reads from the heavy fractions ( $^{13}\text{C}$ -DNA) from DNA-SIP experiments, indicating the relative abundance of bacterial taxa that derived carbon from  $^{13}\text{C}$ -methane in sediment collected from Lake Q (0-1 cm depth). Reprinted from He et al. (2012c).**



methanotrophs have been reported to vary with environmental conditions, including methane and oxygen concentration as well as temperature and nitrogen content. Type I methanotrophs were reported to dominate sites with high oxygen and low methane concentrations. In arctic lakes/ponds, freezing begins to occur in September and continues until the water is frozen, in many places, to the bottom. When arctic lakes are ice-covered, sediment methane concentrations can be high, while oxygen concentration can be low. When lakes are ice free, the open water and wave action generated by high winds allow for oxygen mixing into the water, creating conditions favorable to aerobic methane consumption. This may generate an inverse relationship between oxygen and methane concentrations, with a decrease in methane concentration occurring when oxygen concentrations are elevated at the sediment-water interface.

Interestingly, methylotrophs, including the genera *Methylophilus* and/or *Methylotenera*, were also abundant in the  $^{13}\text{C}$ -DNA obtained during our SIP experiments (Figure 34). Methylotrophs especially important in deriving carbon from methane in the deeper sediments (15-20 cm) at low temperatures (4°C and 10°C), and showed a good linear relationship with the relative abundances of methanotrophs in pyrosequencing reads (He et al., 2012b). Methylophilaceae is a family of obligate methylotrophs that utilize methanol as the sole source of carbon and energy. No methanol was added to our microcosms. Methanotrophic bacteria generally metabolize methane completely to carbon dioxide, with methanol, formaldehyde, and formate formed as intermediates (Hanson and Hanson, 1996), and this series of reactions occurs intracellularly with no methanol being produced extracellularly (Corder et al., 1986). We did not monitor methanol levels in our microcosms, so we cannot confirm if extracellular methanol accumulation occurred. Future studies with larger quantities of sediment incubated over a time course that includes shorter incubations might help reveal the mechanism of methane-derived carbon utilization by the Methylophilaceae in arctic lake sediments.

**Figure 34. Relative abundances of known methanotrophs and methylotrophs within sediment microbial populations that derived carbon from methane during SIP, based on the abundances of 16S rRNA gene sequences detected in  $^{13}\text{C}$ -labeled DNA by use of pyrosequencing. Taxonomic assignments were made using the classifier of the Ribosomal Database Project (confidence threshold, 80%). Sediments subjected to SIP were analyzed after about 0.2 mmol  $^{13}\text{C}$ -methane g<sup>-1</sup> (wet weight) was consumed at incubation temperatures of 4°C, 10°C, and 21°C. (a) Methanotrophs; (b) methylotrophs. Reprinted from He et al. (2012b).**



PLFA-SIP studies provided additional support for our observations that Gram negative bacteria including type I and type II methanotrophs were the most abundant microorganisms involved in methane-derived carbon flow, followed by Gram positive bacteria, fungi and actinomycetes (He et al., 2012d). As incubation time increased, carbon flowed from methanotrophs out into non-methanotrophic members of the microbial community. This indicates that secondary and tertiary feeding on  $^{13}\text{C}$ -derived carbon in the microbial food web might be a critical linkage between benthic anoxic and aerobic microbial pathways for transferring methane-derived carbon in arctic lakes (He et al., 2012d).

### 3.2.2 Comparison of methanotrophs among lakes

Our study of surface sediments from Lake Q indicated that type I methanotrophs, including *Methylobacter*, *Methylosoma*, *Methylovulum miyakonense*, and *Methylomonas*, were present and active in methane oxidation at environmentally relevant low temperatures (4°C), and thus likely play an important role in situ in limiting the flux of methane (He et al., 2012c). In order to better understand the controls on greenhouse gas emissions from arctic lakes, we performed additional studies to determine how the identity and activity of methanotrophs vary with sediment depth, temperature and methane source in sediments and water of this and other arctic lakes.

The identity of methane oxidizers was compared among different lakes and sampling locations using DNA-SIP (Table 6) (He et al. 2012a). A diverse bacterial community was involved directly or indirectly in acquiring methane-derived carbon. Members of the phylum Proteobacteria predominated methane-C assimilation, especially in the sediments from the subarctic lake (LK-NW) site and the deep (15-20 cm) sediment from an arctic lake (LQ-WEST) site, where Proteobacteria accounted for more than 91% of the total pyrosequencing reads. In the deep (15-20 cm) sediment at the active methane seepage site (LQ-BGC) and the uppermost (0-1 cm) sediment from the LQ-WEST site, the phyla Actinobacteria, Firmicutes, Bacteroidetes, Acidobacteria, Verrucomicrobia, Planctomycetes and Chloroflexi were all found to be active in methane oxidation.

Members of type I (*Methylomonas*, *Methylobacter*, *Methylosoma* and unclassified Methylococcaceae) and type II methanotrophs (*Methylocystis*, *Methylosinus* and *Methylocella*) were detected in the  $^{13}\text{C}$ -DNA from our lake sediments (Table 7). Relative to type II methanotrophs, type I methanotrophs were more dominant in  $^{13}\text{C}$ -DNA from the uppermost (0-1 cm) sediment, especially at the LK-NW site, where *Methylobacter* accounted for 60.3% of the pyrosequencing reads (Table 7). Both type I (*Methylobacter*) and type II methanotrophs (*Methylocystis*, *Methylosinus* and *Methylocella*) were detected in the deeper (15-20 cm) sediment from the LK-NW site. The type II methanotroph, *Methylocystis*, was the most abundant methanotroph in the deeper sediment from the seep site (LQ-BGC) at Lake Q, but the type I methanotroph, *Methylobacter*, was the most abundant type in deeper sediments from LQ-WEST site in the same lake (He et al. 2012a).



**Table 6. Relative abundance (% of total reads) and phylogenetic affiliations of 16S rRNA pyrosequencing reads from DNA of enrichment cultures in methanotroph medium cultivated from lake water samples. Reprinted from He et al. (2012a).**

Phylogenetic affiliation	Sampling site		
	LQ-BGC	LQ-WEST	LK-NW
<i>Proteobacteria</i>			
<i>Alphaproteobacteria</i>			
<i>Methylocystaceae</i>			
<i>Methylocystis</i>	74.1 (1436) <sup>a</sup>	75.4 (2028)	33.6 (1005)
<i>Methylosinus</i>	0.2 (3)	— <sup>b</sup>	1.9 (58)
Unclassified	0.8 (15)	0.8 (21)	18.9 (564)
<i>Methylocystaceae</i>			
<i>Hyphomicrobiaceae</i>			
<i>Hyphomicrobium</i>	1.4 (27)	1.9 (52)	1.2 (35)
Other	6.6 (127)	6.8 (184)	6.6 (196)
<i>Alphaproteobacteria</i>			
<i>Betaproteobacteria</i>			
<i>Methylophilales</i>			
<i>Methylophilus</i>	7.9 (154)	3.2 (86)	25.2 (754)
Unclassified	0.1 (1)	0.2 (6)	0.2 (7)
<i>Methylophilaceae</i>			
<i>Rhodocyclales</i>	0.1 (2)	—	0.1 (2)
<i>Burkholderiales</i>	4.1 (80)	5.4 (146)	2.6 (77)
Other	1.1 (22)	0.5 (13)	1.4 (43)
<i>Betaproteobacteria</i>			
<i>Gammaproteobacteria</i>			
<i>Methylococcales</i>			
<i>Methylomonas</i>	—	—	0.4 (12)
<i>Methylobacter</i>	—	—	0.5 (14)
Unclassified	—	—	0.8 (25)
<i>Methylococcaceae</i>			
Other	1.5 (30)	2.3 (61)	1.6 (49)
<i>Gammaproteobacteria</i>			
<i>Actinobacteria</i>	1.1 (21)	0.6 (15)	0.1 (3)
<i>Bacteroidetes</i>	0.6 (11)	2.2 (59)	1.7 (51)
<i>Verrucomicrobia</i>	0.2 (3)	0.2 (5)	1.1 (34)
Unclassified Bacteria	0.2 (3)	0.4 (11)	1.1 (34)
Other	0.2 (3)	0.1 (4)	0.9 (27)
Total	100 (1938)	100 (2691)	100 (2990)

Taxonomic assignments were generated using the Ribosomal Database Project's classifier.

<sup>a</sup>The numbers of pyrosequencing reads assigned using the RDP classifier (80% confidence threshold) are shown in parentheses.

<sup>b</sup>No pyrosequencing reads from this group were detected.

### 3.2.3 Effect of temperature on the identity of methane oxidizing bacteria

As arctic temperatures continue to rise, understanding the effects of temperature on the activity and of methanotrophs in arctic lake sediments is important to predicting future methane emissions. As described above, methane oxidation potential observed in our lake sediments varied with incubation temperature. We applied DNA-SIP and other molecular methods to characterize methanotrophic communities active at a range of temperatures (4°C, 10°C and 21°C) in sediments (to 25 cm depth) sampled from Lake Q. Interestingly, the identity and

relative abundance of active methanotrophs differed with incubation temperature (Table 8) (He et al. 2012b).

Q-PCR of 16S rRNA genes of type I and type II methanotrophs and *pmoA* gene, and pyrosequencing of 16S rRNA gene in the heavy fractions ( $^{13}\text{C}$ -DNA) demonstrated that type I methanotrophs were more abundant and active than type II methanotrophs in the sediments examined (Table 8). Of the methanotrophs active at 4°C, approximately 95.1-100% of methanotrophs active at 4°C were type I methanotrophs. *Methylocystis* was the only type II

**Table 7. Relative abundance (% of total reads) and phylogenetic affiliations of pyrosequencing reads from  $^{13}\text{C}$ -DNA obtained from SIP of lake sediments incubated with  $^{13}\text{C}$ -methane. Taxonomic assignments were generated using the Ribosomal Database Project's classifier. Reprinted from He et al. (2012a).**

Phylogenetic affiliations	LQ-BGC		LQ-WEST		LK-NW	
	0-1 cm	15-20 cm	0-1 cm	15-20 cm	0-1 cm	15-20 cm
<i>Proteobacteria</i>						
<i>Alphaproteobacteria</i>						
<i>Methylocystaceae</i>						
<i>Methylocystis</i>	1.7 (43)*	25.4 (719)	1.0 (9)	0.2 (6)	0.2 (5)	40.4 (1166)
<i>Methylosinus</i>	—	—	—	—	—	1.5 (43)
Unclassified <i>Methylocystaceae</i>	0.1 (2)	0.5 (13)	0.4 (4)	0.2 (4)	1.6 (45)	7.6 (220)
<i>Beijerinckiaceae</i>						
<i>Methylocella</i>	0.1 (2)	—	—	—	0.1 (2)	2.3 (66)
<i>Methylovirgula</i>	—	—	—	—	0.7 (21)	1.1 (32)
Unclassified <i>Beijerinckiaceae</i>	2.2 (56)	—	0.3 (3)	0 (1)	0.2 (7)	2.1 (62)
<i>Hyphomicrobiaceae</i>						
<i>Hyphomicrobium</i>	6.8 (173)	4.4 (124)	5.8 (52)	0.8 (22)	—	0.2 (6)
<i>Methylobacteriaceae</i>						
<i>Methylobacterium</i>	—	—	—	—	—	1.6 (45)
Other <i>Alphaproteobacteria</i>	15.6 (396)	22.3 (631)	8.9 (80)	6.8 (178)	1.2 (36)	9.6 (278)
<i>Betaproteobacteria</i>						
<i>Methylophilales</i>						
<i>Methylophilus</i>	2.9 (74)	0.3 (8)	1.7 (15)	29.3 (765)	—	—
Unclassified <i>Methylophilaceae</i>	1.1 (27)	0 (1)	0.7 (6)	1.0 (27)	—	0.2 (2)
<i>Rhodocyclales</i>	0.1 (3)	0 (1)	1.4 (13)	6.7 (174)	6.4 (184)	2.0 (59)
<i>Burkholderiales</i>	1.1 (29)	1.1 (31)	3.1 (28)	5.6 (146)	2.0 (57)	0.6 (17)
Other <i>Betaproteobacteria</i>	15.9 (403)	0.7 (21)	12.2 (110)	2.3 (59)	16.0 (462)	0.9 (25)
<i>Gammaproteobacteria</i>						
<i>Methylococcaceae</i>						
<i>Methylobacter</i>	0 (1)	0 (1)	0.1 (1)	30.3 (790)	60.3 (1742)	20.0 (578)
<i>Methylosoma</i>	—	0 (1)	7.0 (63)	1.2 (30)	—	—
<i>Methylosoma</i>	3.2 (82)	—	0.4 (4)	—	—	—
Unclassified <i>Methylococcaceae</i>	2.4 (60)	0 (1)	1.3 (12)	0.1 (2)	4.7 (136)	0.1 (4)
Other <i>Gammaproteobacteria</i>	4.8 (121)	6.5 (184)	6.1 (55)	0.9 (23)	2.7 (77)	3.5 (101)
<i>Deltaproteobacteria</i>	5.7 (144)	5.2 (146)	13.6 (123)	4.9 (127)	0 (1)	0.5 (14)
Unclassified <i>Proteobacteria</i>	1.7 (42)	5.1 (144)	2.3 (21)	1.2 (31)	0.3 (8)	0.6 (18)
<i>Actinobacteria</i>	0.7 (18)	0 (1)	0.9 (8)	5.4 (140)	0.6 (17)	1.3 (38)
<i>Firmicutes</i>	—	0.1 (3)	0.1 (1)	1.1 (29)	2.1 (60)	0.2 (6)
<i>Bacteroidetes</i>	2.6 (67)	0.7 (20)	5.9 (53)	0 (1)	—	1.4 (39)
<i>Acidobacteria</i>	11.3 (286)	0.7 (19)	3.5 (32)	0.1 (2)	—	0.4 (11)
<i>Verucomicrobia</i>	0.7 (18)	0.6 (16)	2.7 (24)	—	0 (1)	—
<i>Planctomycetes</i>	4.1 (103)	0.5 (15)	3.4 (31)	0.2 (5)	0.3 (9)	0.5 (13)
<i>Chloroflexi</i>	2.0 (51)	2.4 (67)	0.4 (4)	—	0.1 (2)	0.1 (2)
Unclassified <i>bacteria</i>	12.2 (310)	22.3 (629)	12.7 (115)	1.4 (37)	0.3 (10)	0.9 (25)
Other	1.1 (27)	1.2 (30)	4.0 (36)	0.3 (8)	0.2 (7)	0.5 (14)
Total	100 (2538)	100 (2826)	100 (903)	100 (2607)	100 (2889)	100 (2884)

Taxonomic assignments were generated using the Ribosomal Database Project's classifier.

\*The numbers of pyrosequencing reads assigned using the RDP classifier (80% confidence threshold) are shown in parentheses.

\*No pyrosequencing reads from this group were detected.

methanotroph active in our sediment samples. An increase in incubation temperature from 4°C to 21°C corresponded to an increase in the relative abundance of *Methylocystis*, indicating that high temperatures favored the growth of these type II methanotrophs. Similar results have been previously reported in landfill cover soils where it was found that type I methanotrophs were more dominant at 10°C than 20°C, while type II methanotrophs were highly elevated only at 20°C (Börjesson et al., 2004).

**Table 8. Effects of temperature on the relative abundances of organisms that derived carbon from <sup>13</sup>C-methane during SIP experiments. Relative abundance as % and number of pyrosequencing reads (in parentheses) from <sup>13</sup>C-labeled DNA assigned to different taxa by using the Ribosomal Database Project Classifier. Reprinted from He et al. (2012b).**

Phylogenetic affiliation <sup>a</sup>	% (no.) of pyrosequencing reads <sup>b</sup> from <sup>13</sup> C-labeled DNA at:					
	4°C		10°C		21°C	
	0-1 cm	15-20 cm	0-1 cm	15-20 cm	0-1 cm	15-20 cm
<i>Proteobacteria</i>						
<i>Alphaproteobacteria</i>						
<i>Methylocystaceae</i>						
<i>Methylocystis</i> (type II)	0.5 (12)	0 (1)	1.4 (10)	1.1 (19)	2.5 (30)	0.2 (4)
Unclassified <i>Methylocystaceae</i>	— <sup>c</sup>	—	0.3 (2)	0.1 (2)	0.2 (3)	—
<i>Hyphomicrobiaceae</i> , <i>Hyphomicrobium</i> <sup>d</sup>	—	—	2.0 (14)	0.3 (5)	4.2 (51)	0.3 (8)
Other <i>Alphaproteobacteria</i>	6.1 (149)	11.1 (325)	6.6 (46)	10.8 (193)	13.5 (164)	15.2 (359)
<i>Betaproteobacteria</i>						
<i>Methylophilales</i>						
<i>Methylophilus</i> <sup>d</sup>	13.2 (322)	20.0 (586)	4.6 (32)	26.2 (467)	0.4 (5)	9.8 (230)
Unclassified <i>Methylophilaceae</i> <sup>d</sup>	0.3 (7)	0.2 (5)	0.1 (1)	1.7 (31)	—	6.6 (156)
<i>Burkholderiales</i> , <i>Methylobium</i> <sup>d</sup>	0.8 (19)	0 (1)	—	—	0.2 (3)	0.1 (2)
Other <i>Betaproteobacteria</i>	7.7 (188)	16.2 (474)	31.8 (222)	7.5 (133)	17.9 (217)	19.1 (449)
<i>Gammaaproteobacteria</i>						
<i>Methylococcaceae</i>						
<i>Methylobacter</i> (type I)	8.7 (212)	39.7 (1166)	1.7 (12)	5.9 (106)	0.4 (5)	21.6 (509)
<i>Methylomonas</i> (type I)	0.4 (10)	—	4.0 (28)	0.1 (1)	5.2 (63)	0.3 (6)
<i>Methylosoma</i> (type I)	0.2 (4)	—	5.4 (38)	25.3 (450)	—	—
Unclassified <i>Methylococcaceae</i> (type I)	0.4 (9)	0.1 (2)	0.4 (3)	0.7 (12)	0.6 (7)	—
Other <i>Gammaaproteobacteria</i>	6.6 (161)	1.0 (29)	6.4 (45)	1.7 (31)	7.6 (92)	2.7 (64)
<i>Deltaproteobacteria</i>	9.6 (234)	1.8 (52)	7.7 (54)	0.3 (5)	10.8 (131)	0.8 (18)
Unclassified <i>Proteobacteria</i>	0.8 (19)	0.7 (22)	1.1 (8)	0.8 (15)	2.9 (35)	0.6 (13)
<i>Actinobacteria</i>	1.4 (35)	3.3 (96)	1.6 (11)	4.9 (88)	1.2 (14)	6.4 (150)
<i>Bacteroidetes</i>	4.5 (109)	0.6 (19)	3.4 (24)	3.0 (53)	3.1 (37)	5.2 (122)
<i>Acidobacteria</i>	3.5 (86)	0.1 (4)	2.9 (20)	0.4 (8)	9.1 (110)	0.5 (11)
<i>Verrucomicrobia</i>	5.7 (138)	0.1 (4)	2.3 (16)	0.5 (9)	0.8 (10)	1.7 (41)
<i>Planctomycetes</i>	3.5 (85)	1.5 (43)	1.3 (9)	4.7 (84)	1.6 (19)	4.8 (113)
Unclassified bacteria	22.2 (542)	1.4 (40)	12.3 (86)	1.8 (32)	14.1 (171)	1.7 (40)
Other	4.1 (99)	2.2 (65)	2.6 (18)	2.1 (38)	3.6 (44)	2.5 (60)
Total	100 (2,440)	100 (2,934)	100 (699)	100 (1,782)	100 (1,211)	100 (2,355)

<sup>a</sup> "Type I" and "type II" stand for type I and type II methanotrophs.

<sup>b</sup> The numbers of pyrosequencing reads were assigned using the RDP classifier (80% confidence threshold).

<sup>c</sup> —, no pyrosequencing reads assigned.

<sup>d</sup> Methylophilus.

We found that the relative abundance of type I and type II methanotrophs active in methane oxidation changed with temperature, and also the taxonomic composition of type I methanotrophs was influenced by temperature. This may be due to the difference in relative optimum temperatures for these organisms (He et al. 2012b). Based on the relative abundance of different methanotrophic taxa in our pyrosequencing libraries, we hypothesize that *Methylosoma* in the sediment was psychrophilic with an optimum temperature of about 10°C. Members of the

genus *Methylomonas* were likely psychrotolerant or mesophilic, based on their decrease in activity and growth at 4°C in comparison to 21°C. *Methylobacter* was likely psychrotolerant, as evidenced by substantial growth at 21°C and 4°C.

The findings of our temperature study (He et al., 2012b) indicate that methane oxidation can occur at low temperatures characteristic of arctic lake sediments, down to at least 4°C. As temperatures rise, methane oxidation potential also increases and shifts in the community structure of bacteria actively growing at the expense of methane also shifts. We detected these shifts within temperature ranges that already occur seasonally in arctic lakes (Miller et al., 1980), suggesting that active methanotrophic populations may also change seasonally. Our data suggest that as temperatures continue to increase in the Arctic, predominant oxidation rates and active methanotrophic populations will also shift. Whether these changes can offset predicted increases in methanogenesis is an important question underlying models of future methane flux and resultant climate change.

### 3.3 Conclusions

Our studies revealed that type I methanotrophs, including *Methylomonas*, *Methylobacter* and *Methylosoma*, and type II methanotrophs, including *Methylocystis* and *Methylosinus*, are abundant and active in assimilating methane in these arctic and sub-arctic lakes. Type I methanotrophs, including *Methylobacter*, *Methylosoma*, *Methylovulum miyakonense*, and *Methylomonas*, were present and active in methane oxidation at environmentally relevant low temperatures (4°C), and thus likely play an important role in limiting the flux of methane from arctic lake sediments. The community structure and activity of methanotrophs varied alongside the physical-chemical properties of the sediments and water, such as sediment composition, oxygen and methane concentrations. The observed flow of carbon derived from methane into other non-methanotrophic members of the microbial community, including Gram positive bacteria, fungi and actinomycetes, may provide an important source of carbon in these microbial communities and to higher trophic levels. Our data suggest that as temperatures increase in the Arctic, predominant oxidation rates and active methanotrophic populations will also shift. Whether these changes can offset predicted increases in methanogenesis is an important question underlying models of future methane flux and resultant climate change. Our study is the first to identify methane oxidizing organisms active in arctic lakes. Additionally, we describe for the first time how methanotrophic communities in arctic lake sediments respond to temperature variation. Our findings provide new fundamental information regarding the activity and diversity of methanotrophs in cold regions that may aid predicting and modeling future methane flux from warming arctic and sub-arctic environments. Future studies in this area are needed to better understand how methane oxidation rates compare to rates of methane production in arctic lake ecosystems, in order to more accurately predict how future climate warming will affect global methane concentrations and ultimately climate feedbacks. An important component of future studies should be attention to anaerobic methane oxidation, since our study provided evidence that anaerobic methane oxidation may be important in these systems.

Fatty acid and alcohol lipid biomarkers extracted from suspended particulate matter collected from Lake Q in May (ice-cover) and July (ice-free) support rate-based evidence that methane oxidation is more prevalent in May than July and that carbon released by methane oxidation is

distributed into other carbon reservoirs (e.g. plant and algal biomass). These data are important supporting evidence that suggest methane oxidation during a time when the lake was previously assumed to be biologically quiescent is, to the contrary, vigorous. Evidence that methane carbon is transferred into biomarkers during times when methane availability and oxidation are high, confirms that biomarkers recovered from the sediment record are useful proxies for reconstructing methane activity in the past. Data analyzed by that model provide provocative evidence that periods of known warming in the past (i.e. the Holocene Thermal Maximum) are associated with an increase in the abundance and methane carbon contribution in methanotrophic biomarkers. Furthermore, warming during the past two millennia and continuing toward the present time indicate an increasingly active methane availability in the lake.

#### **4 Establishing a long-term record of the variability in methane emissions in relation to arctic climate change**

Arctic lakes and wetlands make a substantial contribution to the atmospheric methane budget. Methane trapped in ice cores records global-scale responses of methane reservoirs (e.g., gas hydrates, wetlands) affected by abrupt climate change (e.g., Sowers 2006). However, profound knowledge gaps remain regarding past methane emissions from the Arctic and relationships to climate change (Sowers 2010). Understanding how methane emissions will respond to contemporary climate change in the Arctic requires a basic understanding of how the methane cycle and environmental conditions (e.g. temperature and hydrology) have varied in the past. Multi-year studies have assessed seasonal differences in methane emissions from individual lakes (Walter et al. 2006). On longer time scales (i.e. multi-millennial), Arctic wetlands have been identified as a significant source of atmospheric methane since the last deglaciation (Sowers 2006; Walter et al. 2006). The intensity and timing of their contribution have been distinct from the tropics and Southern Hemisphere. Longer temporal records of methane flux from Arctic wetlands in relation to climate change are needed. In this regard, analyses of proxies of past methane release preserved in sediments taken from lakes and wetlands have been proposed (Wooller et al. 2009). These proxies are based on the stable carbon isotope composition (expressed as  $\delta^{13}\text{C}$  values) of various components (e.g. chironomid head capsules) preserved in lake sediments. Specifically, incorporation of  $^{13}\text{C}$ -depleted methane carbon ( $\delta^{13}\text{C}$  typically  $< -40\text{‰}$ ) into the biomass of aquatic microbes and invertebrates yields  $\delta^{13}\text{C}$  values that are more negative than other primary production sources, such as terrestrial plants in the Arctic that use  $\text{C}_3$  photosynthesis ( $\sim -27\text{‰}$ ) (Wooller et al. 2007).



## 4.1 Materials and Methods

During field work (Figure 35) we took a series of sediment cores from Lake Q (Figure 36).

Sub samples were taken from an organic rich sediment core and sent to NOSAMS facility for radiocarbon dating. Sub-samples were also taken from along the core for a series of chemical analyses to characterize past availability of methane and past environmental conditions (habitat type, hydrology and temperature). We used a multi-proxy paleoecological reconstruction to examine relative changes in methane production over a multi-millennial time scale from a wetland in Arctic Alaska.

**Figure 35. Project field-work and sediment coring operations in Alaska. Coring from a frozen lake allows a stable platform from which to work.**

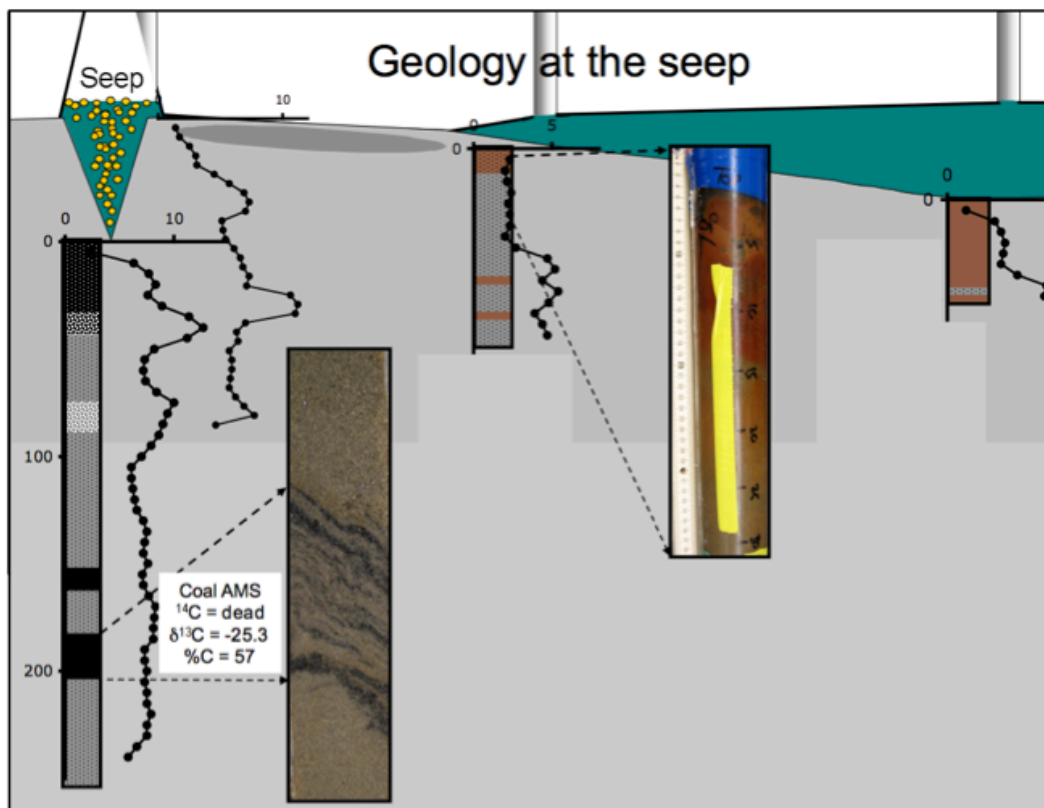


Specifically, we analyzed  $\delta^{13}\text{C}$  values of aquatic invertebrate (chironomids and cladocerans with head capsules and ephippia, respectively) remains preserved in a sediment core taken from a lake in Arctic Alaska (Figure 37).  $\delta^{13}\text{C}$  values from some chironomids and cladocerans that are low relative to associated total organic carbon (TOC) have been interpreted as evidence for the incorporation of methane-derived carbon by grazing on methane oxidizing microbes (Grey and Deines 2005; Grey et al. 2004; Jones and Grey 2004). Notably, significant relationships have



been demonstrated between methane fluxes from northern lakes and the  $\delta^{13}\text{C}$  values of some chironomid and cladoceran species, with relatively low  $\delta^{13}\text{C}$  in some invertebrates from lakes with higher methane flux. These findings along with laboratory and field incubation experiments support the use of these organisms as proxies for methane production in lakes. Similarly, some submerged bryophytes have also been shown to utilize carbon derived from oxidized methane, which can result in relatively low  $\delta^{13}\text{C}$  values from mosses.

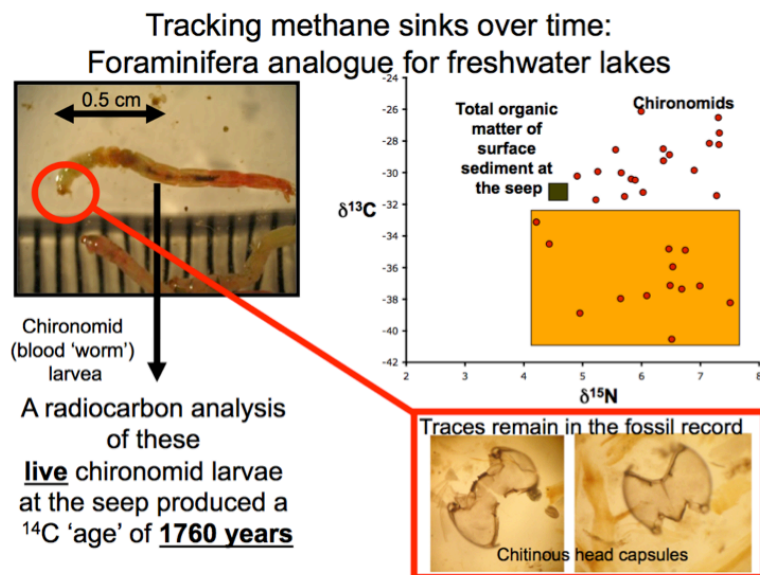
**Figure 36. A schematic of the sediment cores taken from Lake Q.**



The remains from aquatic organisms in cores of lake sediment retain the signature of the original whole organism. Consequently, researchers have proposed using  $\delta^{13}\text{C}$  values from lacustrine biota as a proxy for past incorporation of methane-derived carbon and therein past changes in methane emissions from lakes (Wooller et al. 2009). In this study, we applied these principles to examine a ~12,000 yr record of the methane cycle in an Arctic lake of Alaska. We applied isotopic mixing models to estimate alterations in the proportional contribution of methane-derived carbon to pelagic (cladocerans) and benthic (chironomids) organisms from a radiocarbon-dated sediment core from which we also describe environmental changes (i.e. temperature, hydrology, and habitat) that occurred at this location during the Holocene. We used changes in the assemblages of chironomids preserved in the sediment core as a proxy of past temperature (Langdon et al. 2011). We also used changes in the past oxygen isotope values ( $\delta^{18}\text{O}$ ) of lake water inferred from the  $\delta^{18}\text{O}$  of chironomid head capsules preserved in the sediments as a proxy for hydrologic change (Wooller et al., 2004) and plant macrofossils coupled

with sediment characteristics (lithological description and elemental composition) as proxies for local habitat change.

**Figure 37. Photos of chironomid fossils used to chemically analyze for signatures of past methane availability in lakes. Chironomids found at the seep in Lake Q had low  $\delta^{13}\text{C}$  values and 'old' radiocarbon ages indicating consumption of methane oxidizing bacteria. Wooller 2012**



Lipid biomarkers were organic solvent extracted from particulate matter and sediments and analyzed as part of our cost sharing agreement with Prof. Dr. Kai Uwe Hinrichs at the MARUM Institute, University of Bremen, Germany. Dr. Marcus Elvert was the lead collaborating scientist from MARUM. Lipid analysis entails chemical separation of different lipid classes from the bulk lipid extract followed by analysis by gas chromatography-flame ionization to quantify the lipids, analysis by gas chromatography-mass spectrometry to identify the

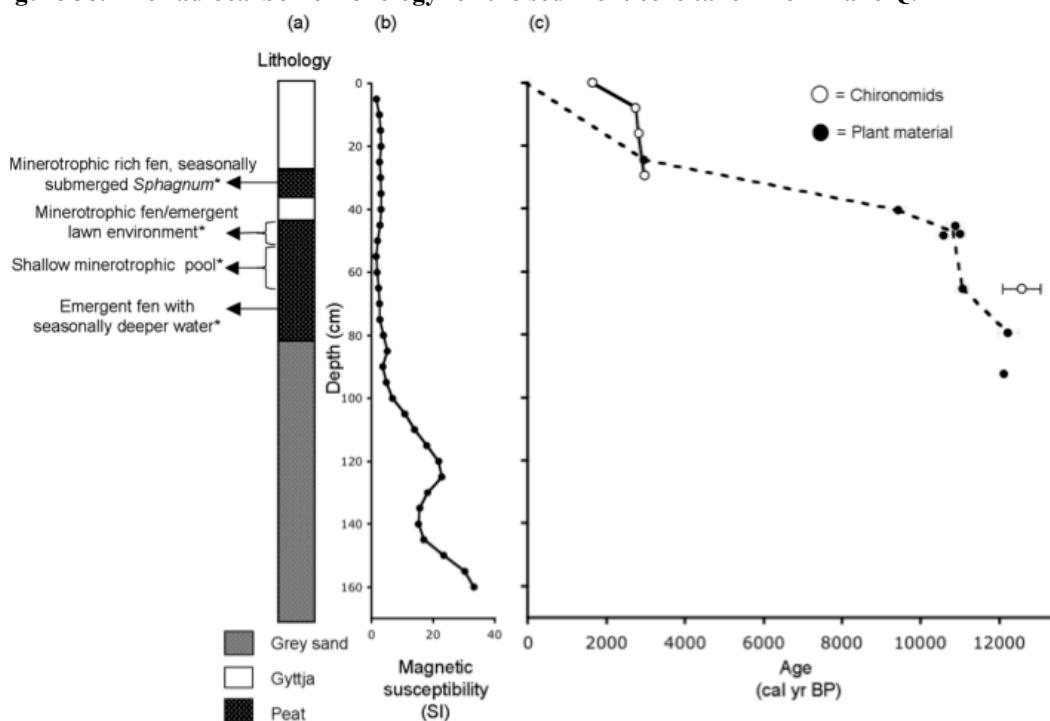
compounds and analysis by gas chromatography-isotope ratio mass spectrometry to measure the carbon isotope content of the compounds. Additionally, liquid chromatography-mass spectrometry analyses were performed to obtain mean annual air temperatures (MATs).

## 4.2 Results and Discussion

A radiocarbon chronology was established for the sediment core taken from Lake Q. The record showed the sediment represented the last approximately 12,000 years (Figure 38).

Stable carbon isotopic values of photosynthetic biomarkers and methane were utilized to estimate the proportional contribution of methane-derived carbon to lake-sediment-preserved benthic (chironomids) and pelagic (cladocerans) components over the last ~12,000 years (Figure 39). These results were compared to temperature, hydrologic, and habitat reconstructions from the same site using chironomid assemblage data, oxygen isotopes of chironomid head capsules, and radiocarbon ages of plant macrofossils. Cladoceran ephippia from ~4,000 cal yr BP sediments have  $\delta^{13}\text{C}$  values that range from ~-39 to -31‰, suggesting peak methane carbon assimilation at that time. These low  $\delta^{13}\text{C}$  values coincide with an apparent decrease in effective moisture and development of a wetland that included *Sphagnum subsecundum*. Incorporation of methane-derived carbon by chironomids and cladocerans decreased from ~2,500 to 1,500 cal yr BP, coinciding with a temperature decrease. Live-collected chironomids with a radiocarbon age of 1,640 cal yr BP, and fossil chironomids from 1,500 cal yr BP in the core illustrate that 'old' carbon has also contributed to the development of the aquatic ecosystem since ~1,500 cal yr BP.

**Figure 38. The radiocarbon chronology for the sediment core taken from Lake Q.**



The relatively low  $\delta^{13}\text{C}$  values of aquatic invertebrates (as low as  $-40.5\text{‰}$ ) provide evidence of methane incorporation by lake invertebrates, and suggest intermittent climate-linked methane release from the lake throughout the Holocene. Lipid biomarker data from the radiocarbon-dated sediment core from Lake Q was paired with the invertebrate biomarker data to reconstruct the evolution of Lake Q and to infer methane activity during the Holocene. A record based on temperature-dependent branching and ring patterns of soil derived glycerol dialkyl glycerol tetraether (GDGT) lipids was used to construct the MAT record at the lake (left side of Figure 40). The highest temperatures occurred during the Holocene Thermal Maximum (HTM), when the lake site was an emergent fen. Concentration and carbon isotope values for hop-17(21)-ene, another biomarker for aerobic methanotrophy, was most abundant and had lowest  $\delta^{13}\text{C}$  values indicating an intense methane cycle during the HTM (right side of Figure 40). After establishment of thermokarst Lake Q, most negative MATs and intermittent methane activity were observed in the period from  $\sim 10,000$  to  $\sim 2,000$  years BP. Increasing concentrations of hop-17(21)-ene with relatively low  $\delta^{13}\text{C}$  values and rising MATs for the past 2,000 years BP suggest methane activity (and potentially emissions) is also increasing.

### 4.3 Conclusions

Our data imply that past methane production and incorporation into aquatic invertebrates at Lake Q have changed over the last  $\sim 12,300$  cal yr BP in response to climate change in the Arctic. Low  $\delta^{13}\text{C}$  values for cladoceran and chironomid remains relative to those of TOC are evident intermittently. The most notable period of low  $\delta^{13}\text{C}$  values from cladocerans took place at  $\sim 4,000$

cal yr BP, correlating with a peak in reconstructed lake water  $\delta^{18}\text{O}$  values, which imply significant evaporation from the lake. Older-than-expected radiocarbon ages from chironomids, relative to the age of the enclosing sediment, coupled with low  $\delta^{13}\text{C}$  values (relative to TOC), imply the intermittent use of old methane by aquatic organisms during the last ~12,300 years and in the lake today. This approach needs to be applied at greater spatial resolution to examine broad geographic patterns.

**Figure 39. (a) Estimated proportional contribution (%) of methane-derived carbon to chironomids and ephippia from the LQ-West core, (b)  $\delta^{18}\text{O}$  values of modern lake water from Qalluuraq Lake plotted relative to reconstructed  $\delta^{18}\text{O}$  values from analyses of chironomid head capsules (see methods) from the LQ-West core, and (c) chironomid assemblage, inferred mean July air temperature from the LQ-West core (also plotted relative to inferred temperature from Burial Lake, Alaska, Kurek et al. 2009). (Wooller et al. 2012).**

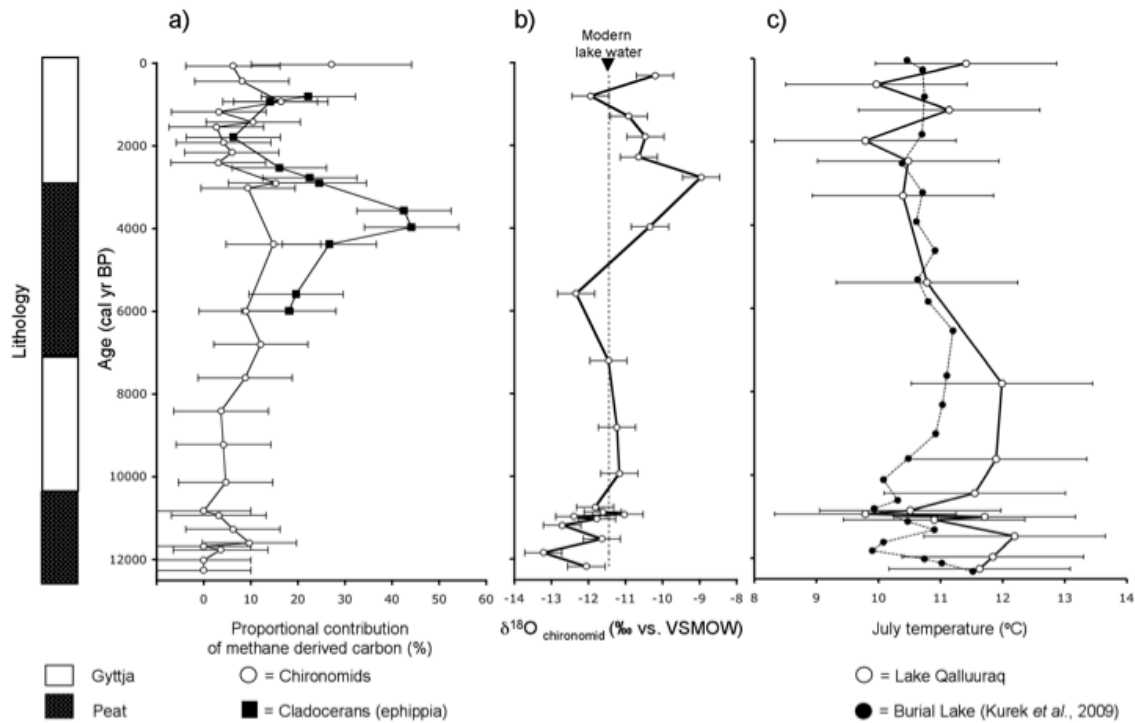
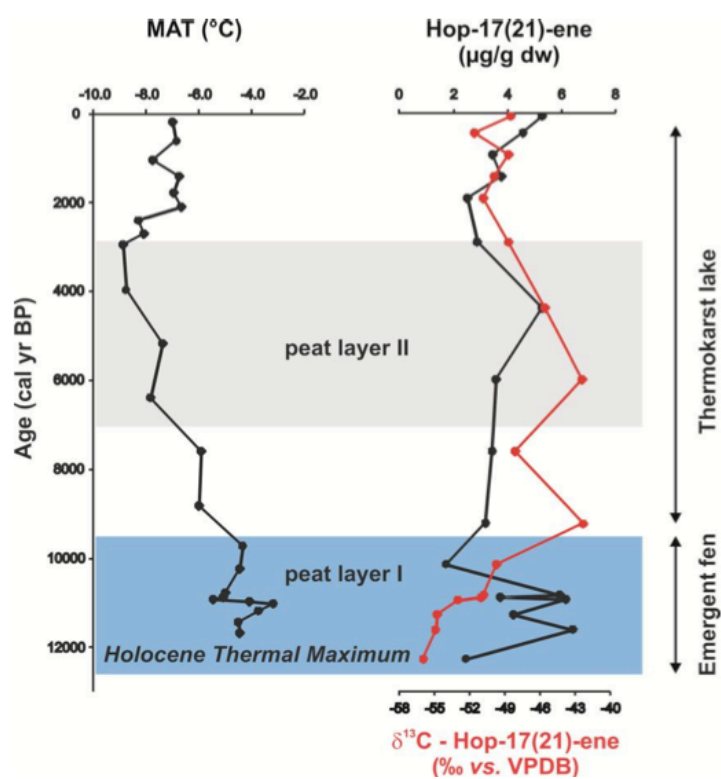


**Figure 40.** Lipid biomarker based Holocene records of mean annual air temperature (left) and methane activity (right) at Lake Q.





## LIST OF FIGURES

Figures	Page
Figure 1. Location map showing primary study sties (Lake Q and Lake Teshekpuk) and the reference sites (Fairbanks lakes).	7
Figure 2. Sources and sinks for methane beneath a thermokarst lake (TKL) with a well-developed thaw bulb.	7
Figure 3. Schematic of potential sources of methane that could me emitted at or near a thermokarst lake.	8
Figure 4. Nominal relationship among permafrost, gas hydrate, and gas-charged sediments in a permafrost area, from Ruppel (2007).	8
Figure 5. Calculated thickness of gas hydrate stability zone on the Alaskan North Slope based on analyses by T. Collett of USGS borehole temperature data and supplementary data. The positions of the Lake Q and Lake Teshekpuk study sites are also shown.	10
Figure 6. Classification of superficial (ecological) ebullition seeps by methane bubble-clusters patterns in lake ice; methane concentrations in bubble gas; and summer, winter, and annual ebullition determined by long-term flux measurements. Error estimates (standard error of n seeps) represent differences in methane concentrations and ebullition between individual seeps in each category. The lines on the meter sticks in the photos of type A and B mark 10cm wide intervals. [From Walter Anthony et al. 2010].	16
Figure 7. The effect on lake ice formation of the largest superficial seeps (a) and the smallest (b) and largest (c) subcap macroseeps. Even the strongest superficial seeps are ice-covered in late winter. Further, ebullition does not occur simultaneously among superficial seeps (a). In contrast, bubbles breaking the surface of all open holes indicate high, simultaneous ebullition among subcap seeps (b). Clustering of subcap seeps is apparent in the aerial photograph (d). Photographs were taken near Fairbanks, Interior Alaska (a), Cook Inlet, Southcentral Alaska (b), and (Lake Q) Atkasuk, Northern Alaska (c, d) one, eight, and three weeks respectively following freeze-up. Locations are shown in Figure 8. [From Walter Anthony et al. 2012].	17
Figure 8. Map of Alaska seeps, aerial flight path, study regions, lakes, yedoma deposits and hydrocarbon basins. Yellow dots, representing 77 subcap seep sites identified across Alaska in this study, and green dots (superficial study lakes, panel a) are scaled by the magnitude of methane flux ( $\text{kg methane site}^{-1} \text{d}^{-1}$ ) at each site. Black dashed lines show sections of the flight path omitted from analysis due to fog. Additional information is provided in Walter Anthony et al. [2012].	19
Figure 9. Distinctions between seep types based on bubbling rates and isotope compositions. Alaska subcap ebullition seeps (solid symbols) were distinct from superficial seeps (open circles and bars) based on (a) vigorous rates of bubbling; (b) predominately fossil radiocarbon ages [percent modern carbon (pmC), mean $\pm$ SE of 1-12 seeps per lake]; and (c) enriched stable isotope values originating from thermogenic and microbial hydrocarbon reservoirs or buried glacial organics. In (d) $\delta^{13}\text{C}$ -methane and $\text{C1}/(\text{C2}+\text{C3})$ ratios in subcap seeps (solid circles) were similar to those in nearby gas wells (open squares) in South Central Alaska (Cook Inlet, blue, Claypool et al. 1980) and Northern Alaska near the Meade River (green, Burruss et al. 2003) and Walakpa (orange, Burruss et al. 2003). [From Walter Anthony et al. 2012].	20
Figure 10. Lake sediment core locations on the Alaskan North Slope, near Lake Teshekpuk. The white rectangle in the Alaska map inset demarcates the area of the larger map.	22

Figure 11. Subcap (macroseep) and superficial methane seep emissions in Alaska. In 50-km wide bins along the north-south Alaska transect, (a) the number of subcap-seep sites normalized by survey area; (b) total number of lakes surveyed; (c) methane emissions from subcap macroseeps and superficial seeps (yedoma-type and non-yedoma lakes); and a schematic cross-section (d, not to scale) of major topographic and subsurface features along the Alaska transect: permafrost distribution and thickness; examples of open and closed thaw bulbs in conjunction with faults and permeable strata providing gas migration conduits; examples of primary structural and stratigraphic gas traps beneath the secondary cryosphere cap; and potential methane sources contributing to ebullition emissions in Alaska including superficial ecosystem methane from surface lake and taberal (thawed permafrost) sediments and five subcap sources: microbial methane in buried glacial sediments, coalbed methane (biogenic or thermogenic), thermogenic methane from deep conventional hydrocarbons; and possibly methane derived from hydrate dissociation. [From Walter Anthony et al. 2012].	23
Figure 12. Crossplot of sodium (Na) and chloride (Cl) concentrations from Lake Q and surrounding lakes in May and July 2009.	26
Figure 13. Methane concentration profiles from May 2009 sediment cores from Lake Q (lower panels). The upper panel is a conceptual diagram for factors controlling the sediment methane distribution during ice cover.	28
Figure 14. Methane concentration profiles from July 2009 sediment cores from Lake Q (lower panels). The upper panel is a conceptual diagram for factors controlling the sediment methane distribution during ice-free conditions.	29
Figure 15. Sediment methane concentration profiles from A) Lake Teshekpuk, B) Lake Helen, C) Lake 21, and D) Lake Kogru.	30
Figure 16. Noble gas ratio crossplots of Ne, Kr and Xe, expressed as ‘F’ values. Purple triangles are the samples from Lake Q. The other symbols represent atmospheric (ATM), air saturated seawater (ASSW) and samples from gas hydrate and thermogenic sources. The absence of noble gas enrichment in the Lake Q samples is inconsistent with a gas hydrate derived source.	31
Figure 17. Deployment of the Chirp 424 subbottom profiling fish in Lake Teshekpuk in 2010 (left) and use of a waterproofed RTA ground penetrating radar cable in Smith Lake near Fairbanks in 2009 (right).	33
Figure 18. Towed AGI Supersting DC resistivity system on Lake Q in 2009 (left) and Humminbird display showing sidescan results and water column image on Lake Teshekpuk in 2010 (right).	34
Figure 19. Boat operations for geophysical surveys in 2009 at Lake Q (left) and 2010 at Lake Teshekpuk (right).	35
Figure 20. Tracklines for geophysical surveys at Lake Q: Subbottom profiling with the Chirp 424 system in white; GPR in red; and DC resistivity transects in green. The July 2009 cores are shown in yellow, and the seep site is marked with a blue cross.	37
Figure 21. Bathymetry of Lake Q (red to blue shading) mapped by compiling lake bottom first arrival picks from the Chirp 424 data, automatic depth recordings collected during the DC resistivity tows, and lake bottom radar reflections from the GPR data. Standard ArcGIS routines were used to merge and grid the data, and the lake’s edge as digitized from the underlying high-resolution photo-mosaic was arbitrarily set to 0 depth. Deepest blue corresponds to ~2.5 m depth. Red areas are less than half a meter deep. The seep is located at the boundary between the two main basins, where the blue circles and red squares overlap close to the star symbols. Blue circles denote locations of July 2009 cores. The area enclosed by the hatched contour bounds the limit of grounded ice (ticks face	38

into the grounded ice) as digitized from SAR data collected in May 2010.

Figure 22. Raw Chirp 424 subbottom profiling data across the Lake Q seep. Most of the reflectors below the lake bottom are multiples. Line 6 runs from west to east through the seep, and Line 7 runs from north to south, nearly perpendicular to the first line. Note that the seep is vigorous enough that Chirp frequencies (4-24 kHz) can detect the gas in the water column. Depth conversions (right axis on Line 7) are automatically made using 1500 m/s for seismic velocity, which is slightly too fast for this freshwater setting. Note the bright reflector about 8 m south of the seep at ~1 ms below the lake bottom in Line 7 and a bright reflector just beneath the surface to the west of the seep in Line 6. Distance marks along the bottom at 10 m intervals and will not be evenly distributed if the boat's speed changed along track. 40

Figure 23. Lake Teshekpuk and surrounding areas. The Beaufort Sea is at the top of the image. Red circles denote cores collected for this project in April 2010. The white survey lines at the northernmost part of the lake show the geophysical transects acquired in July 2010. Reconnaissance surveys in 2009 had revealed the existence of methane seeps in this part of the lake. Bathymetry provided by Ben Jones, USGS Anchorage. In Lake Teshekpuk, the deepest colors correspond to ~8 m depth. 41

Figure 24. Chirp image collected with USGS Woods Hole equipment by Ben Jones (USGS Anchorage) and Chuck Worley (USGS Woods Hole) during reconnaissance in July 2009. This image shows a seafloor pockmark with well-developed rims, gas charging directly beneath the lake bottom at the seep, and gas in the water column right above the lake bottom at the pockmark. It was on the basis of imagery like this that the decision was made to pursue work in Lake Teshekpuk for Year 2 of the study. Lake Teshekpuk also had a clear advantage over the Prudhoe Bay area, where entry to the field sites would have been complicated by regulations controlling access. 42

Figure 25. Example Chirp profile in Lake Teshekpuk. Shallow gas occurs nearly everywhere in these profiles. The depth conversion on the right was done automatically with 1500 m/s, which is slightly too fast for freshwater and not reliable within the sedimentary section. Uneven spacing of distance marks on the bottom indicates varying speed of the vessel. 43

Figure 26. Example of mini-boomer data recorded in northern Lake Teshekpuk in 2010. 43

Figure 27. Primary sampling locations and study sites for methane oxidation and microbial studies: Lake Q, previously discussed in this report, and Lake Killarney, a subarctic taiga lake with moderate methane ebullition in Fairbanks. Reprinted from He et al., 2012a. 46

Figure 28. Stable isotope probing methods overview. 47

Figure 29. Sediment depth profile for dissolved methane concentration in the sampling sites. (a) LQ-BGC site; (b) LQ-WEST site; and (c) LK-NW site. Reprinted from He et al., 2012a. 48

Figure 30. Methane oxidation at 21° C of water samples from indicated depths: top (20 cm under the water's surface); middle (1 m below the water's surface); bottom (10 cm above the sediment-water interface). Different letters within the graph refer to significant difference at 5% level based on the least significant difference (LSD) method. Reprinted from He et al. (2012a). 49

Figure 31. Methane oxidation potential of sediment from LQ-BGC site at 10°C and 4°C. Reprinted from He et al., 2012a (supplement). 49

Figure 32. Methane oxidation potential of sediment from (a) LQ-BGC; (b) LQ-WEST site; and (c) LK-NW site at 21°C incubated for 2 (white bar), 5 (shaded bar) and 10 (black bar) days. Note different scales on y-axes. Reprinted from He et al., (2012a). 50

Figure 33. Phylogenetic distribution of all pyrosequencing reads from the heavy fractions ( $^{13}\text{C}$ -DNA) from DNA-SIP experiments, indicating the relative abundance of bacterial taxa that derived carbon from $^{13}\text{C}$ -methane in sediment collected from Lake Q (0-1 cm depth). Reprinted from He et al. (2012c).	52
Figure 34. Relative abundances of known methanotrophs and methylotrophs within sediment microbial populations that derived carbon from methane during SIP, based on the abundances of 16S rRNA gene sequences detected in $^{13}\text{C}$ -labeled DNA by use of pyrosequencing. Taxonomic assignments were made using the classifier of the Ribosomal Database Project (confidence threshold, 80%). Sediments subjected to SIP were analyzed after about 0.2 mmol $^{13}\text{C}$ -methane g <sup>-1</sup> (wet weight) was consumed at incubation temperatures of 4°C, 10°C, and 21°C. (a) Methanotrophs; (b) methylotrophs. Reprinted from He et al. (2012b).	53
Figure 35. Project field-work and sediment coring operations in Alaska. Coring from a frozen lake allows a stable platform from which to work.	60
Figure 36. A schematic of the sediment cores taken from Lake Q.	61
Figure 37. Photos of chironomid fossils used to chemically analyze for signatures of past methane availability in lakes. Chironomids found at the seep in Lake Q had low $\delta^{13}\text{C}$ values and ‘old’ radiocarbon ages indicating consumption of methane oxidizing bacteria. Wooller 2012	62
Figure 38. The radiocarbon chronology for the sediment core taken from Lake Q	63
Figure 39. (a) Estimated proportional contribution (%) of methane-derived carbon to chironomids and ephippia from the LQ-West core, (b) $\delta^{18}\text{O}$ values of modern lake water from Qalluuraq Lake plotted relative to reconstructed $\delta^{18}\text{O}$ values from analyses of chironomid head capsules (see methods) from the LQ-West core, and (c) chironomid assemblage, inferred mean July air temperature from the LQ-West core (also plotted relative to inferred temperature from Burial Lake, Alaska, Kurek et al. 2009). (Wooller et al. 2012).	64
Figure 40. Lipid biomarker based Holocene records of mean annual air temperature (left) and methane activity (right) at Lake Q.	65

## LIST OF TABLES

<b>Tables</b>	<b>Page</b>
Table 1. Researchers involved in this project. Table does not include support personnel from UAF and the USGS.	5
Table 2. Dates of aerial surveys and ground truth field campaigns for subcap seeps, supported by this project (North Slope) and other projects. From Walter Anthony et al. (2012).	18
Table 3. Core locations for sediment biogeochemistry studies.	21
Table 4. The occurrence of subcap seep sites in relation to permafrost ice content and soil texture in the Northern Alaska continuous permafrost region.	25
Table 5. Comparison of seep association with fluvial deposits among the three Alaska study regions.	26
Table 6. Relative abundance (% of total reads) and phylogenetic affiliations of 16S rRNA pyrosequencing reads from DNA of enrichment cultures in methanotroph medium cultivated from lake water samples. Reprinted from He et al. (2012a).	55
Table 7. Relative abundance (% of total reads) and phylogenetic affiliations of pyrosequencing reads from $^{13}\text{C}$ -DNA obtained from SIP of lake sediments incubated with $^{13}\text{C}$ -methane. Taxonomic assignments were generated using the Ribosomal Database Project's classifier. Reprinted from He et al. (2012a).	56
Table 8. Effects of temperature on the relative abundances of organisms that derived carbon from $^{13}\text{C}$ -methane during SIP experiments. Relative abundance as % and number of pyrosequencing reads (in parentheses) from $^{13}\text{C}$ -labeled DNA assigned to different taxa by using the Ribosomal Database Project Classifier. Reprinted from He et al. (2012b).	57



## REFERENCES

- Bellefleur, G., Riedel, M., Ramachandran, K., Brent, T., and S. Dallimore, (2009). Recent advances in mapping deep permafrost and gas hydrate occurrences using industry seismic data, Richards Island Area, Northwest Territories, Canada, 2009 CSPG CSEG CWLS Convention, Calgary, Alberta, 603-607.
- Collett, T. S. (1997), "Gas hydrate resources of northern Alaska." *Bulletin of Canadian Petroleum Geology* 45(3): 317-338.
- Grey, J., and Deines, P. (2005), Differential assimilation of methanotrophic and chemoautotrophic bacteria by lake chironomid larvae. In "Aquat Microb Ecol." pp. 61-66.
- He, R. M. J. Wooller, J. W. Pohlman, J. Quensen, J. M. Tiedje, M. B. Leigh. (2012a), Diversity of active aerobic methanotrophs along depth profiles of arctic and subarctic lake water column and sediments. *The ISME Journal*. doi:10.1038/ismej.2012.34
- He, R. M. J. Wooller, J. W. Pohlman, J. Quensen, J. M. Tiedje, M. B. Leigh. (2012b), Shifts in identity and activity of methanotrophs in arctic lake sediments in response to temperature changes. *Applied and Environmental Microbiology* 78(13):4715-4723.
- He, R. M. J. Wooller, J. W. Pohlman, C. Catranis, J. Quensen, J. M. Tiedje, M. B. Leigh. (2012c), Identification of functionally active aerobic methanotrophs in sediments from an arctic lake using stable isotope probing. *Environmental Microbiology* 14(6):1403-1419.
- Jepsen, S.M., Voss, C.I., Walvoord, M.A., Minsley, B.J., and J. Rover, (2013), Linkages between Lake Shrinkage/Expansion and Sublacustrine Permafrost Distribution Determined from Remote Sensing of Interior Alaska, USA, *Geophys. Res. Lett.*, in press, DOI: 10.1002/grl.50187
- Kessler, M. A., L. Plug, and K. Walter Anthony (2012), Simulating the decadal to millennial scale dynamics of morphology and sequestered carbon mobilization of two thermokarst lakes in N.W. Alaska, *J. Geophys. Res.*, doi:10.1029/2011JG001796
- Lachenbruch, A.H., J.H. Sass, L.A. Lawver, M.C. Brewer, G.V. Marshall, R.J. Munroe, J.P. Kennelly, Jr., S.P. Galanis, Jr., and T.H. Moses, Jr. (1982), Temperature and depth of permafrost on the arctic slope of Alaska. In: Gryc, G., ed., *Geology and Exploration of the National Petroleum Reserve in Alaska, 1974-1982*, U.S. Geological Survey Professional Paper 1399, 645-656.
- Minsley, B. J., et al. (2012), Airborne electromagnetic imaging of discontinuous permafrost, *Geophys. Res. Lett.*, 39, L02503, doi:10.1029/2011GL050079.
- Ruppel, C. (2007), "Tapping methane hydrates for unconventional natural gas." *Elements* 3: 193-199.
- Reeburgh, W. S. (2007), Oceanic methane biogeochemistry. In "Chem Rev." pp. 486-513.
- Schuur, E. A. G., J. G. Vogel, et al. (2009), "The effect of permafrost thaw on old carbon release and net carbon exchange from tundra." *Nature* 459(7246): 556-559.
- Shakhova, N., I. Semiletov, et al. (2010), "Methane from the East Siberian Arctic Shelf Response." *Science* 329(5996): 1147-1148.
- Sowers, T. (2006), Late quaternary atmospheric CH<sub>4</sub> isotope record suggests marine clathrates are stable. In "Science." pp. 838-840.
- Walter, K. M., Zimov, S. A., Chanton, J. P., Verbyla, D., and Chapin, F. S. (2006), Methane bubbling from Siberian thaw lakes as a positive feedback to climate warming. In "Nature." pp. 71-75.
- Walter Anthony, K. M., D. Vas, L. Brosius, F. S. Chapin III, S. A. Zimov, Q. Zhuang. (2010) Estimating methane emissions from northern lakes using ice bubble surveys. *Limnology and Oceanography Methods* 8, 592-609.
- Walter Anthony, K. M., P. Anthony, G. Grosse, J. Chanton. In press, (2012), Geologic methane seeps along boundaries of arctic permafrost thaw and melting glaciers, *Nature Geoscience*, DOI doi:org/10.1038/Ngeo1480
- West, J. J., and L. J. Plug (2008), Time-dependent morphology of thaw lakes and taliks in deep and shallow ground ice, *J. Geophys. Res.*, 113, F01009, doi:10.1029/2006JF000696.
- Wooller, M., Zazula, G. D., Edwards, M., Froese, D. G., Boone, R. D., Parker, C., and Bennett, B. (2007c), Stable carbon isotope compositions of Eastern Beringian grasses and sedges: Investigating their potential as paleoenvironmental indicators. In "Arct Antarct Alp Res." pp. 318-331.
- Wooller, M. J., Francis, D., Fogel, M. L., Miller, G. H., Walker, I. R., and Wolfe, A. P. (2004), Quantitative paleotemperature estimates from delta O-18 of chironomid head capsules preserved in arctic lake sediments. In "J Paleolimnol." pp. 267-274.

- Wooller, M.J., Ruppel, C., Pohlman, J.W., Leigh, M.B., Heintz, M., and Walter Anthony, K., (2009), Permafrost gas hydrates and climate change; lake-based seep studies on the Alaskan North Slope: Fire in the Ice (U.S. Department of Energy, National Energy Technology Laboratory Methane Hydrate Newsletter), summer 2009, p. 6-9.
- Wooller, M. J., Pohlman, J. W., Gaglioti, B. V., Langdon, P., Jones, M., Walter Anthony, K. M., Becker, K. W., Hinrichs, K. U., Elvert, M. (2012), Reconstruction of past methane availability in an Arctic Alaska wetland indicates climate influenced methane release during the past ~12,000 years. *Journal of Paleolimnology* DOI 10.1007/s10933-012-9591-8.
- Zimov, S. A., Voropaev, Y. V., Semiletov, I. P., Davidov, S. P., Prosiannikov, S. F., Chapin III, F. S., Chapin, M. C., Trumbore, S., and Tyler, S. (1997), North Siberian Lakes: A Methane Source- Fueled by Pleistocene Carbon. *Science* 277, 800-802.

## LIST OF ACRONYMS AND ABBREVIATIONS

AGI	Advanced Geosciences, Inc.
ANS	Alaska North Slope
BLM	U.S. Bureau of Land Management
DC	Direct current
DNA	Deoxyribonucleic acid
GDGT	glycerol dialkyl glycerol tetraether
GC-FID	Gas Chromatograph Flame Ionization Detector
GPR	Ground penetrating radar
GPS	Global positioning system
HTM	Holocene Thermal Maximum
MAT	Mean annual air temperatures
MARUM	Center for Marine Environmental Studies, U. Bremen
PI	Principal investigator
PLFA	Phospholipid Fatty Acid
Q-PCR	Quantitative real time polymerase chain reaction
RNA	Ribonucleic acid
RTA	Remote terrain antenna (for GPR)
SAR	Synthetic aperture radar
SEG Y	Society of Exploration Geophysics seismic format
SIP	Stable isotope probing
TKL	Thermokarst lake
UAF	University of Alaska-Fairbanks
USGS	U.S. Geological Survey

## **National Energy Technology Laboratory**

626 Cochrans Mill Road  
P.O. Box 10940  
Pittsburgh, PA 15236-0940

3610 Collins Ferry Road  
P.O. Box 880  
Morgantown, WV 26507-0880

13131 Dairy Ashford, Suite 225  
Sugarland, TX 77478

1450 Queen Avenue SW  
Albany, OR 97321-2198

Arctic Energy Office  
420 L Street, Suite 305  
Anchorage, AK 99501

Visit the NETL website at:  
[www.netl.doe.gov](http://www.netl.doe.gov)

Customer Service:  
1-800-553-7681

